

December 2013

# Techniques for Engine Mount Modeling and Optimization

Fadi Alkhatib

*University of Wisconsin-Milwaukee*

Follow this and additional works at: <https://dc.uwm.edu/etd>



Part of the [Mechanical Engineering Commons](#)

---

## Recommended Citation

Alkhatib, Fadi, "Techniques for Engine Mount Modeling and Optimization" (2013). *Theses and Dissertations*. 344.  
<https://dc.uwm.edu/etd/344>

This Dissertation is brought to you for free and open access by UWM Digital Commons. It has been accepted for inclusion in Theses and Dissertations by an authorized administrator of UWM Digital Commons. For more information, please contact [open-access@uwm.edu](mailto:open-access@uwm.edu).

**TECHNIQUES FOR ENGINE MOUNT MODELING AND  
OPTIMIZATION**

By

Fadi Alkhatib

A Dissertation Submitted in  
Partial Fulfillment of the  
Requirements for the Degree of

Doctor of Philosophy

in

Engineering

at

The University of Wisconsin – Milwaukee

December 2013

## **ABSTRACT**

# **TECHNIQUES FOR ENGINE MOUNT MODELING AND OPTIMIZATION**

By

Fadi Alkhatib

The University of Wisconsin-Milwaukee, 2013

Under the Supervision of Professor Anoop Dhingra

This dissertation presents techniques for the design of engine mounting system to address the issue of vibration isolation. While the techniques presented herein are general, the application of proposed techniques is demonstrated primarily through applications in motorcycles. The dynamic loads that are generated due to the shaking forces within the engine and the road loads that are transmitted to the engine through the tire patch are discussed. The geometrical shape of the engine mount is also considered in this work. All models discussed herein deal with solving the optimization problem for the engine mount system such that the transmitted forces to and from the engine are minimized in which the mount parameters are used as design variables.

While work has been done in the past in the area of engine mount design, this dissertation tries to fill in the gap when it comes to designing a comprehensive mounting system that takes into account modeling of the mount characteristics, the excitation load present in the system, and a determination of the final geometrical shape of the engine mount.

The work presented in this dissertation discusses three major problems. The first problem addresses comprehensive mount modeling wherein mathematical mount models range from a simple Voigt model to a complex Voigt model that captures hysteresis and nonlinear behavior are presented. The issue of mechanical snubbing is also considered in these models. An optimization problem is formulated to determine the mount parameters by minimizing the difference between the transmitted loads predicted by the theoretical model and experimentally measured values.

The second problem addressed in this dissertation deals with mounting system optimization. The optimization is carried out such that the loads transmitted through the mount system from/to the frame are minimized. The road loads that are generated due to the irregularities in the road profile and the shaking loads that are generated due to the engine imbalance are discussed in detail. The mount parameters are considered as design variables. Displacement constraints, both static and dynamic are considered to account for packaging requirements and to prevent mechanical snubbing of the engine mount. Numerical examples dealing with mount system optimization are presented first for a six degree of freedom model that deals only with the powertrain assembly. This is followed by twelve degree of freedom model that builds on the previous model by considering the swing-arm assembly dynamics in addition to the powertrain assembly.

The third problem presented in this dissertation deals with finding the optimum geometrical shape of the mount itself. The shape optimization of the mount is done using a nonlinear finite element model of the mount developed in ANSYS<sup>®</sup>. An optimization problem is formulated to minimize the difference between the target stiffness obtained from the dynamic analysis and stiffness values obtained from the mount geometry. The

mount geometrical parameters such as the mount diameter and the thickness are used as design variables. Numerical examples are provided quantifying how mount geometrical parameters vary for different operating engine speeds.

All the models and techniques developed in this work will help designers comprehensively design a mounting system that achieves an effective vibration isolation of the powertrain assembly.

## ACKNOWLEDGMENTS

I would like to thank my advisor, Professor Anoop Dhingra, for his continuous guidance, patience, support and friendship throughout my dissertation work. I appreciate my dissertation committee members: Dr Ron Perez, Dr Ilya Avdeev, Dr Nidal Abu Zahra and Dr Rani El-Hajjar for their support, insights and suggestions. I would like to thank Dr Sudhir Kual for sharing experimental data used in chapter 3 and for discussing the general aspects of mount design. I would like also to thank all my colleagues in the Design Optimization group for their continuous support. I would like also to thank the University of Wisconsin-Milwaukee for providing me financial support that enabled me to do this research.

I also would like to thank my father and mother for their influence and support throughout these long years.

Finally, special thanks to my wife Arwa Shalhout, without her support and patience this success would not have been possible.

*Dedicated to my wife Arwa and my Parents who always encouraged me and supported me throughout these long years of education.*

# TABLE OF CONTENTS

<b>ACKNOWLEDGMENTS .....</b>	<b>v</b>
<b>Chapter 1 - Introduction .....</b>	<b>1</b>
1.1 Introduction .....	1
1.2 Vibration Isolation.....	2
1.3 Engine Mounts .....	3
1.3.1 Elastomeric Mounts .....	3
1.3.2 Passive Hydraulic Mounts .....	4
1.3.3 Active Engine Mounts .....	5
1.4 Modeling of Engine Mounts .....	7
1.5 Dissertation Objectives .....	9
1.6 Dissertation Organization.....	10
<b>Chapter 2 – Literature Review .....</b>	<b>12</b>
2.1 Vibration Isolation.....	12
2.2 Vibration Modes Decoupling.....	14
2.3 Mount Modeling.....	17
2.4 Load Estimation .....	18
2.5 Shape Optimization .....	20
2.6 Summary .....	21
<b>Chapter 3 – Mount Characterization and Determination of Mount Parameters.....</b>	<b>23</b>
3.1 Load Estimation .....	23
3.2 Elastomeric Mount .....	25
3.3 Mount Modeling.....	27
3.3.1 Model 1 - Voigt Model .....	28
3.3.2 Model 2 - Maxwell-Voigt Model.....	30
3.3.3 Model 3 - Voigt Model with Bouc-Wen Element .....	31
3.3.4 Model 4 - Voigt Model with Bouc-Wen Element and Nonlinear Stiffness	33
3.4 Parameter Identification .....	35
3.4.1 Numerical example .....	37
3.5 Summary .....	43



<b>Chapter 4 – Mount Modeling and Design.....</b>	<b>44</b>
4.1 Mathematical Modeling .....	44
4.1.1 Six DOF Model.....	44
4.1.2 Twelve DOF Model .....	51
4.2 Mount Optimization .....	56
4.2.1 Sequential Quadratic Programming .....	57
4.2.2 Six DOF Model.....	60
4.2.3 Twelve DOF Model .....	66
4.3 Isolator Inclining .....	75
4.3.1 Numerical Example .....	77
4.4 Vibration Modes Decoupling.....	79
4.4.1 Numerical Example .....	79
4.5 Summary .....	85
<b>Chapter 5 – Optimum Design of a Mount System for a V-Twin Engine.....</b>	<b>87</b>
5.1 Shaking Loads .....	87
5.1.1 Transmitted Shaking Loads .....	88
5.1.2 Numerical Example .....	98
5.2 Road Loads.....	103
5.2.1 Transmitted Road Loads .....	104
5.2.2 Numerical Example .....	106
5.3 Summary .....	113
<b>Chapter 6 – Shape Optimization of Engine Mounts.....</b>	<b>114</b>
6.1 Finite Element Modeling.....	114
6.2 Parameter Optimization.....	118
6.3 Design Model and Analysis .....	119
6.4 Examples .....	121
6.4.1 Example I.....	122
6.4.2 Example II.....	126
6.5 Summary .....	129
<b>Chapter 7 - Conclusion.....</b>	<b>130</b>

7.1	Theoretical Modeling .....	130
7.2	Mounting system optimization.....	131
7.3	Shape Optimization .....	132
7.4	Future Work .....	133
<b>References .....</b>		<b>135</b>
<b>APPENDIX A .....</b>		<b>140</b>
<b>APPENDIX B .....</b>		<b>142</b>
<b>APPENDIX C .....</b>		<b>144</b>
<b>APPENDIX D .....</b>		<b>146</b>

## LIST OF FIGURES

Figure 1.1: Mechanical Model for Elastomeric Mounts .....	4
Figure 1.2: Simple Hydraulic Mount .....	5
Figure 1.3: (a) Mechanical Model for Active Elastomeric Mount, (b) Mechanical Model for Active Hydraulic Mount.....	6
Figure 1.4: Engine Six DOF Modes (Ye, et. al. 2001) .....	8
Figure 1.5: (a) Engine Mount, (b) Tri-Axial Engine Mount Model (Kaul, 2006).....	8
Figure 3.1: Schematic Diagram Showing the Tire Patch.....	24
Figure 3.2: Tri-axial Engine Mount Model.....	27
Figure 3.3: Voigt Model .....	29
Figure 3.4: Maxwell-Voigt Model .....	31
Figure 3.5: Voigt Model with Bouc-Wen Element.....	33
Figure 3.6: Voigt Model with Bouc-Wen Element and Nonlinear Stiffness .....	34
Figure 3.7: Measured Force – Displacement Curve. ....	38
Figure 3.8: Force Displacement Curve (Voigt Model).....	38
Figure 3.9: Force Displacement Curve (Maxwell-Voigt Model) .....	39
Figure 3.10: Force Displacement Curve (Voigt Model with Bouc-Wen Element) .....	39
Figure 3.11: Force Displacement Curve (Voigt Model with Bouc-Wen Element and Nonlinear Stiffness) .....	40
Figure 4.1: Six DOF Model (Cocco, 2001) .....	45
Figure 4.2: Twelve DOF Model (Cocco, 2001).....	54
Figure 4.3: Twelve DOF Engine-Swingarm Layout.....	55
Figure 4.4: Mount System Layout .....	63

Figure 4.5: Mode Shapes for the Optimized Configuration (6 DOF Model) .....	64
Figure 4.6: Mode Shapes - 1 to 6 (12 DOF Model – Shaking Load only) .....	69
Figure 4.7: Mode Shapes - 7 to 12 (12 DOF Model – Shaking Load only) .....	70
Figure 4.8: Road Profile.....	72
Figure 4.9: Mode Shapes - 1 to 6 (12 DOF Model – Combined Loading).....	73
Figure 4.10: Mode Shapes - 7 to 12 (12 DOF Model – Combined Loading).....	73
Figure 4.11: Schematic diagram of equipment supported by inclined isolators.....	76
Figure 4.12: Mount Arrangement .....	77
Figure 4.13: Decoupled Modes Along with the Associated Natural Frequency .....	78
Figure 4.14: Decoupled Modes and the Corresponding Frequencies (Case I) .....	84
Figure 4.15: Decoupled Modes and the Corresponding Frequencies (Case II) .....	84
Figure 4.16: Decoupled Modes and the Corresponding Frequencies (Case III).....	85
Figure 5.1: Slider Crank Mechanism .....	89
Figure 5.2: V-twin Engine Configuration.....	92
Figure 5.3: Free Body Diagram of the Piston .....	96
Figure 5.4: Shaking Force in the x and y Directions (800 rpm) .....	99
Figure 5.5: Shaking Force in the x and y Directions (3000 rpm) .....	99
Figure 5.6: Shaking Force in the x and y Directions (5000 rpm) .....	100
Figure 5.7: Shaking Torque (800 rpm) .....	100
Figure 5.8: Shaking Torque (3000 rpm) .....	101
Figure 5.9: Shaking Torque (5000 rpm) .....	101
Figure 5.10: Road Profile #1.....	107
Figure 5.11: Magnitude Plot of the Spectrum for Road Profile #1.....	107

Figure 5.12: Reconstructed Time Plot for Road Profile #1 .....	108
Figure 5.13: Road Profile #2.....	109
Figure 5.14: Magnitude Plot of the Spectrum of Road Profile #2 .....	109
Figure 5.15: Reconstructed Time Plot for Road Profile #2 .....	110
Figure 6.1: Mount Geometry .....	115
Figure 6.2: Solid 186 Element (ANSYS, 2009) .....	116
Figure 6.3: Isometric View Showing the Boundary Conditions.....	116
Figure 6.4: Front View Showing the Boundary Conditions .....	117
Figure 6.5: Isometric View Showing the Constraint Equation.....	117
Figure 6.6: Front View Showing the Constraint Equation .....	118
Figure 6.7: Isometric View of the Initial Geometry .....	123
Figure 6.8: Front View of the Initial Geometry .....	123
Figure 6.9: Isometric View of the Optimized Geometry (Example I).....	124
Figure 6.10: Front View of the Optimized Geometry (Example I) .....	124
Figure 6.11: Design Variables Vectors Vs. Steady State Speed .....	125
Figure 6.12: Isometric View of the Optimized Geometry (Example II).....	127
Figure 6.13: Front View of the Optimized Geometry (Example II).....	128

## LIST OF TABLES

Table 3.1: Computed Parameters for the Four Models.....	41
Table 4.1: Bounds for Design Variables.....	64
Table 4.2: Inertia Tensor of Powertrain Assembly.....	64
Table 4.3: Optimization Results (6 DOF Model) .....	65
Table 4.4: Optimization Results for Position and Orientation (6 DOF Model).....	65
Table 4.5: Inertia Tensor of the Swing-arm Assembly.....	68
Table 4.6: Optimization Results (12 DOF Model – Shaking Load only).....	68
Table 4.7: Optimization Results for Position and Orientation (12 DOF Model – Shaking Load only).....	69
Table 4.8: Optimization Results (12 DOF Model – Combined Loading) .....	71
Table 4.9: Optimization Results for location and Orientation (12 DOF Model – Combined Loading) .....	72
Table 4.10: Stiffness Values and the Distance.....	77
Table 4.11: Inertia Tensor for the Engine.....	80
Table 4.12: Initial Guess of the Mount Locations in (m) .....	80
Table 4.13: Initial Guess of the Mount Orientations (deg.).....	81
Table 4.14: Initial Guess of the Mount Stiffness (N/m) .....	81
Table 4.15: Optimum Mount Stiffness (Case I).....	81
Table 4.16: Stiffness Matrix Showing Off-Diagonal Terms (Case I).....	82
Table 4.17: Optimum Mount Stiffness (Case II) .....	82
Table 4.18: Stiffness Matrix Showing Off-Diagonal Terms (Case II) .....	82
Table 4.19: Optimum Mount Stiffness (Case III).....	83

Table 4.20: Stiffness Matrix Showing Off-Diagonal Terms (Case III) .....	83
Table 5.1: Shaking Force Vector at Different Speeds .....	102
Table 5.2: Optimization Results for the Shaking Force Vector Corresponding to 800 rpm .....	102
Table 5.3: Optimization Results for the Shaking Force Vector Corresponding to 3000 rpm .....	102
Table 5.4: Optimization Results for the Shaking Force Vector Corresponding to 5000 rpm .....	103
Table 5.5: Optimization Results for Road Profile #1 .....	110
Table 5.6: Optimization Results for location and Orientation (Profile #1) .....	111
Table 5.7: : Optimization Results for Road Profile #2 .....	111
Table 5.8: Optimization Results for location and Orientation (Profile #2) .....	112
Table 6.1: Parameter Optimization Results .....	125
Table 6.2: Design Variables Vector Corresponding to different Steady State Speeds...	126
Table 6.3: Transmitted Loads at Different Operating Speeds .....	126
Table 6.4: Parameter Optimization Results .....	128

## Chapter 1 - Introduction

The mounting system is the primary interface between the powertrain and the frame; therefore, it's vital to the determination of the vibration isolation characteristics. Different types of engine mount are presented in this chapter, but the only engine mount that will be used in the work herein are the elastomeric mounts. The elastomeric mounts are made of rubber which withstands large amount of deformation under loads with the ability to almost retain its original shape when the load is removed. This is due to the inherent material property of rubber. Rubber is a viscoelastic material which enables it to be used as an isolator and as a damper.

### *1.1 Introduction*

There are two major problems that engineers must deal with when it comes to vibration isolation. The first problem is force isolation, which is frequently encountered in rotating or reciprocating machinery with unbalanced masses. The main objective in this problem is to minimize the force transmitted from the machine to the supporting foundation. The second problem is motion isolation. In this case, we are interested in minimizing the transmitted vibration amplitude such that the mounted equipment is shielded from vibrations coming from the supporting structure. This is broadly achieved by mounting equipment on a resilient support or an isolator such that the natural frequency of the equipment-support system is lower than the frequency of the incoming vibrations to be isolated.



## *1.2 Vibration Isolation*

Vibration isolation can be simply defined as isolating an object from the source of vibration. In order for this objective to be achieved, isolators must be used. There are two major types of isolation. The first type is the passive isolation in which passive techniques such as rubber pads or mechanical springs are used. The isolation is achieved by limiting the ability of vibrations to be coupled to the structure being isolated. This is done using a mechanical connection which dissipates or redirects the energy of vibration before it gets to the structure to be isolated. Passive methods sometimes involve electromechanical controls for adjusting the system, but the isolation mechanism is passive. Passive systems are cost effective and their relative simplicity makes them more reliable and safe. Elastomers which are used in the automotive industry to isolate the engines are one of the most widely used passive isolators.

The second type of isolation is active isolation which contains along with the spring, a feedback circuit which consists of a sensor such as a piezoelectric accelerometer, a controller and an electromagnetic transducer. The acceleration (vibration) signal is processed by a control circuit in which is feed to the electromagnetic actuator which amplifies the signal. As a result of such a feedback system, a considerably stronger suppression of vibration is achieved compared to the ordinary damping. Most active vibration isolation systems are relatively complex, costly, and often provide only marginal improvements in performance compared with conventional passive vibration isolation techniques. They are also more difficult to set up, and their support electronics often require adjustment. Nonetheless, active systems can provide function which is simply not possible with purely passive systems. However, due to their cost

effectiveness, reliability and relative simplicity passive isolators will be used in the design of the mounting system throughout this study.

### *1.3 Engine Mounts*

To achieve the best vibration isolation for the powertrain, a mounting system is used to mount the powertrain in place. The mounting system will provide isolation that will in turn minimize the transmitted forces to/from the engine to the frame. On the other hand, it will also prevent engine bounce caused from shock excitation. This goal is achieved by making the dynamic stiffness and damping of the mounting system frequency and amplitude dependent. Three different types of engine mount systems are listed below:

#### *1.3.1 Elastomeric Mounts*

Elastomeric mounts, which are made of rubber, have been used to isolate engines since 1930s. A lot of changes have been made over the years to improve the performance of the elastomeric mounts. For proper vibration isolation, elastomeric mounts are designed for the necessary elastic stiffness rate characteristics in all directions. They are maintenance free, cost effective and compact. The elastomeric mounts can be represented by a Voigt model which consists of a spring and a viscous damping as shown in Fig. 1.1.

It is difficult to design a mounting system that satisfies a broad array of design requirements. A mount with high stiffness or high damping rates can yield low vibration transmission at low frequency, but its performance at high frequency might be poor. On the other hand, low stiffness and low damping will yield low noise levels but it will induce high vibration transmission. A compromise is needed to obtain balance between

engine isolation and engine bounce. In order to achieve low vibration transmissibility, the mount stiffness must be as low as possible. However, this causes increased static deflection. Lower damping is also desirable for lower transmissibility at higher frequency range. On the other hand, handling and maneuverability are enhanced with higher stiffness. Elastomeric mounts provide a trade-off between competing requirements of low static deflection and enhanced vibration isolation.

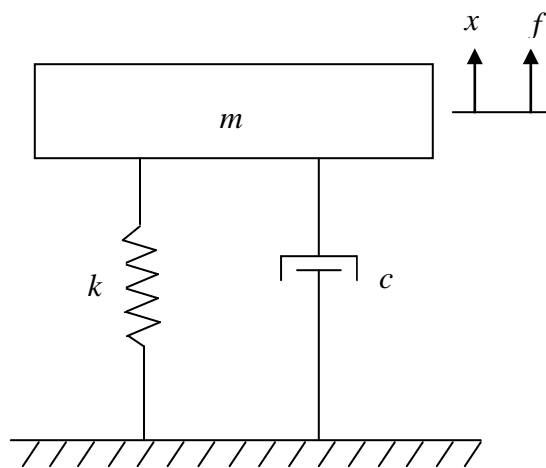


Figure 1.1: Mechanical Model for Elastomeric Mounts

### 1.3.2 Passive Hydraulic Mounts

Hydraulic mounts were first introduced in 1962 for use as vehicle mounting systems. Since then, their popularity has improved for two reasons. The first one is that the current vehicles tend to be small, lightweight and front wheel drive with low idle speeds. The second one is that the hydraulic mounts have developed into highly tunable devices. Three types of hydraulic mounts are in use these days and these are: hydraulic mount with simple orifice, hydraulic mount with inertia track, and hydraulic mount with inertia track and decoupler. A general schematic diagram of the hydraulic mount is

shown in Fig. 1.2. Although there are differences between orifice and inertia track mounts, all of them cause damping at low frequency ranges. These mounts can be tuned to have high damping at the shock excitation frequency which is used to reduce the vibration levels. The dynamic stiffness of these mounts is usually higher than that of the elastomeric mounts. Although the damping in these mount is high at low frequency, the isolation at higher frequencies is degraded. This problem is handled by adding a decoupler to the hydraulic mount which operates as amplitude limited floating piston. It allows the mount to behave like an elastomeric mount to provide good vibration isolation at large displacement. On the other hand, it allows it to behave like a normal hydraulic mount providing the damping for shock excitation.

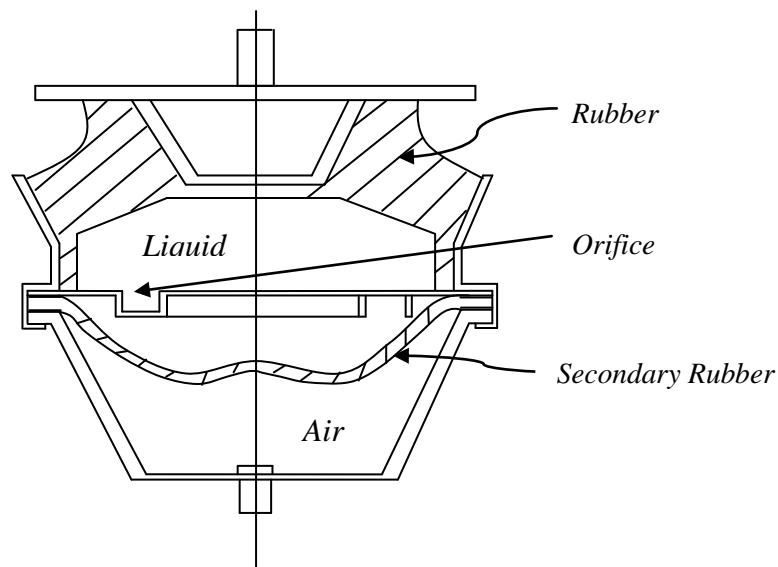


Figure 1.2: Simple Hydraulic Mount

### 1.3.3 Active Engine Mounts

In active vibration control, a counteracting dynamic force is created by one or more actuators in order to suppress the transmission of the system disturbance force. A general active mount consists of a passive mount (elastomeric or hydraulic), force

generating actuator, a structural vibration sensor and an electronic controller. The passive mount is used to support the structure in case of an actuator failure. The controller can either be feedback or feed forward. The vibration control is implemented with a closed loop controller that utilizes the sensor measurement. The mechanical models of elastomeric and hydraulic active mounts are shown in Fig. 1.3. The active mount stiffness is equivalent to the stiffness of the passive mount (elastomeric or hydraulic). The active mounts can overcome the limitations of passive mounts. Active elastomeric mounts can be very stiff at low frequencies and very soft at high frequencies. Meanwhile the active hydraulic mounts can be tuned to achieve adequate damping at engine bounce frequency and have very low dynamic stiffness at high frequency. Semi active mounts are used to improve the low frequency features of the system like increasing damping. By providing superior isolation, active engine mounts can allow large engine vibration levels. This may reduce balance shaft requirements and enable the vehicle chassis to be lighter.

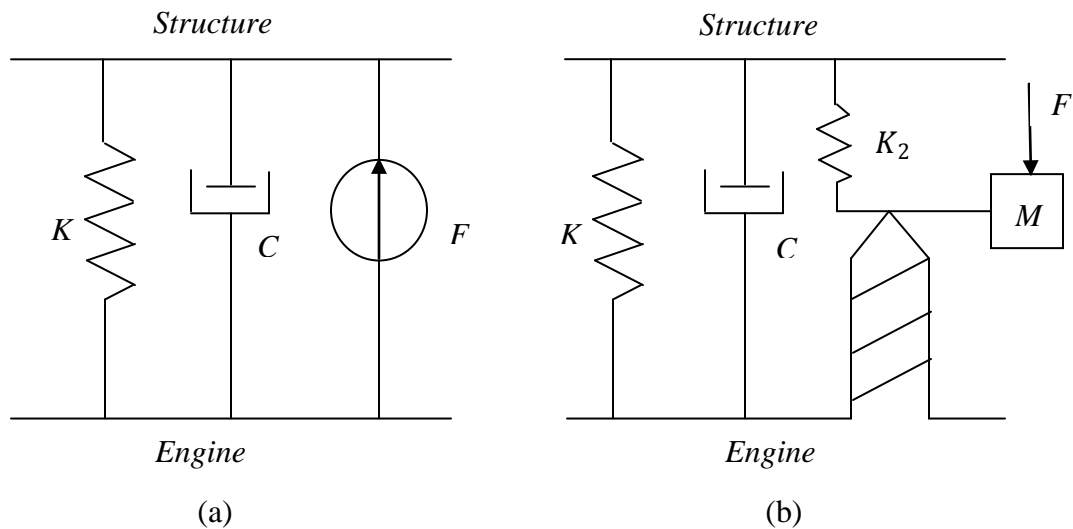


Figure 1.3: (a) Mechanical Model for Active Elastomeric Mount, (b) Mechanical Model for Active Hydraulic Mount.

### *1.4 Modeling of Engine Mounts*

A typical mounting system consists of powertrain and a number of mounts that connect the powertrain to the supporting frame. The major objective of the engine mount is to isolate the engine disturbances from being transferred to the supporting structure. These disturbances will excite the engine 6 DOF vibration modes shown in Fig. 1.4. For example, the torque caused by the firing pulse will cause engine pitch vibration. To isolate vibrations caused by engine unbalanced disturbances, low elastic stiffness as well as low damping are used since the transmitted forces depends on the values of the stiffness and damping of the mounts. The mounts are modeled as a spring and hysteresis damping or viscous damping along each of the three principal directions shown in Fig. 1.5. The mounts used herein are elastomeric mounts in which the stiffness, orientation and location are the main variables that need to be determined in order to achieve the desired isolation. This type of engine mount is modeled as Voigt Model which is shown in Fig. 1.1. The frame is always modeled as a rigid body thorough out this dissertation.

The natural frequency of the mounting system should be lower than the engine disturbance frequency to avoid the excitation of the mounting system resonance. This will ensure a low transmissibility.

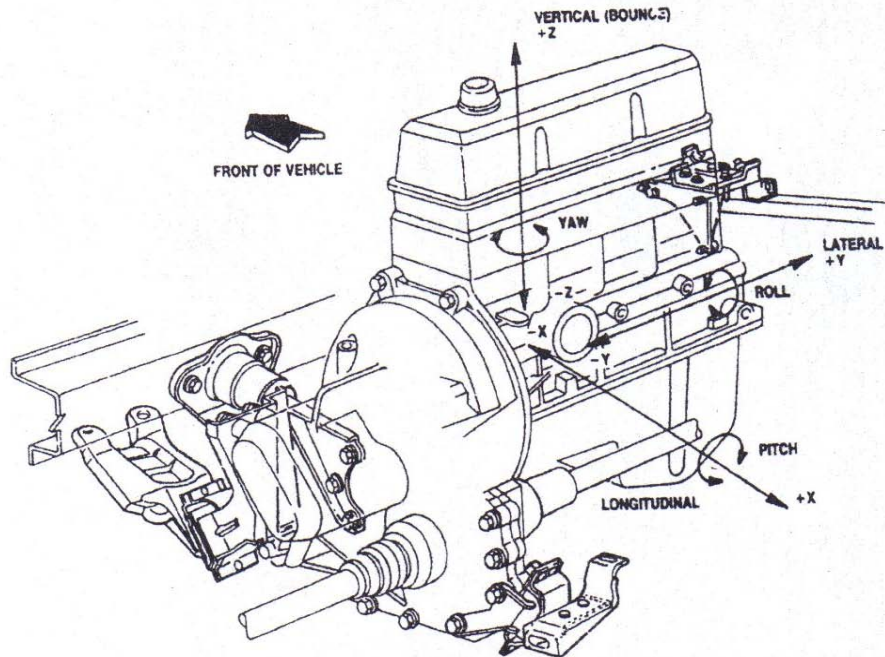


Figure 1.4: Engine Six DOF Modes (Ye, et. al. 2001)

Figure 1.4, shows an engine and its six degrees of freedom that will be excited as result of the inertia forces acting on the its block and the oscillator torque acting about the crankshaft. Fig. 1.5, shows a typical engine mount alongside its tri-axial model consisting of a spring and damper along each principal direction.

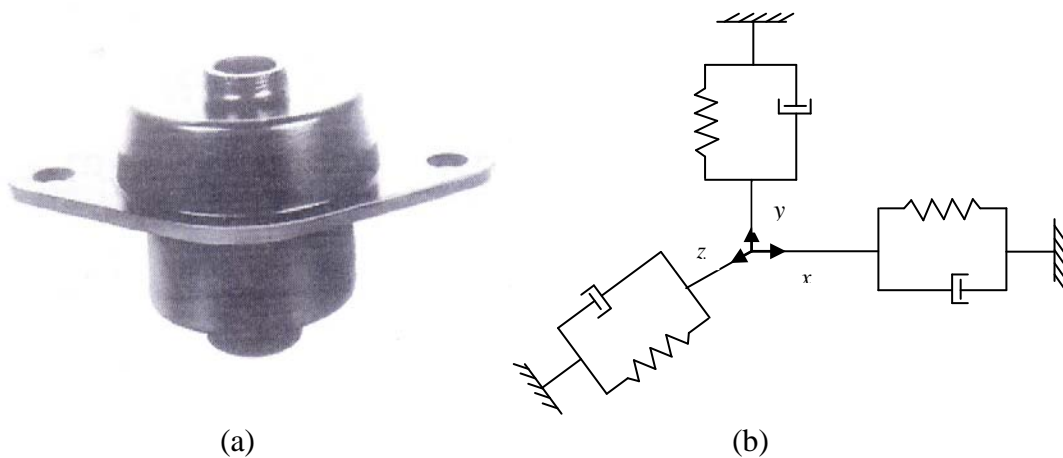


Figure 1.5: (a) Engine Mount, (b) Tri-Axial Engine Mount Model (Kaul, 2006)

### *1.5 Dissertation Objectives*

The emphasis in this work is to develop a complete mounting system such that the transmitted forces to/from the engine to the supporting frame are minimized. The loads can be described as external or internal. The external loads are due to external disturbances from the environment such as irregularities in the road profile and road bumps. These disturbances can be transmitted through the tire patch to the engine causing it to hit nearby components. The engine movement needs to be constrained due to packaging space limitations surrounding the engine. In order to do so, these transmitted external loads must be minimized by the use of the mounting system. Once the mounting system is defined and the transmitted loads are minimized, the focus is switched to the balancing masses inside the engine. This is done to minimize the internal loads. The loads that need to be minimized are the loads due to the shaking force resulting from the rotating unbalance due to eccentric masses. Material imperfections, faulty assembly and machining inaccuracy are among other factors that will cause eccentric masses. This will introduce an offset between the center of gravity and the axis of rotation leading to unbalanced forces. These forces, which vary in magnitude and direction, can be eliminated by introducing a counter force that eliminates the effect of the original unbalanced force.

In order to minimize the transmitted external loads to the engine, we first need good load estimates. The technique used herein is to estimate the force transmitted through the tire patch for different load profiles. The next step after defining the external transmitted loads is to design the mounting system. Two different performance metrics will be used to solve this problem. The first one involves decoupling the vibration modes



through minimizing the off-diagonal terms of the global stiffness matrix. This insures that only the diagonal terms in the stiffness matrix are dominant, which leads to clean decoupled modes. The second method deals with minimizing the transmitted loads. Several alternate mount models will be explored. These include the Voigt model, Maxwell Voigt model, Voigt model with a Bouc-Wen element and Voigt model with Bouc-Wen element and a variable stiffness. All of these models will have a component that represents mechanical snubbing. Mechanical snubber is used to absorb large amount of energy within small displacement amplitudes. In order to capture the hysteretic behavior over large range of operating frequencies, a Bouc-Wen model is added.

After fully defining the mounting system, as a final step, an optimum geometrical shape of the mount will be determined using topology optimization.

## *1.6 Dissertation Organization*

This work has been divided into five main parts. Chapter two discusses the available literature on vibration isolation, vibration modes decoupling, mount design and shape optimization.

Chapters three and four present the work regarding mount modeling and design. These chapters provide the necessary mathematical modeling along with the equations of motion for various mount models used in this work. Numerical examples utilizing experimental mount data are presented to demonstrate extraction of mount parameters from solution of an optimization problem.

Chapter five discusses the issue of the load transmitted from/into the engine and the balancing masses. All the mathematical formulation for the internal forces and moments are presented along with numerical examples. External loads imposed on the

system due to irregularities in the road profile are discussed and different road profiles are analyzed. This road profile information is used to determine the force transmitted the tire patch in the vehicle.

Chapter six discusses mount shape optimization problem providing examples that ties it to the mount modeling and design discussed in the previous chapters showing the effect of different engine operating speeds on the final mount shape. A nonlinear finite element analysis is performed to determine the optimum mount shape.

Chapter seven summarizes the main results and conclusion of the dissertation and provides an outline for possible future work.

## Chapter 2 – Literature Review

Over the years, much work has been done in the area of vibration isolation. Throughout this thesis, the focus is on vibration isolation through the use of a mounting system. There are various methods that have been used to minimize vibration transmitted to and from the engine. Among these techniques, mount system optimization stands out. The mount optimization problem typically involves finding the optimum stiffness, orientation and location of the mounting system that will result in the best possible vibration isolation. Once the necessary mount characteristics are known, the problem of finding the optimum geometrical shape of the engine mount is also considered in this thesis.

### 2.1 *Vibration Isolation*

Spiekermann, et al. (1985) discussed the issue of minimizing forces that are transmitted through the mounting system. These forces can be caused as a result of rotational imbalance and reciprocating masses. The authors argue that in the case of small damping and frequencies below the natural frequency, the force transmitted through the mounts is proportional to the mount stiffness. Nevertheless, when the excitation frequency is near the rigid body natural frequency, the rigid body displacement and the transmitted forces may be large. The procedure used in the optimization technique is removing the natural frequencies from the undesired range and keeping the others. This is done by using an objective function in the optimization procedure that penalizes the natural frequencies in the undesired range without affecting other design parameters. For simulation purposes, a three dimensional rigid body is used. The rigid body consists of

six degrees of freedom (DOF) that includes three translational DOF and three rotational DOF.

Ford (1985) presents a design procedure for the front wheel drive engine idle isolation. In this procedure, a six degree of freedom lumped system is used to represent engine mounts. Then decoupling the highest five natural frequencies from the idle torque pulse direction is achieved. The baseline mounting system and the decoupled mounting system are tested on a three cylinder engine with similar inertia properties to the four cylinder engine. The main disturbance at the idle is the crankshaft torque vibration caused as a result of the gas pressure firing pulse. The approach is to decouple the torque generated by gas pressure pulse from five of six powertrain rigid body modes. This is done by introducing an objective function which is the sum of the square of the roll component in modes two through six.

Sui (2003) emphasized on the role of mounts in achieving better vehicle handling characteristics and rider comfort as well as a resulting vibration caused by engine firing force and other sources. This is achieved only when there is a mounting system that exhibits decoupled vibration modes. In order to achieve decoupling, the following assumptions must be considered. The powertrain is infinitely rigid and mounted to the ground. The excitations are assumed to be of a harmonic or periodic nature with known frequencies and the resulting displacements are small. The author lays down some basic concepts that include the following definitions of different coordinate systems: the vehicle coordinate system, engine coordinate system, principal moment of inertia (MOI) coordinate system, torque roll axis coordinate system, elastic axes and elastic center and center of percussion.

## 2.2 *Vibration Modes Decoupling*

Six vibration modes will be generated for the engine mass since it possesses six degrees of freedom in 3-D space. Three of the modes are translational and three are rotational. Generally speaking, the shaking force will cause the engine to respond in six degrees of freedom. The work is done to decouple the modes or make the coupling weak. This technique will be used as one of the proposed methods to optimize the mounting system.

Timpner (1965) suggested different techniques to eliminate vibrations due to internal and external disturbances. In order to decouple the modes, the elastic center of the mounts must coincide with the center of gravity of the engine. As a result, the ideal locations of the mounts are inside the mass (engine) which is infeasible. Luckily, the mounts can be still placed outside the engine and still achieve the goal of having the elastic center and the center of gravity coincide. The author discusses three different engine mounts orientations. First: two equal mounts symmetrically located. Second: two equal mounts with axes normal to each other. Third: two vertical mounts with different rates

Liu (2003) presents a method used in the optimization design of engine mounts. The constraint problem is solved using some of the known parameters such as engine center of gravity, mount stiffness rates and mount location and/or orientation. The main objective of this work is decoupling vibration modes. This work is done using a computer code DynaMount. Generally speaking, it's hard to come up with a mount design that decouples vibration modes. However, there are few special cases in which vibration modes can be completely decoupled. Throughout the study, the author used two different

coordinate systems. The first one is the vehicle coordinate system which is located at the engine center of gravity, and the equation of motion of the system is written with respect to it. The second one is a local coordinate system used to describe the engine mount properties. A rotation matrix that relates the local coordinate system to the global coordinate system is used in this case. The mounts are considered to be cylinders with the top surface attached to the engine and the bottom surface attached to the vehicle. The origin of the local coordinate system is located at the center of the mount.

Jeong and Singh (2000) examined the issue of torque roll axis (TRA) decoupling for a multi-dimensional mounting system of an automotive engine and gear box. They consider only the rigid body modes of the powertrain and the chassis is considered to be rigid. Since pulsating torque of the multi cylinder engine is a major source of vibration, therefore a mathematical model of the engine mounting system necessary to understand the design issues.

Iwahara and Sakai (1999) discussed various possibilities to isolate the engine. The engine mount layout consists of four mounts supporting the engine. The three and five mount layouts among other layouts are also investigated. Eigen value analysis, frequency response and transient response are used to determine the best way to isolate the engine.

Derby (1973) presents two techniques for decoupling. The first one is locating the isolators symmetrically in the same plane with the center of gravity. The second one is locating the isolators symmetrically about a ring in which the center of gravity is higher than the center of the ring. The author presents the necessary condition to decouple the translational modes from the rotational modes as well as decoupling natural frequencies. The isolators are located at the corners of a plane rectangle and the center of the

equipment is located within the rectangle formed by the isolators. In the paper, it's assumed that the damping matrix is proportional to the stiffness matrix. Furthermore, it's assumed that the stiffness values for all isolators are equal. Finally, the center of gravity is located above the center of the rectangle pattern of the isolators which reduces the number of equation to only two instead of eight, and the number of parameters to five.

Akanda and Adulla (2005) studied a six cylinder four wheel drive vehicle. In such a vehicle, the powertrain includes engine, transmission and transfer case. The torque roll axis approach is used to decouple the modes and come up with the mounting system locations. The author suggests locating the mounts at the nodal points of the fundamental bending modes of the powertrain may reduce the transmitted forces to the body.

Bretl (1993) presents a new simulation method to design the mounting system. The author sets the goal to come up with a mounting system that minimizes the response regardless of the resulting rigid modes. The technique computes response sensitivity to determine changes to the mounting system that will result into a minimum response. The design variables are the mount location, stiffness and damping. The response sensitivities are used to construct a set of linear equations that represent the total difference in response between the target and computed as a summation of design variable changes. The updated factors are approximated to the design variables that are required to minimize response.

Courteille and Mortier (2005) present a new technique to find an optimized and robust solution for the mounting system. Multi objective algorithm (Pareto optimization) is used as a base to the multi objective robust optimization problem. The use of this technique enhances the vehicle isolation characteristics. The method focuses on the use

of the optimization to minimize the vibration due to pulsating torque of the crankshaft at idle speed without paying any attention to the unbalanced forces due to the forces of the engine pistons. Since there is no accurate definition of the vehicle at early stages of design process, the author uses a probability distribution of the system parameters. This leads to a random change of the system's parameters. In order to have a sound design for an engine mount that will perform the intended job in isolation, a good estimate of the loads acting on the structure is very important. Reviewed next are some methods that can be used to estimate the loads acting on the mount system.

### *2.3 Mount Modeling*

The first step in mount design is modeling of the mount itself. Simple Voigt model is frequently employed to model the mount. The model consists of a spring and a damper connected in parallel and supporting the isolated mass. While the Voigt model is sufficient in many applications, it cannot capture certain mount characteristics such as hysteresis behavior, mount snubbing when shock loading is present, nonlinearity in mount systems, etc.

Zhang and Richards (2006) presented a study of the dynamic analysis and parameter identification of a rubber isolator using Maxwell-Voigt model. In the study, they noticed the difference between the Voigt model which simply consists of a spring damper connected in parallel and the Maxwell-Voigt model which includes another spring and a damper connected in series the Maxwell model. The Voigt model does not accommodate the inertial effect of the fluid present in the system and it becomes invalid. The Maxwell-Voigt model is used instead. Voigt model and Maxwell-Voigt model are good enough when it comes to capturing the characteristics of isolators that are used in



applications that possesses small range of frequency and over small bands of displacements amplitudes. On the other hand, when it comes to applications where the isolators are used over a large operating frequency range, the above models may not be sufficient to capture the hysteretic behavior. In this case the hysteretic model based on Bouc-Wen model is used. Bouc-Wen model is a nonlinear model that has the capability of capturing the time dependency by introducing an additional state variable.

Ye and Wang (2007) conducted a study to estimate the Bouc-Wen model parameters. The proposed approach use particle swarm optimization (PSO) which is based on the movement and intelligence of swarms. The results of the PSO method are compared to the genetic algorithms (GAs) in terms of parameter accuracy. It is shown that higher quality solution and better computational efficiency can be achieved by using the PSO method.

Ikhouane, et al. (2006) focus on the fact that even if there is a good approximation of the true hysteresis modeled using the Bouc-Wen model, it may not keep significant physical properties which are inherent in the real data. The work in this paper presents a characterization of the different classes of Bouc-Wen models in terms of their bounded input bounded output stability and as a result reproducing the physical properties inherent in true systems that have been modeled.

## *2.4 Load Estimation*

Generally speaking, in order to accurately design any component, good estimate of the loads acting on the component is vital. The stresses induced in a component are a function of the loads applied. The accuracy of estimating the loads applied to the engine mount plays an important role in designing the mounting system and its components (i.e.

stiffness and damping). The major problem that arises is measuring the loads. The simplest way of estimating the loads is by a direct measure using load cells. In some cases, inserting load cells is almost impossible due the nature of the structure. Another approach which is recently attracting attention is treating the structure as a load transducer. In this technique, the measured strains on some parts of the structure can provide a history of the loads acting on it

Masroor and Zachary (1990) proposed a procedure to select the location of strain gauges on a structure. The procedure is valid for linear elastic static problems. It can accommodate both isotropic and nonisotropic materials. The procedure involves applying a unit load each time and collecting the corresponding strains. This will produces a matrix that contains the strain information at the candidate locations of the strain gauges. The selection of the final location of the strain gauges is determined by the best approximate solution (BAS) that minimizes the sum of the squared errors.

Wickham et al. (1995) presented a computational tool that uses the D-optimal design technique to find the location and orientation of the strain gauges. The tool insures a precise location of the selected strain gauges. This in return will insure an accurate load recovery.

Dhingra and Hunter (2003) proposed a technique that considers the whole structure as a load transducer. The technique is valid for both 2 dimensional and 3 dimensional structures as well. The procedure delivers the location as well as the orientation of the strain gauges to be used through the help of finite element software. The selection of the strain gauge locations and orientation is done by using optimization

technique. This is achieved by using the D-optimal design procedure which maximizes the determinant of the matrix ( $A^T A$ ).

While load estimation using strain gauges mounted on the structure is a promising approach, it is not used herein due to resources limitations. Instead, the approach adopted estimates external loads transmitted through the mount system by monitoring the road profile in contact with the tire patch.

## 2.5 *Shape Optimization*

Once the mount is designed, i.e. the stiffness and damping values of the mount are known, the next step is to translate these numerical values into physical mount. This involves determining geometrical dimensions of the mount such that it have desired stiffness and damping characteristics

Kim J. and Kim Heon (1997) conducted a study on bush (shear) type engine mount that is used frequently in the auto industry in order to come up with the optimum geometrical shape of the mount. The study is performed by utilizing nonlinear finite element commercial software. The main objective is to minimize the difference between a set of target stiffness values in the three principal directions obtained from dynamic analysis with the stiffness values in the same directions generated from the geometry of the mount. In this process, a set of variables that fully describes the mount are used as the design vector to be determined from the outcome of the optimization problem.

Ali, et al (2010) conducted a study reviewing the need to different types of constitutive modes for rubber like materials. Modeling of these Elastomers depends on the strain energy function. The selection of the proper rubber elastic material is essential.

The stress-strain response is required in order to define the hyperelastic material behavior.

Scharnhorst and Pain (1978) utilized the Reissner type variational principle to formulate a mixed finite element model of finite strain analysis for Mooney-Rivlin like materials. They have adopted an incremental and stationary Lagrangian formulation. The variables consist of incremental displacements and incremental hydrostatic and distortional stresses. Four node quadrilateral plane strain elements were used in this work to analyze the inflation of an infinitely long thick-walled cylinder subjected to internal pressure.

Swanson (1985) noted that a certain type of problems in which the finite compressibility of high elongation rubber like materials influence the stress distribution, as a result must be taken into consideration. They addressed the problem by introducing a new rubber elasticity model with finite compressibility and improved material representation.

## 2.6 *Summary*

A fair bit of work has been done in the area of mount system design and isolation. The primary goal is to achieve an enhanced performance when it comes to isolation. This is done by better understanding the isolator and its components. Mechanical snubbing is a major aspect that needs to be taken into consideration when designing any mounting system. This dissertation will address the snubbing problem in chapter 3. This will be done in the context of several alternate mount models.

In addition, the dissertation will also look into at the external loads transmitted from road bumps through the mount system. Two criteria are used for designing the

mounting system namely; minimizing the force transmitted through the mount system or designs the system to decouple the vibration modes. Finally, the geometrical shape of the engine mount will be determined at different engine operating speeds.

## Chapter 3 – Mount Characterization and Determination of Mount Parameters

This chapter discusses the basic idea of mount characterization. The process starts with load estimation. The loads are transmitted to the frame through the tire patch. Multiple models for the engine mounts are developed in this chapter. These models vary in complexity from a simple Voigt model to a complex Voigt model that incorporates nonlinear stiffness, mechanical snubbing and a Bouc-Wen element to capture mount hysteresis. The mount parameters are then identified by minimizing the difference between the theoretical transmitted forces and the experimentally measured forces. All the necessary equations of motion and the mathematical equations for the theoretical transmitted forces are developed in this chapter. An optimization problem is formulated to help determine the mount parameters.

### *3.1 Load Estimation*

A mounting system is mainly used to minimize vibrations and shaking forces from the engine from being passed on to the frame, and eventually to the passengers. Also, the mount system might serve another purpose such as minimizing the forces and vibrations due to road bumps from being transmitted to the powertrain. As a result, an important issue when designing a mounting system is figuring out the forces passing through the mount system that needs to be minimized.

The problem occurs when trying to estimate the forces being transmitted through the whole system. The forces can be measured directly by using load cells which might not be easy due to the nature of the structure. One method that can be used in the case of

loads being transmitted from the road bumps through the tire patch is modeling the input force as shown in Eq. 3.1.

$$F_y(t) = k x(t) + c \dot{x}(t) \quad (3.1)$$

In Eq. (3.1)  $F_y(t)$  is the forces transmitted in the y direction through the tire patch due to the displacement  $x(t)$  and velocity  $\dot{x}(t)$  caused by the change of the road profile as shown in Fig. 3.1.  $k$  and  $c$  are the stiffness and damping of the wheels and the suspension in the y direction.

An alternate approach for estimating the forces acting on the system is by treating the structure as a load transducer and by measuring the strains at some previously determined locations. In order to find the most appropriate location and orientation of the strain gauges to place on the structure, there is a need to perform finite element analysis. By knowing the proper location and orientation of the strain gauges, and the use of the principle of superposition, the loads acting on the structure can be determined. This procedure however is not considered in this work.

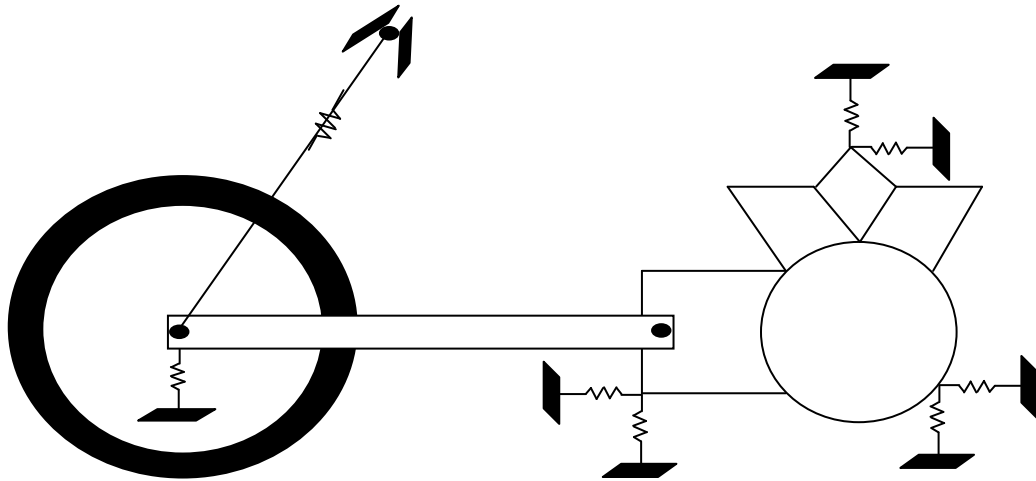


Figure 3.1: Schematic Diagram Showing the Tire Patch

### 3.2 Elastomeric Mount

Engine mounts that are used in automotive industry are primarily made of rubber. The rubber stiffness is categorized as either static or dynamic. In motorcycle or automotive industry, the sag of the powertrain due to the static weight is described using the static stiffness. On the other hand, the dynamic stiffness is used to determine the vibration isolation as a result of the application of a harmonic load. The dynamic stiffness varies with the amplitude and frequency of the applied load or the applied displacement. The relation that governs the static and the dynamic stiffness is as follows:

$$K_{dyn} = \eta K_{st} \quad (3.2)$$

In Eq. (3.2),  $\eta$  is the dynamic to static coefficient which is always greater than 1.  $K_{st}$  is the static stiffness and  $K_{dyn}$  is the dynamic stiffness. The dynamic to static coefficient varies with the input frequency leading to a higher coefficient with higher frequencies and as a result a higher dynamic stiffness.

The complex stiffness for an elastomer that is subjected to a sinusoidal displacement  $x_i(t)$  with an output force  $f_o(t)$  is the output force to the input displacement described as follows:

$$K^* = \frac{F_o^*}{X_i} = \frac{F_o}{X_i} \cos\delta + j \frac{F_o}{X_i} \sin\delta \quad (3.3)$$

The displacement  $x_i(t) = X_i e^{j\omega t}$  and the input force  $f_o(t) = F_o e^{j(\omega t + \delta)} = F_o^* e^{j\delta}$ , where  $F_o^* = F_o e^{j\omega t}$ .

In Eq. (3.3),  $X_i$  is the peak displacement amplitude,  $F_o$  is the peak force amplitude,  $\delta$  is the phase angle between the input displacement and the output force and  $\omega$  is the input frequency. Eq. (3.3) can be generally expressed as follows:



$$K^* = K' + jK'' \quad (3.4)$$

where,

$$K' = \frac{F_o}{X_i} \cos\delta \quad \text{and} \quad K'' = \frac{F_o}{X_i} \sin\delta \quad (3.5)$$

The elastomer dynamic stiffness  $K_{dyn}$  is the magnitude of  $K^*$ .

$$K_{dyn} = |K^*| = \sqrt{(K')^2 + (K'')^2} = \frac{F_o}{X_i} \quad (3.6)$$

The loss factor is defined as follows:

$$\beta = \tan\delta = \frac{K''}{K'} \quad (3.7)$$

The loss factor  $\beta$  is used to determine the damping or the hysteresis of the engine mount. Both the dynamic stiffness and the loss factor are critical parameters in the modeling of the engine mounts.

The engine mount is typically represented as three mutually orthogonal translational springs about the center of elasticity shown in Fig. 3.2. In Fig. 3.2, the coordinate system of the mount is also shown. It is assumed that the mount is attached to the rigid body by means of ball joints. This implies that the resilient element is incapable of applying a moment to the body it is attached to.

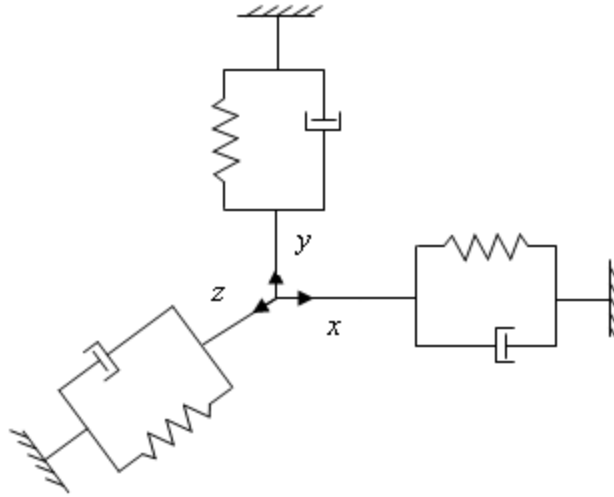


Figure 3.2: Tri-axial Engine Mount Model

### 3.3 Mount Modeling

The main component in designing a mounting system is the design of the mount itself. Identifying the mount parameters such as the mount stiffness and damping is a crucial step in the process of designing an appropriate mounting system. There are four candidate models that are used to represent the mounting system, all of which are assumed to be elastomeric isolators. The first model is the Voigt model shown in Fig. 3.3. This model is formulated using a spring and damper that are connected in parallel to a supporting mass. The second model is the Maxwell-Voigt model shown in Fig. 3.4. This model is formulated like the Voigt model and has an additional spring and a damper connected in series. The third model is the Voigt model with a Bouc-Wen element as shown in Fig. 3.5. This model is formulated like the first model with the addition of a Bouc-Wen element to capture mount hysteresis. The fourth Model is the Voigt Model with a Bouc-Wen element and nonlinear stiffness as shown in Fig. 3.6. This model is the same as the third model with one exception; the snubbing stiffness is modeled as a nonlinear spring.

All of the models presented next will have an element that represents mechanical snubbing. A mechanical snubber is used in mounts to absorb large amount of energy within small displacement amplitudes, and is modeled as a spring with linear stiffness for all of the models except for the last model where snubbing is modeled using spring that possesses a nonlinear stiffness. Mechanical snubbers are very important when it comes to designing an isolation system. It is used as a device to limit the motion of the mounting system when it undergoes overloading conditions.

### 3.3.1 Model 1 - Voigt Model

Fig. 3.3 shows the configuration of model 1. The model consists of a single degree of freedom system where the spring and damper are represented by the stiffness  $k_1$  and damping coefficient  $b_1$ . The snubbing effect is taken into account by adding additional two linear springs  $k_2$  and  $k_3$  that will be engaged when the displacement amplitude  $x$  of the isolated mass exceeds the snubbing gap  $x_o$ . The equations of motion for model 1 are as follows:

$$\begin{aligned}
 m\ddot{x} + b_1\dot{x} + k_1x &= f, \text{ for } |x| < x_o \\
 m\ddot{x} + b_1\dot{x} + (k_1 + k_2)x &= f + k_2x_o, \text{ for } x \geq x_o \\
 m\ddot{x} + b_1\dot{x} + (k_1 + k_3)x &= f - k_3x_o, \text{ for } x \leq -x_o
 \end{aligned} \tag{3.8}$$

In the equation above,  $m$  represents the mass of the isolated system and  $f$  is the excitation force acting on the system. The system of 2<sup>nd</sup> order linear differential equations in Eq. (3.8) can be converted into a system 1<sup>st</sup> order linear differential equations as follows:

$$\begin{bmatrix} \dot{x}_1 \\ \dot{x}_2 \end{bmatrix} = \begin{bmatrix} 0 & 1 \\ \frac{-k_1}{m} & \frac{-b_1}{m} \end{bmatrix} \begin{bmatrix} x_1 \\ x_2 \end{bmatrix} + \begin{bmatrix} 0 \\ \frac{f}{m} \end{bmatrix} \tag{3.9}$$

$$\begin{bmatrix} \dot{x}_1 \\ \dot{x}_2 \end{bmatrix} = \begin{bmatrix} 0 & 1 \\ \frac{-(k_1 + k_2)}{m} & \frac{-b}{m} \end{bmatrix} \begin{bmatrix} x_1 \\ x_2 \end{bmatrix} + \begin{bmatrix} 0 \\ \frac{f}{m} + \frac{k_2 x_o}{m} \end{bmatrix} \quad (3.10)$$

$$\begin{bmatrix} \dot{x}_1 \\ \dot{x}_2 \end{bmatrix} = \begin{bmatrix} 0 & 1 \\ \frac{-(k_1 + k_3)}{m} & \frac{-b}{m} \end{bmatrix} \begin{bmatrix} x_1 \\ x_2 \end{bmatrix} + \begin{bmatrix} 0 \\ \frac{f}{m} - \frac{k_3 x_o}{m} \end{bmatrix} \quad (3.11)$$

In the above equations,  $x_1 = x$  and  $x_2 = \dot{x}$ . Eq. (3.9) is the governing equation of motion for the system shown in Fig. 3.3 when  $|x| < x_o$ . Eq. (3.10) is the governing equation of motion when  $x \geq x_o$  and Eq. (3.11) is the governing equation of motion when  $x \leq -x_o$ . To accommodate varying stiffness in different directions of motion, the snubbing stiffness  $k_2$  and  $k_3$  is assumed to be asymmetrical. This assumption can be relaxed for symmetric systems by making the snubbing stiffness equal for both motion directions.

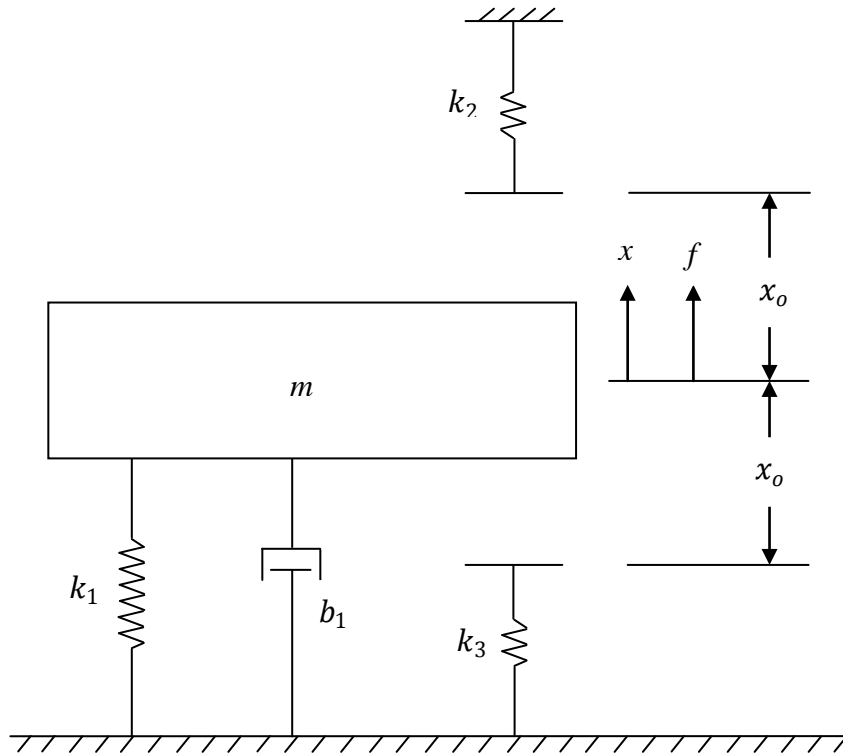


Figure 3.3: Voigt Model

### 3.3.2 Model 2 - Maxwell-Voigt Model

Fig. 3.4 shows the configuration of model 2. This model consists of a single degree of freedom system where the spring and damper are represented by stiffness  $k_1$  and damping  $b_1$  just like in model 1. However, there is an additional spring with stiffness  $k$  and a damper with damping coefficient  $b$  connected in series in reference to Maxwell-Voigt model. The snubbing effect is modeled just like the one presented in model 1. The equations of motion for the system shown in Fig. 3.4 are as follows:

$$\begin{bmatrix} m & 0 \\ 0 & 0 \end{bmatrix} \begin{bmatrix} \ddot{x} \\ \ddot{y} \end{bmatrix} + \begin{bmatrix} b_1 & 0 \\ 0 & b \end{bmatrix} \begin{bmatrix} \dot{x} \\ \dot{y} \end{bmatrix} + \begin{bmatrix} (k_1 + k) & -k \\ -k & k \end{bmatrix} \begin{bmatrix} x \\ y \end{bmatrix} = \begin{bmatrix} f \\ 0 \end{bmatrix} \quad (3.12)$$

$$\begin{bmatrix} m & 0 \\ 0 & 0 \end{bmatrix} \begin{bmatrix} \ddot{x} \\ \ddot{y} \end{bmatrix} + \begin{bmatrix} b_1 & 0 \\ 0 & b \end{bmatrix} \begin{bmatrix} \dot{x} \\ \dot{y} \end{bmatrix} + \begin{bmatrix} (k_1 + k_2 + k) & -k \\ -k & k \end{bmatrix} \begin{bmatrix} x \\ y \end{bmatrix} = \begin{bmatrix} f + k_2 x_o \\ 0 \end{bmatrix} \quad (3.13)$$

$$\begin{bmatrix} m & 0 \\ 0 & 0 \end{bmatrix} \begin{bmatrix} \ddot{x} \\ \ddot{y} \end{bmatrix} + \begin{bmatrix} b_1 & 0 \\ 0 & b \end{bmatrix} \begin{bmatrix} \dot{x} \\ \dot{y} \end{bmatrix} + \begin{bmatrix} (k_1 + k_3 + k) & -k \\ -k & k \end{bmatrix} \begin{bmatrix} x \\ y \end{bmatrix} = \begin{bmatrix} f - k_3 x_o \\ 0 \end{bmatrix} \quad (3.14)$$

In Eq. (3.12) through Eq. (3.14),  $k$  and  $b$  represents the stiffness and damping of the additional spring and the damper added to the Maxwell model as shown in Fig. 3.4. Eq. (3.12) through Eq. (3.14) can be expressed as system of 1<sup>st</sup> order differential equation as follows:

$$\begin{bmatrix} \dot{x}_1 \\ \dot{x}_2 \\ \dot{y} \end{bmatrix} = \begin{bmatrix} 0 & 1 & 0 \\ \frac{-(k + k_1)}{m} & -\frac{b_1}{m} & \frac{k}{m} \\ \frac{k}{m} & 0 & -\frac{k}{m} \end{bmatrix} \begin{bmatrix} x_1 \\ x_2 \\ y \end{bmatrix} + \begin{bmatrix} 0 \\ \frac{f}{m} \\ 0 \end{bmatrix} \quad (3.15)$$

$$\begin{bmatrix} \dot{x}_1 \\ \dot{x}_2 \\ \dot{y} \end{bmatrix} = \begin{bmatrix} 0 & 1 & 0 \\ \frac{-(k + k_1 + k_2)}{m} & -\frac{b_1}{m} & \frac{k}{m} \\ \frac{k}{m} & 0 & -\frac{k}{m} \end{bmatrix} \begin{bmatrix} x_1 \\ x_2 \\ y \end{bmatrix} + \begin{bmatrix} 0 \\ \frac{f}{m} + \frac{k_2}{m} x_o \\ 0 \end{bmatrix} \quad (3.16)$$

$$\begin{bmatrix} \dot{x}_1 \\ \dot{x}_2 \\ \dot{y} \end{bmatrix} = \begin{bmatrix} 0 & 1 & 0 \\ \frac{-(k + k_1 + k_3)}{m} & -\frac{b_1}{m} & \frac{k}{m} \\ \frac{k}{b} & 0 & -\frac{k}{b} \end{bmatrix} \begin{bmatrix} x_1 \\ x_2 \\ y \end{bmatrix} + \begin{bmatrix} 0 \\ \frac{f}{m} - \frac{k_3}{m} x_o \\ 0 \end{bmatrix} \quad (3.17)$$

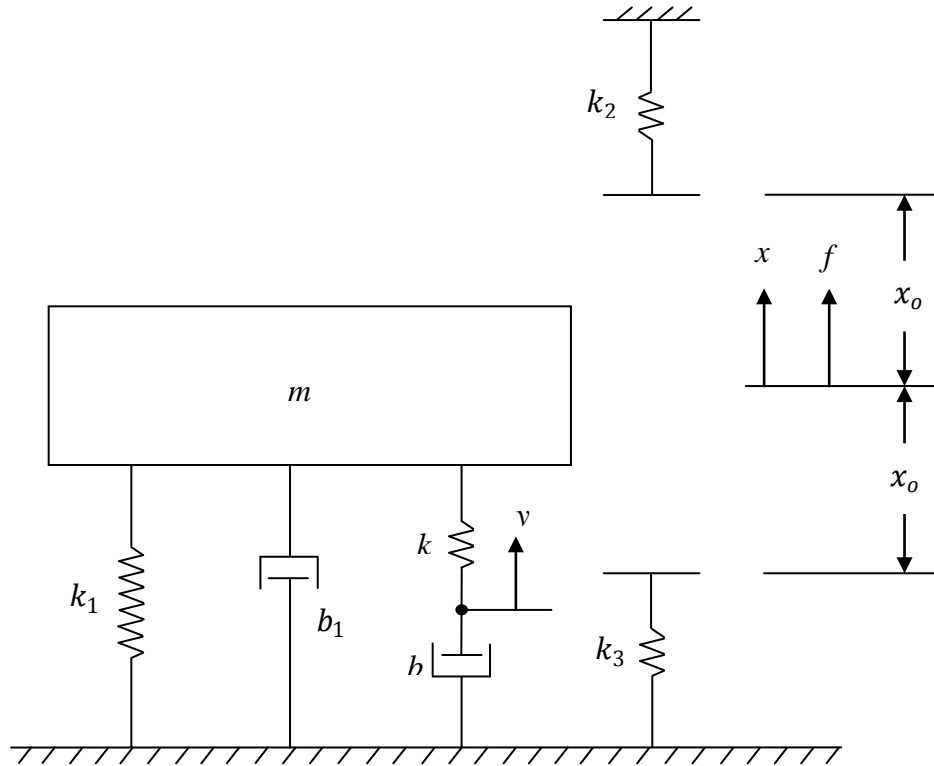


Figure 3.4: Maxwell-Voigt Model

### 3.3.3 Model 3 - Voigt Model with Bouc-Wen Element

Fig. 3.5 shows the configuration of model 3. This model is similar to model 1. In order to capture the hysteretic behavior over large range of operating frequencies, a Bouc-Wen element is added (Ikhouane, 2006). The Bouc-Wen element is a nonlinear element that is added to the model to capture the time dependence by adding the time dependent parameter ( $z$ ).  $\alpha, \beta, \gamma, A$  and  $n$  are the set of Bouc-Wen element parameters

that need to be defined. The model that incorporates the Bouc-Wen element is shown in Fig. 3.5 and can be expressed as a system 1<sup>st</sup> order differential equations as follows:

$$\begin{aligned}\dot{x}_1 &= x_2 \\ \dot{x}_2 &= -\frac{k_1}{m}x_1 - \frac{b_1}{m}x_2 - \frac{\alpha}{m}z + \frac{f}{m} \\ \dot{z} &= -\gamma|x_2|z|z|^{n-1} - \beta x_2|z|^n + Ax_2\end{aligned}\tag{3.18}$$

The nonlinear system shown above in Eq. (3.18) holds when there is no snubbing effect i.e.  $|x| < x_o$ .  $x_1 = x$  and  $x_2 = \dot{x}$ .  $\alpha, \beta, \gamma, A$  and  $n$  are constants referred to as Bouc-Wen parameters.  $z$  is the time varying constant introduced by Bouc-Wen element.

When  $x \geq x_o$ , the equations of motion (EOM) are as follows:

$$\begin{aligned}\dot{x}_1 &= x_2 \\ \dot{x}_2 &= -\frac{(k_1 + k_2)}{m}x_1 - \frac{b_1}{m}x_2 - \frac{\alpha}{m}z + \frac{f}{m} + \frac{k_2}{m}x_o \\ \dot{z} &= -\gamma|x_2|z|z|^{n-1} - \beta x_2|z|^n + Ax_2\end{aligned}\tag{3.19}$$

and finally when  $x \leq -x_o$ , the equations of motion (EOM) are as follows:

$$\begin{aligned}\dot{x}_1 &= x_2 \\ \dot{x}_2 &= -\frac{(k_1 + k_3)}{m}x_1 - \frac{b_1}{m}x_2 - \frac{\alpha}{m}z + \frac{f}{m} - \frac{k_3}{m}x_o \\ \dot{z} &= -\gamma|x_2|z|z|^{n-1} - \beta x_2|z|^n + Ax_2\end{aligned}\tag{3.20}$$

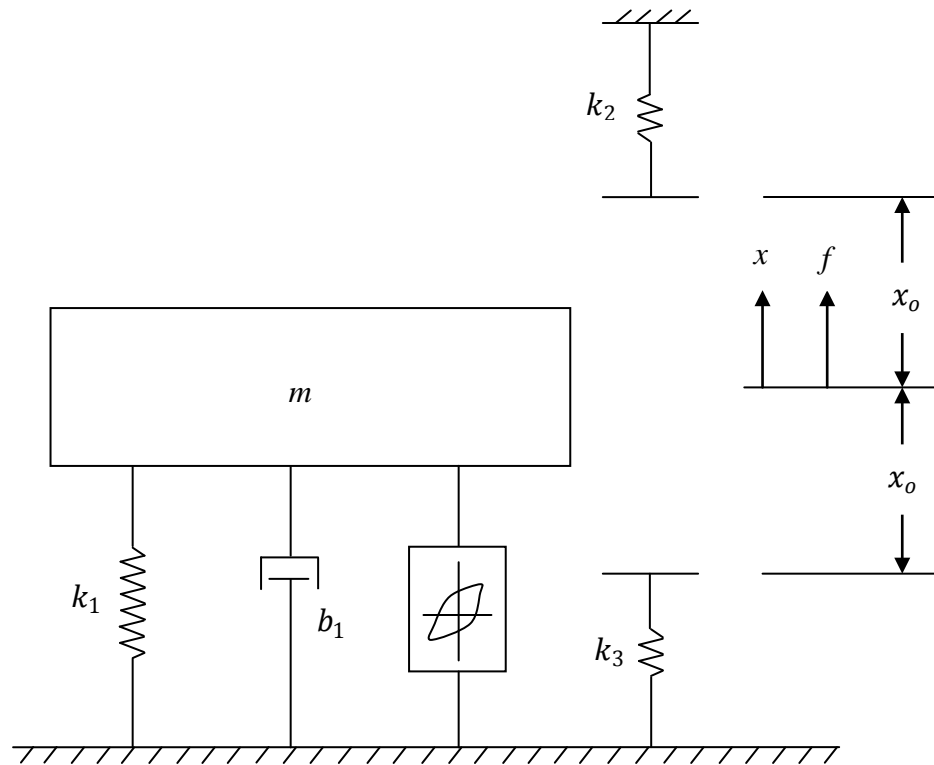


Figure 3.5: Voigt Model with Bouc-Wen Element

### 3.3.4 Model 4 - Voigt Model with Bouc-Wen Element and Nonlinear Stiffness

Fig. 3.6 shows the configuration of model 4. This model is modeled like model 3. However, in all of the models mentioned above, the snubbing is represented as a linear spring. In model 4, snubbing is represented by a nonlinear stiffness to capture the progressive stiffening behavior when the snubber is engaged. The governing EOM for model 4 are the same as defined in Eq. (3.18) when the snubber is not engaged i.e.  $|x| < x_0$ . When  $x \geq x_0$ , the EOM for the model are as follows:



$$\dot{x}_1 = x_2$$

$$\dot{x}_2 = -\frac{k_1}{m}x_1 - \frac{k_2}{m}(x_1 - x_o) - \frac{k_2}{m}(x_1 - x_o)^3 - \frac{b_1}{m}x_2 - \frac{\alpha}{m}z + \frac{f}{m} \quad (3.21)$$

$$\dot{z} = -\gamma|x_2|z|z|^{n-1} - \beta x_2|z|^n + Ax_2$$

In Eq. (3.21),  $k_2$  represents the snubber stiffness which is modeled as a cubic nonlinear relationship instead of the linear snubber stiffness used in the previous models.

The EOM of for  $x \leq x_o$  are as follows:

$$\dot{x}_1 = x_2$$

$$\dot{x}_2 = -\frac{k_1}{m}x_1 - \frac{k_3}{m}(x_1 + x_o) - \frac{k_3}{m}(x_1 + x_o)^3 - \frac{b_1}{m}x_2 - \frac{\alpha}{m}z + \frac{f}{m} \quad (3.22)$$

$$\dot{z} = -\gamma|x_2|z|z|^{n-1} - \beta x_2|z|^n + Ax_2$$

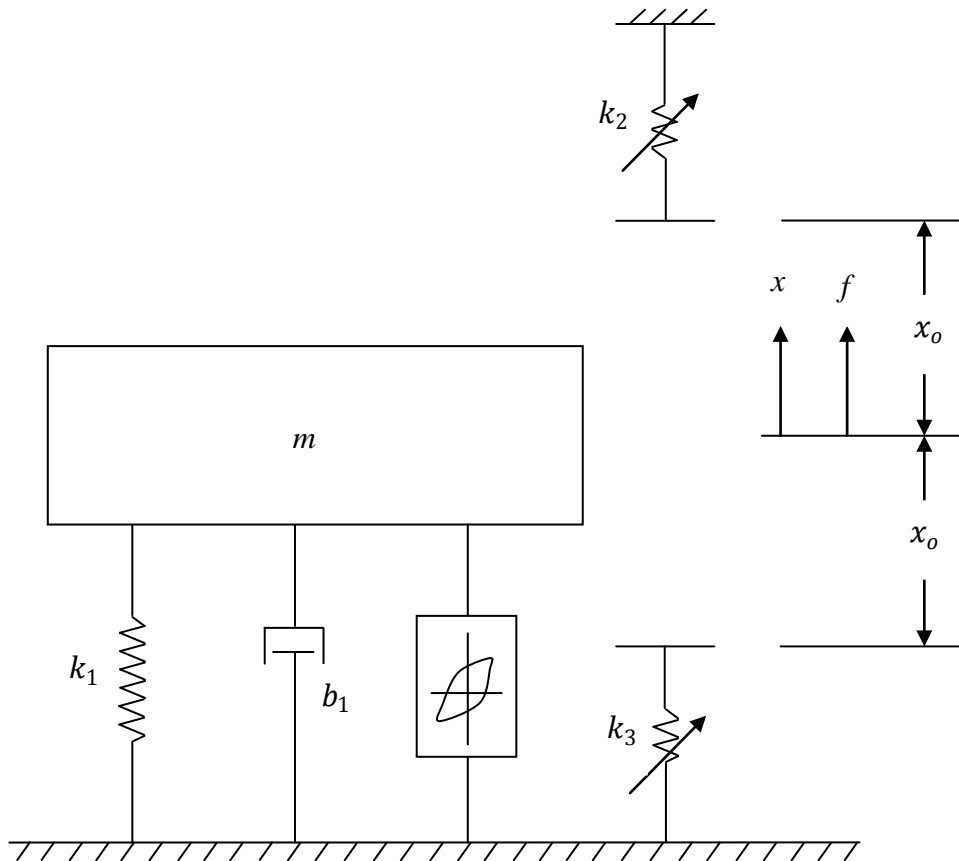


Figure 3.6: Voigt Model with Bouc-Wen Element and Nonlinear Stiffness

### 3.4 Parameter Identification

Parameter identification is used next to find the variables associated with each of the models presented in sections 3.3.1 to 3.3.4. An optimization procedure is used to determine the variables in each of the presented models. The solution technique involves finding the difference between the transmitted force computed from the theoretical models and the measured force. A time history of the measured forces transmitted to the base from a known excitation is used for model reconciliation.

The objective function for the parameter identification is defined as:

$$\|f_t - f_m\| \quad (3.23)$$

In Eq. (3.23),  $f_t$  is the time history of the transmitted force to the base calculated from the theoretical model and  $f_m$  is the time history of the measured force for a specified input. This solution technique works by minimizing the norm of the difference between the time history of the two forces, which results in finding the relevant parameters of the corresponding models. In the optimization problem, the only constraints are the side constraints which provide a limit for the design variables except for the models in section 3.3.3 and 3.3.4, where the presence of the constraints is necessary to limit the Bouc-Wen model parameters in order to insure bounded input bounded output response (Ikhouane, 2006). The Sequential Quadratic Programming (SQP) algorithm is used to the optimization problem. The ‘fmincon’ function in MATLAB<sup>®</sup> optimization toolbox is used to minimize the function in Eq. (3.23).

The force transmitted to the base for the Voigt model, defined in Fig. 3.3, is expressed as follows:

$$\begin{aligned}
f_t &= b_1\dot{x} + k_1x, \quad \text{for } |x| < x_o \\
f_t &= b_1\dot{x} + k_1x + k_2(x - x_o), \quad \text{for } x \geq x_o \\
f_t &= b_1\dot{x} + k_1x + k_3(x + x_o), \quad \text{for } x \leq -x_o
\end{aligned} \tag{3.24}$$

In Eq. (3.24),  $k_1, k_2, k_3$  and  $b_1$  are the system parameters that need to be determined from the parameter identification for the Voigt model.

The force transmitted to the base for the Maxwell-Voigt model, defined in Fig. 3.4, is expressed as follows:

$$\begin{aligned}
f_t &= b_1\dot{x} + k_1x + b\dot{y} \\
&= b_1\dot{x} + k_1x + k(x - y), \quad \text{for } |x| < x_o \\
f_t &= b_1\dot{x} + k_1x + b\dot{y} + k_2(x - x_o) \\
&= b_1\dot{x} + k_1x + k(x - y) + k_2(x - x_o), \quad \text{for } x \geq x_o \\
f_t &= b_1\dot{x} + k_1x + b\dot{y} + k_3(x + x_o) \\
&= b_1\dot{x} + k_1x + k(x - y) + k_3(x + x_o), \quad \text{for } x \leq -x_o
\end{aligned} \tag{3.25}$$

In Eq. (3.25),  $k_1, k_2, k_3, k, b_1$  and  $b$  are the system parameters that need to be determined from the parameter identification for the Maxwell-Voigt model.

The force transmitted to the base for the Voigt model with Bouc-Wen element, defined in Fig. 3.5 is expressed as follows:

$$\begin{aligned}
f_t &= b_1\dot{x} + k_1x + \alpha z, \quad \text{for } |x| < x_o \\
f_t &= b_1\dot{x} + k_1x + \alpha z + k_2(x - x_o), \quad \text{for } x \geq x_o \\
f_t &= b_1\dot{x} + k_1x + \alpha z + k_3(x + x_o), \quad \text{for } x \leq -x_o
\end{aligned} \tag{3.26}$$

In Eq. (3.26),  $k_1, k_2, k_3, b_1$  and  $\alpha$  need to be determined.  $z$  in the equation above is a time varying variable that comes as a result of using Bouc-Wen element which depends on the

parameters  $\beta, \gamma, n$  and  $A$  which need to be determined also for the Voigt model with Bouc-Wen element.

The force transmitted to the base for the Voigt model with Bouc-Wen element and nonlinear stiffness, defined in Fig. 3.6, is expressed as follows:

$$\begin{aligned}
 f_t &= b_1 \dot{x} + k_1 x + \alpha z, & \text{for } |x| < x_o \\
 f_t &= b_1 \dot{x} + k_1 x + \alpha z + k_2(x - x_o) + k_2(x - x_o)^3, & \text{for } x \geq x_o \\
 f_t &= b_1 \dot{x} + k_1 x + \alpha z + k_3(x + x_o) + k_3(x + x_o)^3, & \text{for } x \leq -x_o
 \end{aligned} \tag{3.27}$$

In Eq. (3.27),  $k_1, k_2, k_3, b_1$  and  $\alpha$  need to be determined.  $z$  which depends on  $\beta, \gamma, n$  and  $A$  are also need to be determined for the Voigt model with Bouc-Wen element and nonlinear stiffness.

### 3.4.1 Numerical example

To illustrate the parameter identification procedure, consider the following test situation. Experimental test results obtained from an elastomeric engine mount are used to find the mount parameters. The experimental force-displacement data was furnished by Dr. Kaul. The force-displacement data collected from the experiment is shown in Fig. 3.7. The data computed for the four models is shown in Table 3.1 and the results for the force-displacement relationship for the four models are shown in Figs. 3.8, 3.9, 3.10 and 3.11 respectively.

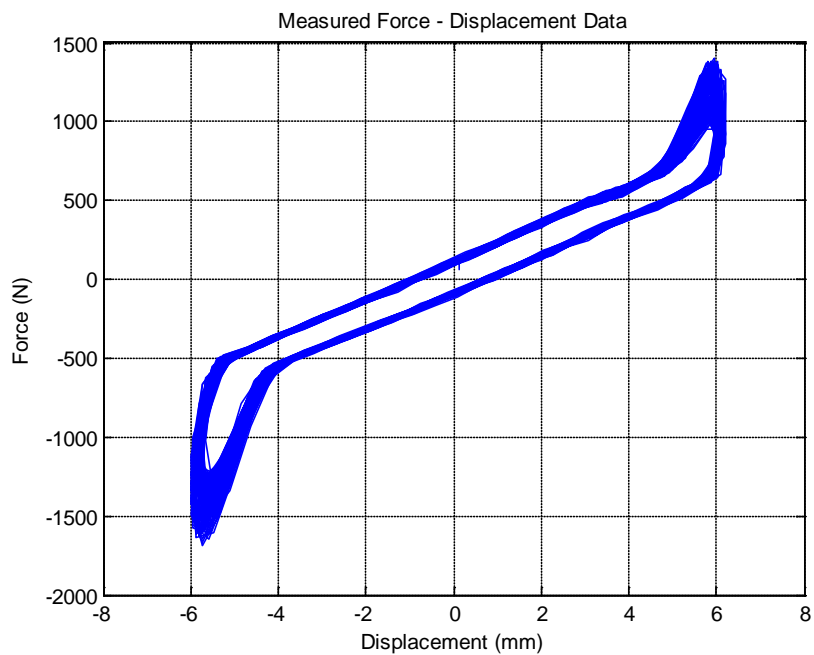


Figure 3.7: Measured Force – Displacement Curve.

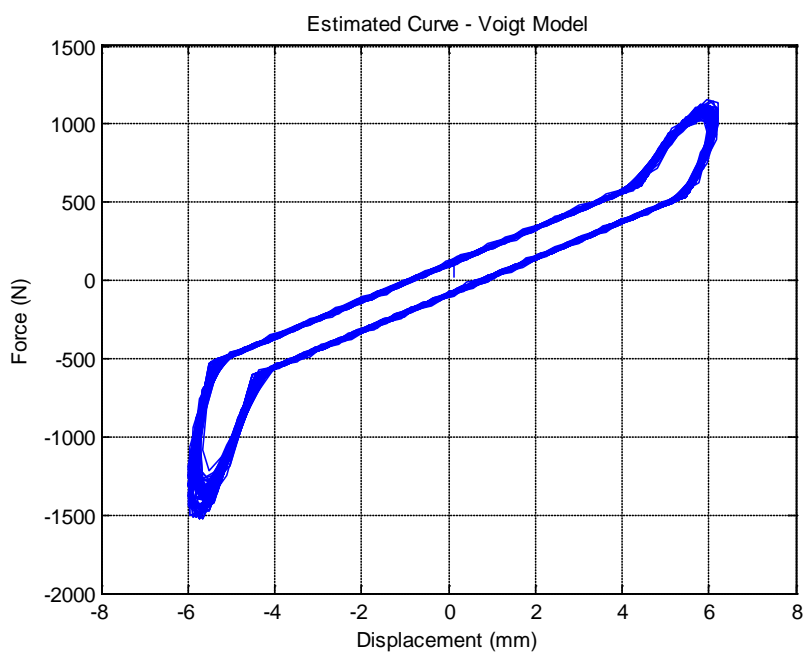


Figure 3.8: Force Displacement Curve (Voigt Model)

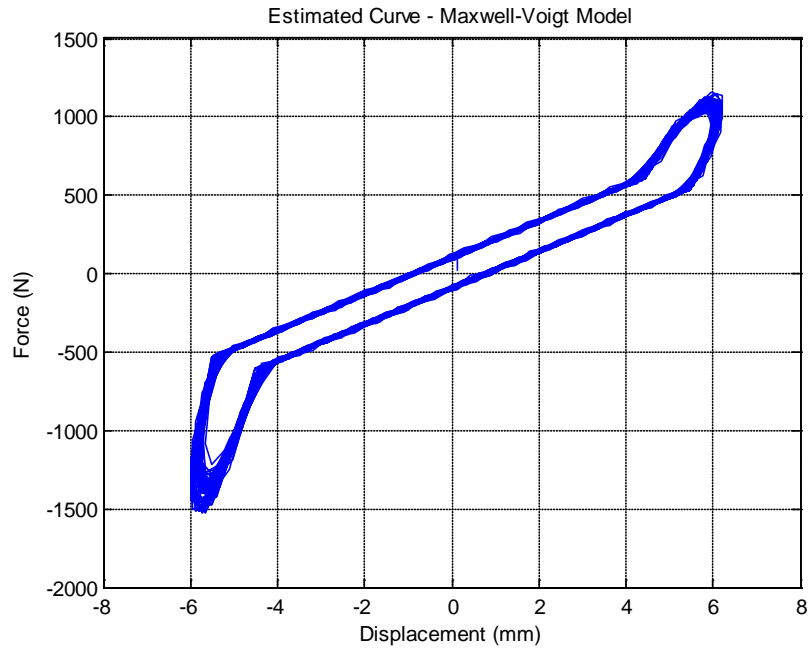


Figure 3.9: Force Displacement Curve (Maxwell-Voigt Model)

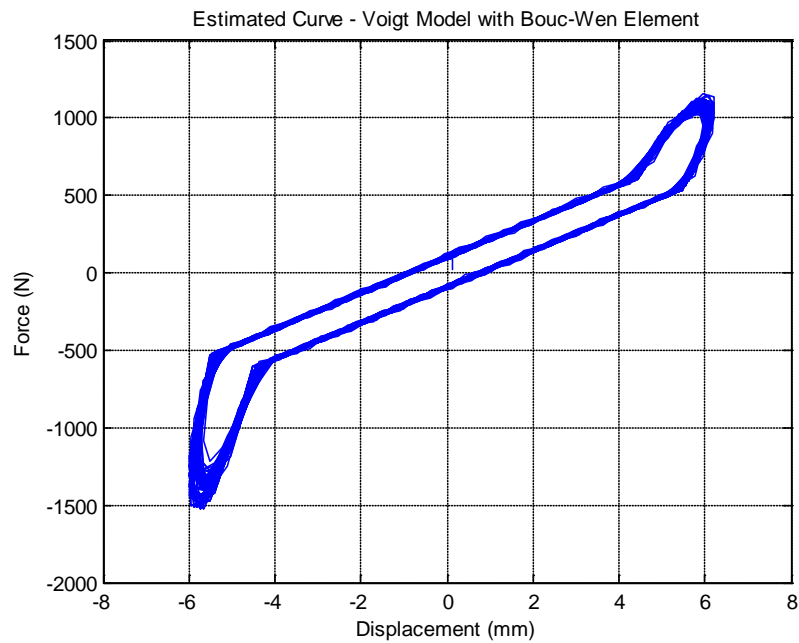


Figure 3.10: Force Displacement Curve (Voigt Model with Bouc-Wen Element)

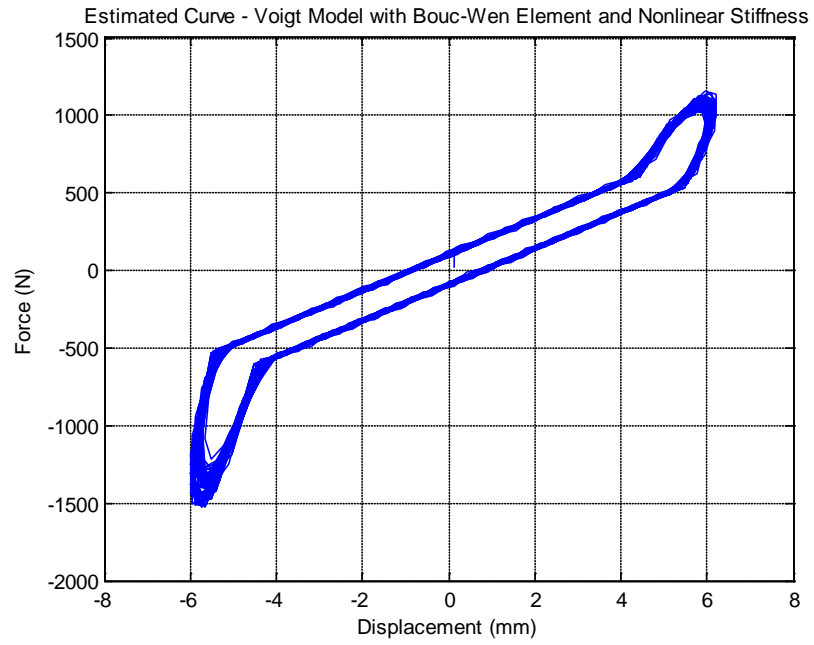


Figure 3.11: Force Displacement Curve (Voigt Model with Bouc-Wen Element and Nonlinear Stiffness)

Table 3.1: Computed Parameters for the Four Models

	Stiffness Parameters (N/mm)	Damping Parameters (N-s/mm)	Bouc-Wen Parameters	Optimized F
Model 1	$k_1 = 116.31$ $k_2 = 314.83$ $k_3 = 746.35$	$b_1 = 1.38$		5.44E+03
Model 2	$k_1 = 112.35$ $k_2 = 299.29$ $k_3 = 732.14$ $k = 45.18$	$b_1 = 0.001$ $b = 2.78$		5.82E+03
Model 3	$k_1 = 116.31$ $k_2 = 314.83$ $k_3 = 746.35$	$b_1 = 1.37$	$\alpha = 0.01$ $\beta = 0.48$ $\gamma = 1$ $n = 1.65$ $A = 1.1$	5.44E+03
Model 4	$k_1 = 118.76$ $k_2 = 154.31$ $k_3 = 429.62$	$b_1 = 1.36$	$\alpha = 0.01$ $\beta = 0.5$ $\gamma = 0.94$ $n = 1.42$ $A = 0.83$	4.81E+03



The parameters for the four models, based on the formulation presented in sections 3.3 and 3.4, are presented in Table 3.1. As can be seen from Table 3.1, the value for the isolation stiffness variable  $k_1$ , varies by 5% between the four models. The same can be said about  $b_1$ , except for the Maxwell-Voigt model, which overestimates damping. The force displacement plots that correspond to the four models are shown in Figs. 3.9 to 3.11. It can be seen that the closest correlation with the experimental plot is achieved in Fig. 3.11 which corresponds to the Voigt model with Bouc-Wen element and nonlinear stiffness. This result is achieved because this particular model is the most comprehensive model among the four models. This model contains a time varying Bouc-Wen element and a cubic relationship to model the transition in stiffness due to snubbing. The Voigt model with Bouc-Wen element shows similar results as the Voigt model with Bouc-Wen element and nonlinear stiffness since it uses a time varying Bouc-Wen element as well. But, it does not capture the transition in stiffness characteristics of the snubbing system. The Voigt model is the easiest model among all of the four models, although it might not be a good candidate if monitoring hysteresis and stiffness transition is the goal. It's best suited for application with little damping and snubbing application with low hysteresis and limited range of excitation frequency. With regards to using the Maxwell-Voigt model, there are no clear advantages in using it over the Voigt model. The Maxwell-Voigt model overestimates the damping as can be seen in Table 3.1.

### 3.5 *Summary*

In this chapter, mount characterization is discussed. The development of the equations of motion for the different mounting systems to characterize the mount and determine its parameters is presented herein. Four different models are proposed; the Voigt model, the Maxwell-Voigt model, Voigt model with Bouc-Wen element and Voigt model with Bouc-Wen element and nonlinear stiffness. In all of these models, mount parameters are identified by solving an optimization problem. The objective is to minimize the transmitted loads to the frame. The hysteresis loop for the four models is generated and compared to the hysteresis loop generated from the experimental data. It is seen that model 4 yields the best correlation with the experimental data.

## Chapter 4 – Mount Modeling and Design

This chapter provides the necessary mathematical equations needed to describe the mounting system. Two different models are formulated. The first one is a six degree of freedom model that treats the powertrain as a six DOF rigid body. The second model is a more elaborate twelve DOF model that treats the powertrain and the swing-arm as two 6 DOF rigid bodies. The main goal is to achieve an appropriate mounting system that fulfils the major task of vibration isolation. The models suggested above are used to formulate the optimization problem such that the mounting system stiffness, orientation and location are estimated. Several examples are provided based on the theoretical models presented herein.

### *4.1 Mathematical Modeling*

This section presents two different configurations of the engine mount system that is used in the motorcycle vibration isolation application. The first one is a six degree of freedom (DOF) model and the second one is a twelve DOF model. The equations of motion are developed for both models. For both models, an optimization problem is set up in order to solve for the engine mount characteristics by minimizing the transmitted loads to the frame due to engine excitation loads and road loads. As mentioned above, the optimization problem used the engine mount parameters i.e. stiffness, location and orientation as the design vector.

#### *4.1.1 Six DOF Model*

In this section, the equations of motion for a six DOF model which captures the engine dynamics are formulated. The model discussed in this section consists of a

powertrain that is treated as a six DOF rigid body. The powertrain assembly consists of the engine and the exhaust system connected to the frame via engine mounts. The powertrain assembly used herein is considered to be rigid; this assumption is used throughout this dissertation. The frame structure is also assumed to be infinitely rigid. Fig. 4.1 shows the layout that represents the model defined above where the powertrain is directly assembled to the frame at points (1, 2, 3) without being coupled to the swing-arm assembly. The swing-arm is attached to the frame below point 2.

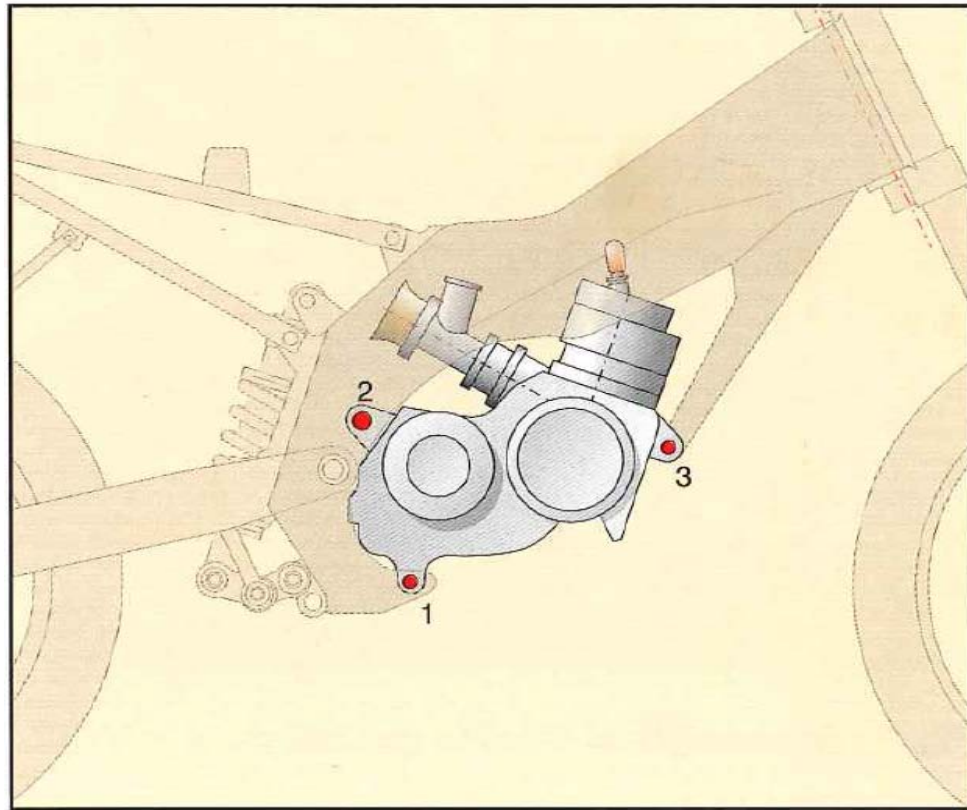


Figure 4.1: Six DOF Model (Cocco, 2001)

The equation of motion of the six DOF system defined above is given as follows:

$$M_e \ddot{X}_e + C_e \dot{X}_e + K_e X_e = F_e e^{j\omega t} \quad (4.1)$$

In Eq. (4.1),  $F_e$  denotes the input force vector which can be caused either by the shaking force due to engine imbalance or due to road load.  $M_e$ ,  $C_e$  and  $K_e$  are  $6 \times 6$  that represents

mass, damping and stiffness matrices respectively. The 6x1 vector  $F_e = [f_{xe} \ f_{ye} \ f_{ze} \ m_{xe} \ m_{ye} \ m_{ze}]^T$ , where the first three terms in the column vector represents the forces in the  $x$ ,  $y$ ,  $z$  directions and the last three terms represents the moments about the  $x$ ,  $y$ ,  $z$  axes. The terms of the generalized inertia matrix  $M_e$  of the powertrain are with respect of the global coordinate system. The 6x1 displacement vector  $X_e$ , consists of three translational  $x$ ,  $y$  and  $z$  and three rotational  $\alpha$ ,  $\beta$  and  $\gamma$  degrees of freedom of the powertrain.

$$X_e = [x \ y \ z \ \alpha \ \beta \ \gamma]^T$$

In order to account for different orientations of the mounts, the stiffness and damping are represented in the local coordinate system of the mount. A transformation matrix is used to express the stiffness and damping in the global coordinate system. The generalized mass matrix of the powertrain is as follows (Harris, 1961):

$$M_e = \begin{bmatrix} m_e & 0 & 0 & 0 & m_e z_e & -m_e y_e \\ 0 & m_e & 0 & -m_e z_e & 0 & m_e x_e \\ 0 & 0 & m_e & m_e y_e & -m_e x_e & 0 \\ 0 & -m_e z_e & m_e y_e & I_{xxe} & -I_{xye} & -I_{xze} \\ m_e z_e & 0 & -m_e x_e & -I_{xye} & I_{yye} & -I_{yze} \\ -m_e y_e & m_e x_e & 0 & -I_{xze} & -I_{yze} & I_{zze} \end{bmatrix} \quad (4.2)$$

In Eq. (4.2),  $m_e$  is the mass of the powertrain,  $(x_e, y_e, z_e)$  is the location of the center of gravity (C.G.) of the powertrain with respect to the origin of the global coordinate system,  $I_{xxe}, I_{yye}, I_{zze}, \dots$  are the inertia terms of the powertrain assembly with respect to the origin of the global coordinate system.

If the center of gravity of the powertrain coincides with the origin of the global coordinate system, the generalized mass matrix simplifies to the following form:

$$M_e = \begin{bmatrix} m_e & 0 & 0 & 0 & 0 & 0 \\ 0 & m_e & 0 & 0 & 0 & 0 \\ 0 & 0 & m_e & 0 & 0 & 0 \\ 0 & 0 & 0 & I_{xxe} & -I_{xye} & -I_{xze} \\ 0 & 0 & 0 & -I_{xye} & I_{yye} & -I_{yze} \\ 0 & 0 & 0 & -I_{xze} & -I_{yze} & I_{zze} \end{bmatrix} \quad (4.3)$$

The stiffness and damping matrices  $k_i^*$  and  $c_i^*$  of an individual mount 'i' expressed in its own local coordinate system is given as follows:

$$k_i^* = \begin{bmatrix} k_{xi} & 0 & 0 \\ 0 & k_{yi} & 0 \\ 0 & 0 & k_{zi} \end{bmatrix} \quad (4.4)$$

$$c_i^* = \begin{bmatrix} c_{xi} & 0 & 0 \\ 0 & c_{yi} & 0 \\ 0 & 0 & c_{zi} \end{bmatrix} \quad (4.5)$$

In Eq. (4.4),  $k_{xi}$ ,  $k_{yi}$ ,  $k_{zi}$  represents the stiffness of the engine mount 'i' in the  $x$ ,  $y$  and  $z$  directions respectively. In the above representation it is assumed that the engine mount is modeled about its center of elasticity which consists of three principal stiffness coefficients without any cross coupling influence. The same can be said about the damping matrix  $c_i^*$  represented in Eq. (4.5). A transformation matrix ( $A_i$ ) is used in order to transform both, the stiffness and damping matrices to the global coordinate system as follows:

$$k_i = A_i^T k_i^* A_i \quad (4.6)$$

$$c_i = A_i^T c_i^* A_i \quad (4.7)$$

$c_i$  and  $k_i$  in Eq. (4.6) and Eq. (4.7) respectively are the individual mount damping and stiffness matrices expressed in the global coordinate system. The matrix  $A_i$  is a transformation matrix which is a combination of three different rotations  $\theta_1, \theta_2$  and  $\theta_3$  about  $x$ ,  $y$  and  $z$  axes with respect to the global coordinate system shown in Eq. (4.8).

Hence, for the systems where the local and global coordinate systems coincide, the transformation matrix  $A_i$  is a 3x3 identity matrix.

$$A_i = \begin{bmatrix} C\theta_{2i}C\theta_{3i} & -C\theta_{1i}S\theta_{3i} + S\theta_{1i}S\theta_{2i}C\theta_{3i} & S\theta_{1i}S\theta_{3i} + C\theta_{1i}S\theta_{2i}C\theta_{3i} \\ C\theta_{2i}S\theta_{3i} & C\theta_{1i}C\theta_{3i} + S\theta_{1i}S\theta_{2i}S\theta_{3i} & -S\theta_{1i}C\theta_{3i} + C\theta_{1i}S\theta_{2i}S\theta_{3i} \\ -S\theta_{2i} & S\theta_{1i}C\theta_{2i} & C\theta_{1i}C\theta_{2i} \end{bmatrix} \quad (4.8)$$

where;  $C\theta_i = \cos(\theta_i)$  and  $S\theta_i = \sin(\theta_i)$ . Euler angles, Bryant angles, etc. can be used to calculate the transformation matrix  $A_i$  as well (Crede, 1965). Appendix A presents a detailed discussion of some alternate transformation matrix formulations.

The transformed damping and stiffness matrices are for the overall six DOF powertrain assembly is as follows:

$$C_e = \begin{bmatrix} C_{11} & C_{12} \\ C_{21} & C_{22} \end{bmatrix} \quad (4.9)$$

$$K_e = \begin{bmatrix} K_{11} & K_{12} \\ K_{21} & K_{22} \end{bmatrix} \quad (4.10)$$

where;

$$K_{11} = \sum k_i$$

$$K_{12} = -\sum k_i \tilde{r}_i, \quad K_{21} = K_{12} \quad (4.11)$$

$$K_{22} = -\sum \tilde{r}_i k_i \tilde{r}_i$$

$$C_{11} = \sum c_i$$

$$C_{12} = -\sum c_i \tilde{r}_i, \quad C_{21} = C_{12} \quad (4.12)$$

$$C_{22} = -\sum \tilde{r}_i c_i \tilde{r}_i$$

$C_e$  and  $K_e$  represents the overall damping and stiffness matrices of the powertrain assembly shown in Eq. (4.9) and Eq. (4.12).  $\tilde{r}_i$  represents the skew-symmetric matrix that corresponds to an individual mount position  $(r_{xi}, r_{yi}, r_{zi})$  and it is given by:

$$\tilde{r}_i = \begin{bmatrix} 0 & -r_{zi} & r_{yi} \\ r_{zi} & 0 & -r_{xi} \\ -r_{yi} & r_{xi} & 0 \end{bmatrix} \quad (4.13)$$

For the powertrain assembly used herein, the connection of the infinitely rigid powertrain is done to an infinitely rigid frame through four engine mounts. The governing equations of motion (EOM) are expanded below. It is assumed that the global coordinate system is not located at the C.G. of the powertrain. The position vector from the origin to the C.G. of the powertrain assembly is  $(x_{be}, y_{be}, z_{be})$ .

$$\begin{aligned} m_e \ddot{x} + m_e z_{be} \ddot{\beta} + m_e y_{be} \ddot{\gamma} + (k_{x1} + k_{x2} + k_{x3} + k_{x4})x + \\ (k_{x1}r_{z1} + k_{x2}r_{z2} + k_{x3}r_{z3} + k_{x4}r_{z4})\beta - \\ (k_{x1}r_{y1} + k_{x2}r_{y2} + k_{x3}r_{y3} + k_{x4}r_{y4})\gamma = f_{xe} e^{j\omega t} \end{aligned} \quad (4.14)$$

$$\begin{aligned} m_e \ddot{y} - m_e z_{be} \ddot{z} + m_e x_{be} \ddot{\gamma} + (k_{y1} + k_{y2} + k_{y3} + k_{y4})y \\ - (k_{y1}r_{z1} + k_{y2}r_{z2} + k_{y3}r_{z3} + k_{y4}r_{z4})\alpha \\ + (k_{y1}r_{x1} + k_{y2}r_{x2} + k_{y3}r_{x3} + k_{y4}r_{x4})\gamma = f_{ye} e^{j\omega t} \end{aligned} \quad (4.15)$$

$$\begin{aligned} m_e \ddot{z} - m_e y_{be} \ddot{\alpha} + m_e x_{be} \ddot{\beta} + (k_{z1} + k_{z2} + k_{z3} + k_{z4})z \\ + (k_{z1}r_{y1} + k_{z2}r_{y2} + k_{z3}r_{y3} + k_{z4}r_{y4})\alpha \\ - (k_{z1}r_{x1} + k_{z2}r_{x2} + k_{z3}r_{x3} + k_{z4}r_{x4})\beta = f_{ze} e^{j\omega t} \end{aligned} \quad (4.16)$$



$$\begin{aligned}
& -m_e z_{be} \ddot{y} + m_e y_{be} \ddot{z} + I_{xxe} \ddot{\alpha} - I_{xye} \ddot{\beta} - I_{xze} \ddot{\gamma} \\
& - (k_{y1}r_{z1} + k_{y2}r_{z2} + k_{y3}r_{z3} + k_{y4}r_{z4})y \\
& + (k_{z1}r_{y1} + k_{z2}r_{y2} + k_{z3}r_{y3} + k_{z4}r_{y4})z \\
& + [(k_{y1}r_{z1}^2 + k_{z1}r_{y1}^2) + (k_{y2}r_{z2}^2 + k_{z2}r_{y2}^2) + (k_{y3}r_{z3}^2 + k_{z3}r_{y3}^2) \\
& + (k_{y4}r_{z4}^2 + k_{z4}r_{y4}^2)]\alpha \\
& - [(k_{z1}r_{x1}r_{y1}) + (k_{z2}r_{x2}r_{y2}) + (k_{z3}r_{x3}r_{y3}) + (k_{z4}r_{x4}r_{y4})]\beta \\
& - [(k_{y1}r_{x1}r_{z1}) + (k_{y2}r_{x2}r_{z2}) + (k_{y3}r_{x3}r_{z3}) + (k_{y4}r_{x4}r_{z4})]\gamma \\
& = m_{xe} e^{j\omega t} \tag{4.17}
\end{aligned}$$

$$\begin{aligned}
& m_e z_{be} \ddot{x} - m_e x_{be} \ddot{z} - I_{xye} \ddot{\alpha} + I_{yye} \ddot{\beta} - I_{yze} \ddot{\gamma} \\
& + (k_{x1}r_{z1} + k_{x2}r_{z2} + k_{x3}r_{z3} + k_{x4}r_{z4})x \\
& - (k_{z1}r_{x1} + k_{z2}r_{x2} + k_{z3}r_{x3} + k_{z4}r_{x4})z \\
& - [(k_{z1}r_{y1}r_{x1}) + (k_{z2}r_{y2}r_{x2}) + (k_{z3}r_{y3}r_{x3}) + (k_{z4}r_{y4}r_{x4})]\alpha \\
& + [(k_{x1}r_{z1}^2 + k_{z1}r_{x1}^2) + (k_{x2}r_{z2}^2 + k_{z2}r_{x2}^2) + (k_{x3}r_{z3}^2 + k_{z3}r_{x3}^2) \\
& + (k_{x4}r_{z4}^2 + k_{z4}r_{x4}^2)]\beta \\
& - [(k_{x1}r_{y1}r_{z1}) + (k_{x2}r_{y2}r_{z2}) + (k_{x3}r_{y3}r_{z3}) + (k_{x4}r_{y4}r_{z4})]\gamma \\
& = m_{ye} e^{j\omega t} \tag{4.18}
\end{aligned}$$

$$\begin{aligned}
& -m_e y_{be} \ddot{x} + m_e x_{be} \ddot{y} - I_{xze} \ddot{\alpha} - I_{yze} \ddot{\beta} + I_{zze} \ddot{\gamma} \\
& - (k_{x1}r_{y1} + k_{x2}r_{y2} + k_{x3}r_{y3} + k_{x4}r_{y4})x \\
& + (k_{y1}r_{x1} + k_{y2}r_{x2} + k_{y3}r_{x3} + k_{y4}r_{x4})y \\
& - [(k_{y1}r_{x1}r_{z1}) + (k_{y2}r_{x2}r_{z2}) + (k_{y3}r_{x3}r_{z3}) + (k_{y4}r_{x4}r_{z4})]\alpha \\
& - [(k_{x1}r_{y1}r_{z1}) + (k_{x2}r_{y2}r_{z2}) + (k_{x3}r_{y3}r_{z3}) + (k_{x4}r_{y4}r_{z4})]\beta \\
& + [(k_{x1}r_{y1}^2 + k_{y1}r_{x1}^2) + (k_{x2}r_{y2}^2 + k_{y2}r_{x2}^2) + (k_{x3}r_{y3}^2 + k_{y3}r_{x3}^2) \\
& + (k_{x4}r_{y4}^2 + k_{y4}r_{x4}^2)]\gamma = m_{ze} e^{j\omega t} \tag{4.19}
\end{aligned}$$

In the equations presented above, Eq. (4.14) to Eq. (4.19), the damping coefficients has been ignored in order to simplify the equations of motion. It may noted that the transformation matrices  $A_1$ ,  $A_2$ ,  $A_3$  and  $A_4$  are represented as identity matrices since the local frame of the individual mounts are aligned with the global coordinate system.

The equations of motion presented above are for a motorcycle application in which the powertrain is directly mounted to the frame as shown in Fig. 4.1. The swing-arm assembly used in this model is not connected to the powertrain. Fig. 4.1 shows the connection points that connect the powertrain to the frame. This type of connection is widely used in the motorcycle industry.

#### 4.1.2 Twelve DOF Model

A six DOF model is used to represent the powertrain assembly that is attached to the frame through engine mounts has been discussed in the previous section. The model developed in section 4.1.1 could come out short in capturing the isolation characteristics

in this layout. Therefore, an alternative model shown in Fig. 4.2, will be developed in this section. This model is a twelve DOF system that takes into consideration a layout that is widely used in the motorcycle industry. This layout assumes that there are two rigid bodies, one represents the powertrain and the second one represents the swing-arm. The swing arm is pivoted to the powertrain through a shaft assembly referred to as the coupler. Fig. 4.3 shows the layout of the twelve DOF model with the two rigid bodies attached. In this section, the EOM of the 12 DOF model are developed. More details regarding the coupler shaft are presented in Appendix C.

The general equations of motion for the twelve DOF system described above are as follows:

$$M \ddot{X} + C \dot{X} + K X = F e^{j\omega t} \quad (4.20)$$

In Eq. (4.20),  $M$ ,  $C$  and  $K$  are a  $12 \times 12$  mass, damping and stiffness matrices respectively.  $X = [x_{sa} \ y_{sa} \ z_{sa} \ \alpha_{sa} \ \beta_{sa} \ \gamma_{sa} \ x_e \ y_e \ z_e \ \alpha_e \ \beta_e \ \gamma_e]^T$  is the displacement vector that contains translational and rotational degrees of freedom for both the swing-arm and the powertrain. The subscript 'sa' represents parameters related to the swing-arm assembly and the subscript 'e' represents parameters related to the powertrain assembly.  $F$  denotes the input force vector due to the shaking force resulting from engine imbalance and/or the road loads due to the irregularities in the road profile. The overall mass matrix of the system is as follows:

$$M = \begin{bmatrix} M_{swingarm} & Z_6 \\ Z_6 & M_{engine} \end{bmatrix} \quad (4.21)$$

In Eq. (4.21),  $M_{engine}$ ,  $M_{swingarm}$  are the  $6 \times 6$  mass matrices of the powertrain and the swing-arm assemblies respectively and  $Z_6$  is a  $6 \times 6$  zero matrix. The powertrain mass matrix and

the swing-arm mass matrix are similar and they are the same as the mass matrix defined in Eq. (4.20). The inertia matrices for both the powertrain and the swing-arm are defined at their local center of gravity.

The stiffness and damping matrices of the twelve DOF system are defined as follows:

$$K = \begin{bmatrix} K_{sa} + K_c & -K_c \\ -K_c & K_e + K_c \end{bmatrix} \quad (4.22)$$

$$C = \begin{bmatrix} C_{sa} + C_c & -C_c \\ -C_c & C_e + C_c \end{bmatrix} \quad (4.23)$$

In Eq. (4.22),  $K_e$  and  $K_{sa}$  are the stiffness matrices of the powertrain and the swing-arm respectively. Both of these stiffness matrices are constructed in the same fashion as described in the previous section. The swing-arm stiffness matrix is constructed using the stiffness characteristics of the two rear shock springs connecting the swing-arm to the frame.  $C_e$  and  $C_{sa}$  shown in Eq. (4.23) are the damping matrices of the powertrain and the swing-arm respectively and they are constructed in the same way as  $K_e$  and  $K_{sa}$ .  $K_c$  and  $C_c$  are the stiffness and damping matrices of the coupler respectively. Both of these matrices are  $6 \times 6$  diagonal matrices. The construction of coupling stiffness and damping matrices of the coupler is discussed in details in Appendix C. A modeling of the shaking forces and the road loads will be discussed in detail in chapter 5.

The model discussed in this section assumes that the frame is infinitely rigid just like the assumption in the previous section. This assumption means that connection points between the engine mounts and the frame as well as the connection points between the frame and the rear suspension undergo zero deflection.

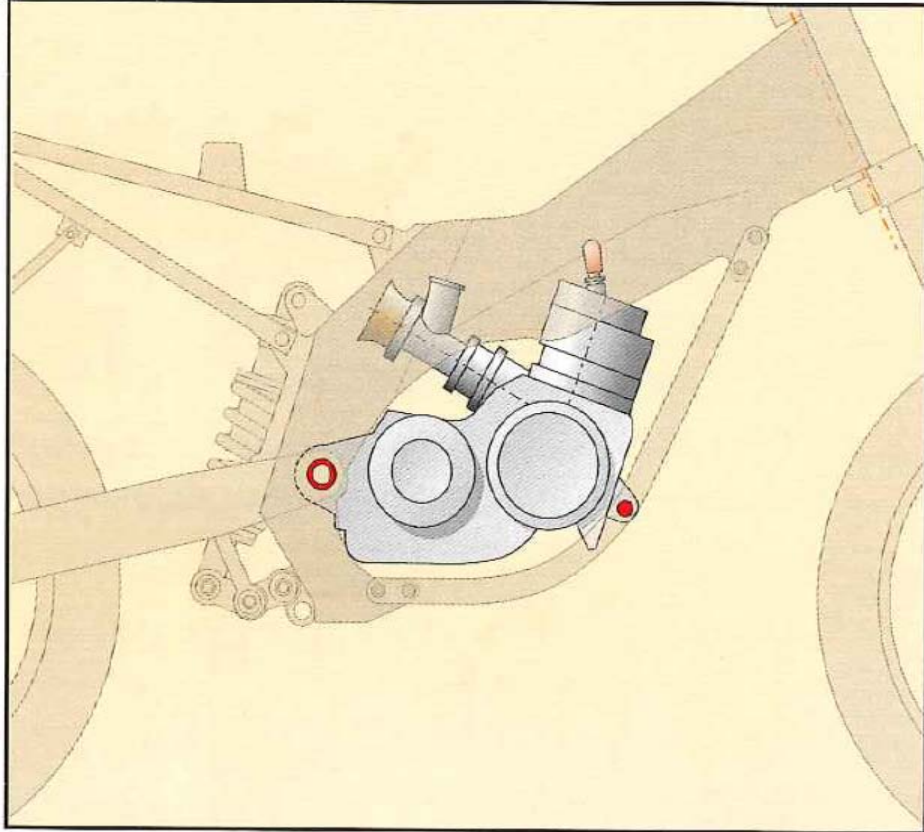


Figure 4.2: Twelve DOF Model (Cocco, 2001)

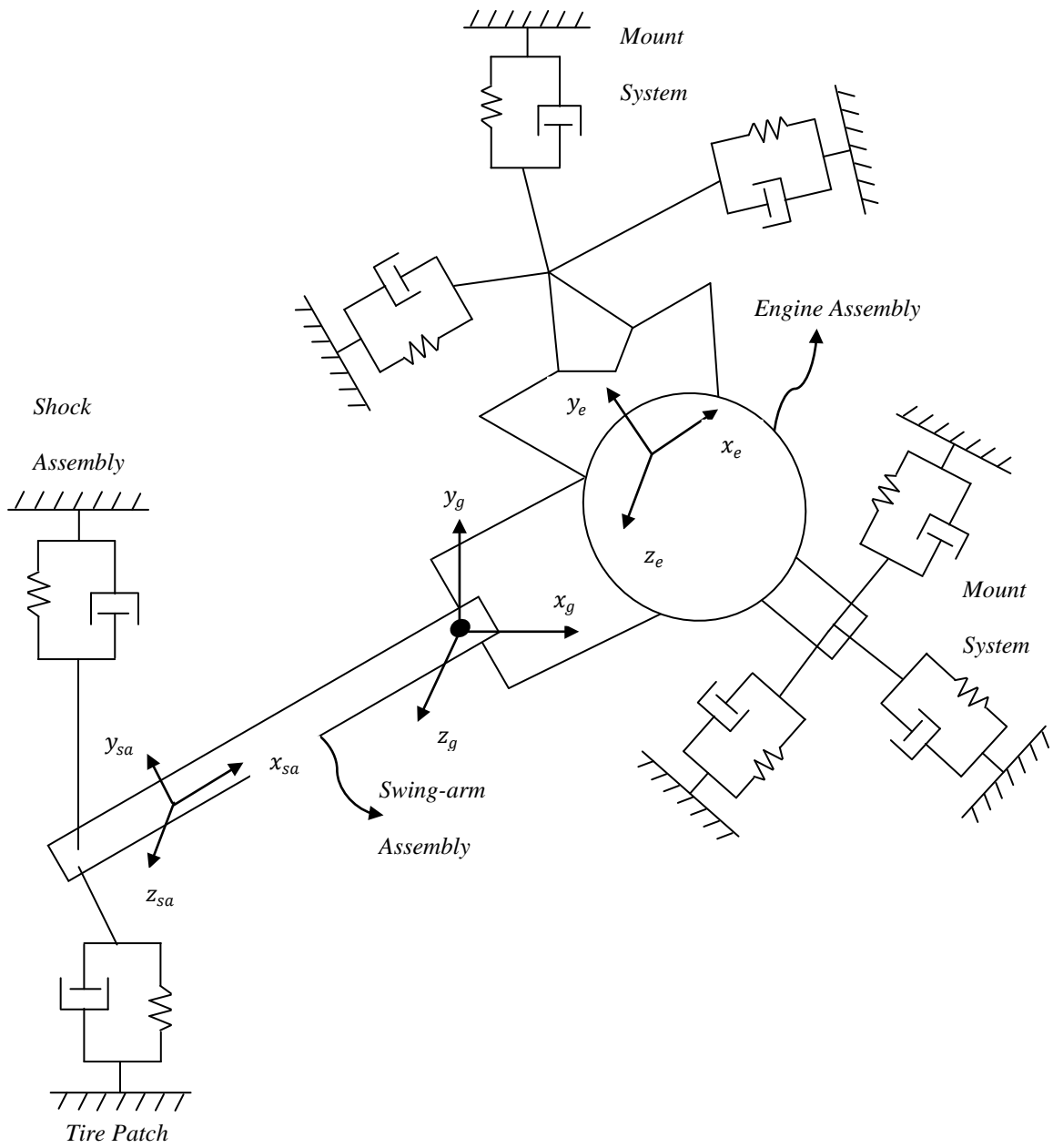


Figure 4.3: Twelve DOF Engine-Swingarm Layout

## 4.2 Mount Optimization

In this section, a formulation of the optimization problem for the models discussed in section 4.1 is presented using. The optimization problem is solved using the method of Sequential Quadratic Programming (SQP). SQP is used throughout this dissertation to solve the engine mount optimization problem.

The objective function that is used in this work is the weighted sum of the transmitted force through each individual mount. The transmitted forces through the mounts are due to the shaking forces generated inside the engine and/or the forces generated from the varying road profile. Loads calculated at several steady speeds can be used to construct the objective function.

The force ' $f_i$ ' transmitted to the frame through the individual mount ' $i$ ' is given as follows:

$$f_i = \begin{bmatrix} -k_i^* & k_i^* \tilde{r}_i \end{bmatrix} \begin{bmatrix} X_{ti} \\ X_{ri} \end{bmatrix} \quad (4.24)$$

In Eq. (4.24),  $X_{ti}$  and  $X_{ri}$  represent the translational and rotational displacement at the center of gravity of the powertrain as result of the input load.  $k_i^*$  is the local stiffness matrix for the individual mount ' $i$ ' and  $\tilde{r}_i$  is the skew symmetric matrix from the position vector of the individual mount ' $i$ '. Both of these matrices are defined in section 4.1.1 by Eq. (4.4) and Eq. (4.13).

The objective function  $f_w$  is assembled by summing the Euclidean norm of the individual force transmitted through each mount as follows:

$$f_w = \sum_j \lambda_j \sum_i \|f_i\| \quad (4.25)$$

In Eq. (4.25),  $\lambda_i$  is the weighting parameter that corresponds to different loading conditions. The complete engine mount optimization problem can be stated as follows:

$$\begin{aligned} & \text{Min } f_w(k_i, r_i, \theta_i) \\ & \text{subject to } g_j(k_i, r_i, \theta_i) \leq 0 \quad j = 1, \dots, N \end{aligned} \quad (4.26)$$

In Eq. (4.26), the mount stiffness, location and orientation  $(k_i, r_i, \theta_i)$  are the design variables that are subjected to a total of  $N$  number of constraints  $g_j$ . The constraints that are used in the above problem consist of constraints on the engine mount stiffness, constraints on the mount location based on the available space, constraints on the mount orientation that is dictated by symmetry and finally a constraint on the deflection of the center of gravity of the powertrain due to the static weight of the powertrain. The objective function  $f_w$  is defined in Eq. (4.25). Both  $f_w$  and  $g_j$  are functions of the design variables  $(k_i, r_i, \theta_i)$ .

The Sequential Quadratic Programming (SQP) method is used to solve the optimization problem. A brief description of the SQP method is presented next.

#### 4.2.1 Sequential Quadratic Programming

The general function of an optimization problem is given below:

$$\begin{aligned} & \text{Minimize } f(x); x \in \mathcal{R}^n \\ & \text{subject to } h_i(x) = 0 \quad i = 1, \dots, p \\ & \quad \quad \quad g_j(x) \leq 0 \quad j = 1, \dots, m \\ & \quad \quad \quad x_l \leq x \leq x_u \end{aligned} \quad (4.27)$$

In Eq. (4.27),  $f(x)$  is the objective function.  $h_i(x)$  and  $g_i(x)$  are the  $i^{\text{th}}$  equality and inequality constraints respectively and  $x$  is the vector of design variables.  $x_l$  and  $x_u$  are the lower and upper bound vectors for the design variables. The optimization problem



defined in Eq. (4.27) consisting of ‘ $p$ ’ equality constraints and ‘ $m$ ’ inequality constraints is said to be linear if the objective function and all the constraints are linear function of the design variables. The problem is said to be quadratic if the objective function is quadratic and the constraints are linear. If the objective function and/or the constraints are nonlinear function of the design variables, then the problem is said to be a nonlinear optimization problem. In the case of the engine mount optimization, the problem is nonlinear, and the Sequential Quadratic Programming (SQP) algorithm is employed to solve the problem. The (SQP) method uses the Newton’s method and Kuhn-Tucker conditions to solve the optimization problem as mentioned in (Rao, 2000).

For the optimization problem with  $p$  equality constraints and  $n$  design variables, a quadratic sub-problem is constructed based on the approximation of the Lagrangian function  $L(x, \lambda)$  which stated as follows:

$$L(x, \lambda) = f(x) + \sum_{k=1}^p \lambda_k h_k(x) \quad (4.28)$$

In Eq. (4.28),  $\lambda_k$  is the Lagrange multiplier for the  $k^{th}$  equality constraint and  $h_k(x)$  is the  $k^{th}$  equality constraint and  $f$  is the objective function.  $x$  is a vector of  $n$  design variables.

The Kuhn-Tucker necessary conditions for the problem stated in Eq. (4.28) can be stated as follows:

$$\nabla L = 0 \quad \text{or} \quad \nabla f + \sum_{k=1}^p \lambda_k \nabla h_k = 0$$

$$h_k(x) = 0, k = 1, \dots, p \quad (4.29)$$

Eq. (4.29) consists of a set of  $(n + p)$  nonlinear equations that is solved using Newton’s method. The above equation can be represented in the following form:

$$F(Y) = 0 \text{ where } F = \begin{bmatrix} \nabla L \\ h \end{bmatrix}_{(n+p) \times 1} \text{ and}$$

$$Y = \begin{bmatrix} x \\ \lambda \end{bmatrix}_{(n+p) \times 1} \quad (4.30)$$

where the  $(n + p)$  system of equation shown in Eq. (4.30) is solved using the Newton's method iteratively as follows:

$$[\nabla F]_j^T \Delta Y_j = -F(Y_j) \quad (4.31)$$

In Eq. (4.31)  $Y_j$  is the solution at the beginning of the the  $j^{\text{th}}$  iteration,  $\Delta Y_j$  is the change in the  $Y_j$  and  $[\nabla F]_j$  is the Jacobian matrix of the  $(n + p)$  nonlinear equations. The updated solution is given as follows:

$$Y_{j+1} = Y_j + \Delta Y_j \quad (4.32)$$

Eq. (4.32) can be rewritten as:

$$\begin{bmatrix} [\nabla^2 L] & [H] \\ [H]^T & [0] \end{bmatrix}_j \begin{bmatrix} \Delta x \\ \Delta \lambda \end{bmatrix}_j = - \begin{bmatrix} \nabla L \\ h \end{bmatrix}_j \quad (4.33)$$

In Eq. (4.33),  $\Delta x_j = x_{j+1} - x_j$  and  $\Delta \lambda_j = \lambda_{j+1} - \lambda_j$  and  $\nabla^2 L$  is the Hessian matrix of the Lagrange function and  $H = [\nabla h_k]$ . The first equation from the system of equation in Eq. (4.33) can be rewritten in the following form:

$$[\nabla^2 L]_j \Delta x_j + [H]_j \lambda_{j+1} = -\nabla L_j + [H]_j \lambda_j = -\nabla f_j \quad (4.34)$$

Eq. (4.33) can be rewritten as:

$$\begin{bmatrix} [\nabla^2 L] & [H] \\ [H]^T & [0] \end{bmatrix}_j \begin{bmatrix} \Delta x_j \\ \lambda_{j+1} \end{bmatrix} = - \begin{bmatrix} \nabla f_j \\ h_j \end{bmatrix} \quad (4.35)$$

Eq. (4.35) can be solved iteratively to determine  $\Delta x_j$  and  $\lambda_{j+1}$ , the design variables and the Lagrange multipliers. For a general problem with both equality and inequality constraints, the optimization problem can be stated as follows:

Find  $X$  that

$$\begin{aligned} \text{Minimize } Q &= \nabla f^T \Delta X + \frac{1}{2} \Delta x^T [\nabla^2 L] \Delta X \\ \text{subject to } g_j + \nabla g_j^T \Delta X &\leq 0 \quad j = 1, \dots, m \\ h_k + \nabla h_k^T \Delta X &= 0 \quad k = 1, \dots, p \end{aligned} \quad (4.36)$$

and the Lagrangian function is given as:

$$\bar{L} = f(x) + \sum_{j=1}^m \lambda_j g_j(x) + \sum_{k=1}^p \lambda_{m+k} h_k(x) \quad (4.37)$$

In Eq. (4.37),  $X$  is the design variable vector and  $L$  is the corresponding Lagrangian function.  $g_j$  and  $h_k$  are the inequality and equality constraints respectively. A first order Taylor series is used to linearize the nonlinear constraint function. This problem can be solved with a similar procedure as the optimization problem with only equality constraints mentioned earlier in this section.

#### 4.2.2 Six DOF Model

In this section, the force transmitted through the engine mount to the frame due to the engine imbalance is used as the objective function. The optimization problem is formulated based on the six DOF model presented in section 4.1.1. The design vector is based on the mount parameters; stiffness, orientation and location. Some constraints imposed on the problem include limits on the powertrain deflection due to the static and

dynamic loads combined with constraints on the lower and upper bounds for the design variables.

#### 4.2.2.1 Numerical Example

The example presented herein is based on the model presented in section 4.1.1 in order to solve the optimization problem of minimizing the transmitted loads formulated in section 4.2. The objective function is compiled by summing the transmitted force through the individual mounts that are supporting the powertrain. The objective function is described as follows:

$$F_{obj} = \|f_1\| + \|f_2\| + \|f_3\| + \|f_4\| \quad (4.38)$$

In Eq. (4.38),  $f_1$ ,  $f_2$ ,  $f_3$  and  $f_4$  are the force vectors transmitted to the frame through the four mounts that are supporting the powertrain due to the shaking force at the engine steady speed of 4000 rpm. The formulation of the shaking force at the steady state speed is discussed in depth in chapter 5. The general layout of the mounting system for this example is shown in Fig. 4.4. Mount parameters which consist of mount stiffness, mount location and mount orientation are compiled to form the design vector. The lower and upper bounds used for the design variables are shown in Table 4.1. A limit that is imposed on the design variables by constraining the deflection of the powertrain as follows:

$$|U_{st}| \leq U_{max} \quad (4.39)$$

In Eq. (4.39),  $U_{st}$  is the static deflection vector of the powertrain due to the static loading at its C.G. and  $U_{max}$  is the maximum allowable displacement due to the static load.  $U_{max} = [0.025 \text{ in} \quad 0.050 \text{ in} \quad 0.025 \text{ in} \quad 0.5 \text{ deg} \quad 0.5 \text{ deg} \quad 0.5 \text{ deg}]$ . An additional constraint is added to the allowable displacement at the mount in the y-

direction to prevent premature snubbing. A maximum displacement of 0.5 in is used as an upper bound for the displacement for all four mount locations. The maximum steady state displacement is as follows:

$$|U_1|_{dyn} \leq U_{max}^{dyn} \quad |U_2|_{dyn} \leq U_{max}^{dyn} \quad |U_3|_{dyn} \leq U_{max}^{dyn} \quad |U_4|_{dyn} \leq U_{max}^{dyn}$$

In this example, the mounting system used herein consists of four identical circular cross section elastomeric mounts. For each mount, two dynamic stiffness parameters completely define the stiffness characteristics. These stiffness parameters are radial and axial stiffness and are used as the design variables. A loss factor of 0.3 (Carfagni, 1998) and a dynamic-to-static stiffness coefficient of 1.2 have been used. In order to reduce the total number of design variables, symmetry constraints are imposed. This is done by symmetrically placing two mounts on each side of the  $x$ - $y$  plane resulting in six position variables instead of twelve and four orientation variables instead of twelve. The radial and axial stiffness values are identical for all four mounts resulting in a total of twelve design variable for the engine mounting system. The mass of the powertrain is 0.5  $lb \cdot s^2/in$  and inertia values of the powertrain are given in Table 4.2.

The optimization problem is solved using the SQP technique to minimize the value of the objective function. The design variables resulting from the optimization process are shown in Table 4.3. The computed mount location and orientation vectors are shown in Table 4.4. The resulting mode shapes are shown in Fig. 4.5. Each mode shape is presented with its corresponding un-damped natural frequency with respect to their degrees of freedom  $x, y, z, \alpha, \beta$  and  $\gamma$  respectively.

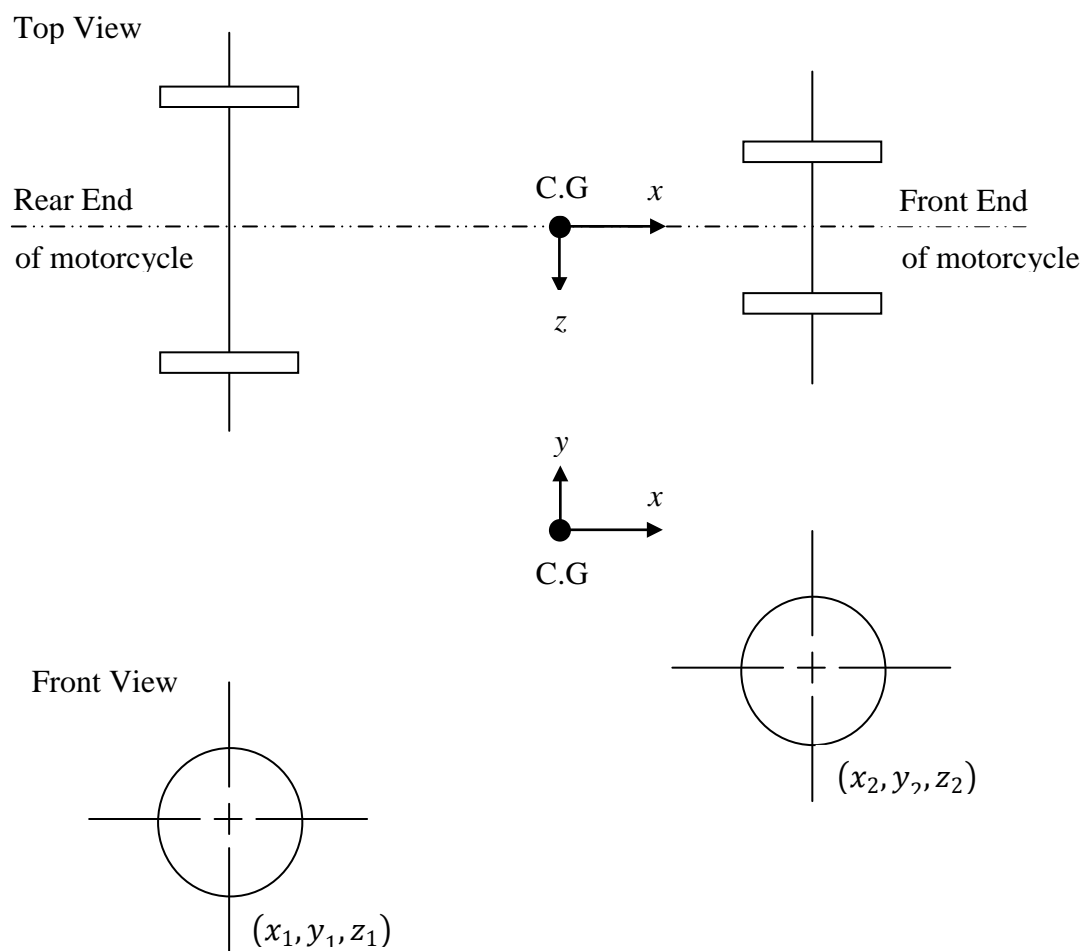


Figure 4.4: Mount System Layout

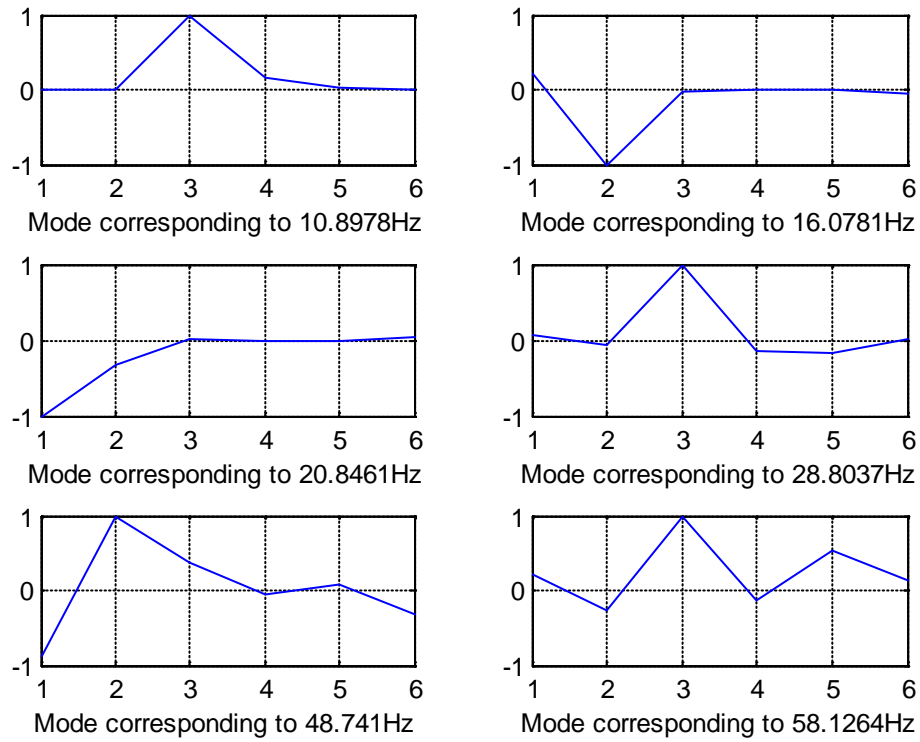


Figure 4.5: Mode Shapes for the Optimized Configuration (6 DOF Model)

Table 4.1: Bounds for Design Variables

	Min.	Max.
Mount Stiffness (x,y)	100	5000
Mount Stiffness (z)	500	10000
Orientation Angles	deg. 0	50

Table 4.2: Inertia Tensor of Powertrain Assembly

	x	y	Z
$I_x$	20.7	1.86	0.12
$I_y$ (lb-in <sup>2</sup> )	1.86	12.81	2.3
$I_z$	0.12	2.3	26.14

Table 4.3: Optimization Results (6 DOF Model)

	Load Transmitted		Mount Stiffness (lb/in)			
	(lb)		x	y		z
Initial Guess	110.90		475	475		7500
Optimized Design	39.90		1016.6	1016.6		7503.5
Natural Frequencies	10.898	16.078	20.846	28.804	48.741	58.126 (un-damped)
(Hz)	10.89	16.07	20.823	28.743	48.447	57.627 (damped)
Damping Coefficients	0.025	0.036	0.047	0.065	0.110	0.131

Table 4.4: Optimization Results for Position and Orientation (6 DOF Model)

	Mount 1	Mount 2	Mount 3	Mount 4
Orientation (deg)				
Starting Guess	(0.1, 50, 0)	(-0.1, -50, 0)	(0.5, 25, 0)	(-0.5, -25, 0)
Results	(16.6, 50, 0)	(-16.4, -50, 0)	(45.7, 12.7, 0)	(-45.7, -12.7, 0)
Position (in)				
Starting Guess	(12, -9, 0)	(12, -9, 0)	(-19, -5, 0)	(-19, -5, 0)
Results	(9.2, -5, -7)	(9.2, -5, 7)	(-11, -10, -3)	(-11, -10, 3)

#### 4.2.2.2 Discussion of Results

It is worth mentioning that for the example presented in section 4.2.2.1, the starting guess for the problem was changed couple of times to make sure that the final optimum solution does not get stuck at local minima. This is due to the fact that the engine mount optimization problem is a highly nonlinear and could easily get stuck at a local minimum as a final solution.



As can be seen in Table 4.3, the optimum stiffness values have changed a lot in the  $x$  and  $y$  direction while barely changing in the  $z$ -direction. The small amount of change in the stiffness along the  $z$ -direction is due to the fact that the force transmitted to the frame is least sensitive to the stiffness in the  $z$ -direction of the engine mount. This fact is used in the motorcycle design by tuning the (out-of-plane) stiffness in the  $z$ -direction to achieve the best handling possible. By tuning the (in-plane) stiffness values in the  $x$  and  $y$  direction, the isolation characteristics of the motorcycle are enhanced with minimal cross coupling between the out-of-plane and the in-plane stiffness coefficients. Table 4.4, shows the optimum values for the mount locations and orientations. It can be seen that the mount locations have not changed a lot, meanwhile the mount orientations have changed significantly. This observation shows the effect of mount orientation on achieving minimum load transmission. On the other hand it also indicates that the effect of mount location on load transmission has less impact than mount orientation.

### *4.2.3 Twelve DOF Model*

The equations of motion of the six DOF model formulated in section 4.1.1 along with the example shown in section 4.1.2 represents a mounting system that is connected to the frame only. Fig. 4.2 shows an alternate twelve DOF model that couples the powertrain and the swing-arm using a shaft assembly. The model presented herein is an extension of the model presented in section 4.2.2. It provides sufficient information to capture the isolation characteristics of such a layout. This model is based on two rigid bodies, one is for the powertrain assembly and the other one is for the swing-arm assembly connected together using a coupler.

This section uses the equations that were formulated in section 4.1.2 to develop an optimization problem in order to solve for the mount parameters. It will also provide examples where the road loads and the shaking loads are present as input loads.

#### *4.2.3.1 Numerical Example I*

The example presented next is based on the model presented in section 4.1.2 in order to solve the optimization problem of minimizing the transmitted loads formulated in section 4.2. The objective function is computed by summing the transmitted force through the individual mounts that are supporting the powertrain. The objective function is described in Eq. (4.38). The input load vector corresponds to the force due to the shaking loads only.

The mounting system used in this example consists of four identical circular cross section elastomeric mounts with symmetry constraints. Two of these engine mount are at the front of the powertrain assembly and the other two are located at the rear of the powertrain assembly as shown in Fig. 4.4. The powertrain assembly and the swing-arm assembly are connected using a shaft assembly which will be referred to as the coupler. The swing-arm assembly is connected to the frame via two shock absorbers one at each side of the motorcycle.

The swing arm assembly used herein (Kaul, 2006) has a mass of  $0.13 \text{ lb-s}^2/\text{in}$ . the inertia properties of the swing arm with respect to its C.G. are listed in Table 4.5. The swing-arm is connected to the frame using two shock absorbers which are inclined by an angle of  $47^\circ$  with respect to the horizontal axis. The shock absorber exhibits an axial stiffness and damping of  $45 \text{ lb/in}$  and  $4.4 \text{ lb-s/in}$  respectively. The stiffness of the coupler used in the example is  $42655 \text{ lb/in}$  in the  $x$  and  $y$  direction and  $658252 \text{ lb/in}$  along the  $z$

axis. The rotational stiffness values is 682493 *lb-in/rad* about the *x* and *y* axes. The rotational stiffness about the *z* axis is zero. A 2% structural damping has been used to compute the coupler damping properties. The input load, the design parameters, bounds and constraints are the same as the example presented in section 4.2.2.1. The results of the optimization problem are presented in Table 4.6 and Table 4.7.

Table 4.5: Inertia Tensor of the Swing-arm Assembly

	x	y	z
$I_x$	0.465	0.002	-0.007
$I_y$ (lb-in <sup>2</sup> )	0.002	30	-0.008
$I_z$	-0.007	-0.008	29

Table 4.6: Optimization Results (12 DOF Model – Shaking Load only)

	Load Transmitted		Mount Stiffness (lb/in)			
	(lb)		x	y	Z	
Initial Guess	88.59		475	475	7500	
Optimized Design	59.32		2341.7	2341.7	2157.9	
Natural Frequencies	1.640	8.719	10.436	21.394	22.221	24.305
	59.842	75.703	103.415	104.025	200.567	1271.369 (undamped)
(Hz)	1.574	8.618	10.426	21.375	22.217	24.244
	59.3309	75.119	103.373	104.024	198.376	1270.350 (damped)
Damping Coefficients	0.005	0.020	0.028	0.040	0.042	0.044
	0.071	0.124	0.130	0.147	0.152	0.282

Table 4.7: Optimization Results for Position and Orientation (12 DOF Model – Shaking Load only)

	Mount 1	Mount 2	Mount 3	Mount 4
Orientation (deg) Starting Guess	(0.1, 50, 0)	(-0.1, -50, 0)	(0.5, 25, 0)	(-0.5, -25, 0)
Results	(50, 50, 0)	(-50, -50, 0)	(50, 50, 0)	(-50, -50, 0)
Position (in) Starting Guess	(12, -9, 0)	(12, -9, 0)	(-19, -5, 0)	(-19, -5, 0)
Results	(12, -9,-3)	(12, -9,3)	(-12.5, -10, -7)	(-12.5, -10, 7)

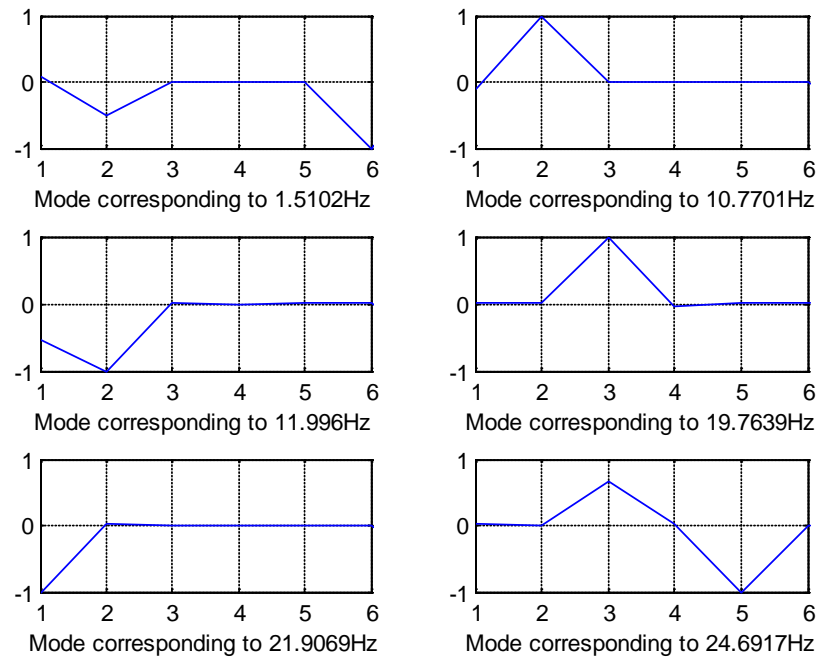


Figure 4.6: Mode Shapes - 1 to 6 (12 DOF Model – Shaking Load only)

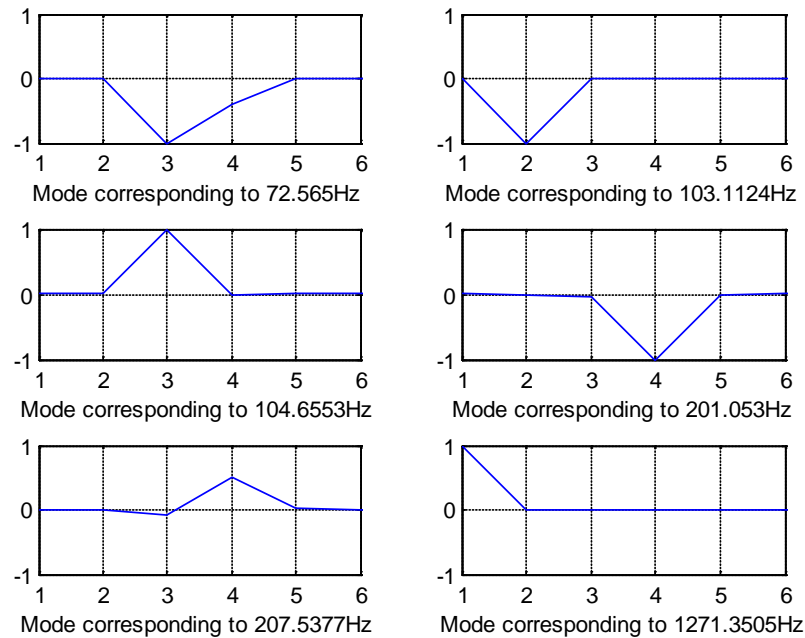


Figure 4.7: Mode Shapes - 7 to 12 (12 DOF Model – Shaking Load only)

#### 4.2.3.2 Numerical Example II

This example is based on the model presented in section 4.1.2 in order to solve the optimization problem of minimizing the transmitted loads formulated in section 4.2. The objective function is computed by summing the transmitted force through the individual mounts that are supporting the powertrain. The objective function is described in Eq. (4.38). The input load vector corresponds to the force is a linear combination of the shaking force and the road load. The example presented in this section is identical to the example presented in the previous section. An additional constraint is added to control the maximum steady state displacement due to the presence of the road load. The load profile used in this example is shown in Fig. 4.8. The governing equation used for the V-Twin engine configuration used for the computation of the shaking force and the road load will be discussed in detail in chapter 5. An elaborate road load model based on

the Pacejka tire model is presented in Appendix B. This model is used to compute the forces and moments acting on the tire patch. The results of the optimization problem are presented in Table 4.8 and Table 4.9.

Table 4.8: Optimization Results (12 DOF Model – Combined Loading)

	Load Transmitted		Mount Stiffness (lb/in)			
	(lb)		x	y	z	
Initial Guess	566.45		475	475	7500	
Optimized Design	122.68		2405	2405	1564.5	
Natural Frequencies	1.482	9.087	10.800	11.639	22.275	35.658
	37.437	103.036	103.396	105.657	200.603	1271.338 (un-damped)
(Hz)	1.41	9.08	10.766	11.621	22.270	35.54
	37.3068	103.002	103.378	103.628	198.41	1270.326 (damped)
Damping Coefficients	0.019	0.021	0.026	0.034	0.040	0.055
	0.079	0.081	0.083	0.147	0.195	0.315

Table 4.9: Optimization Results for location and Orientation (12 DOF Model – Combined Loading)

	Mount 1	Mount 2	Mount 3	Mount 4
Orientation (deg)				
Starting Guess	(0.1, 50, 0)	(-0.1, -50, 0)	(0.5, 25, 0)	(-0.5, -25, 0)
Results	(0.6, 50, 0)	(-0.6, -50, 0)	(4.9, 0, 0)	(-4.9, 0, 0)
Position (in)				
Starting Guess	(12, -9, 0)	(12, -9, 0)	(-19, -5, 0)	(-19, -5, 0)
Results	(8, -8, -3.4)	(8, -8, 3.4)	(-17, -6.8, -3.2)	(-17, -6.8, 3.2)

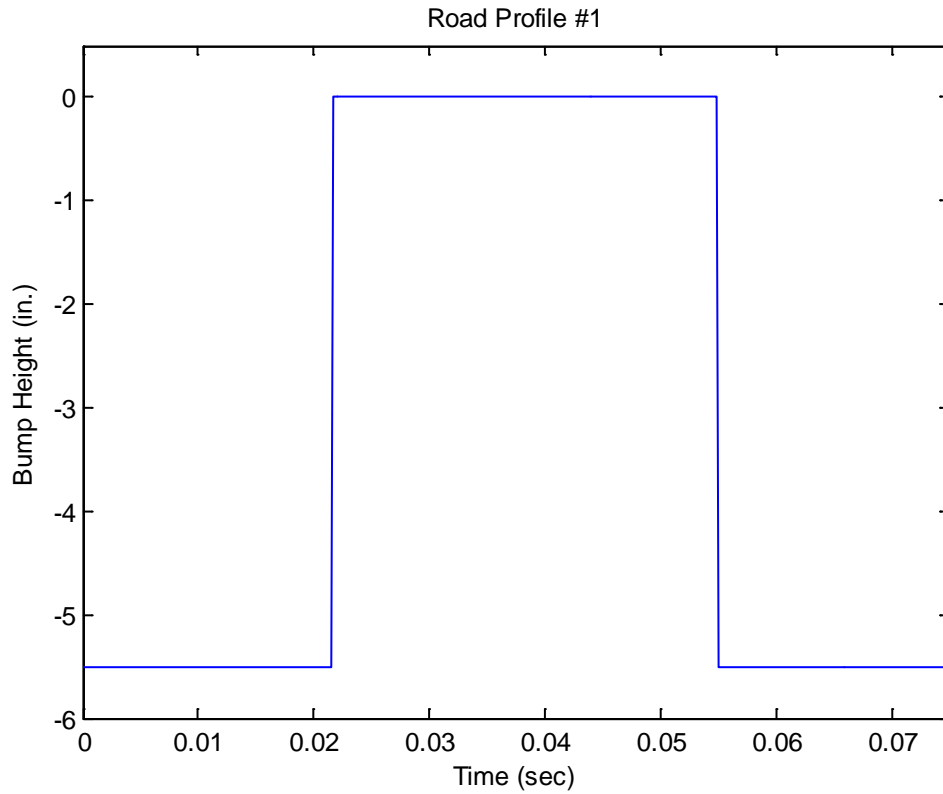


Figure 4.8: Road Profile

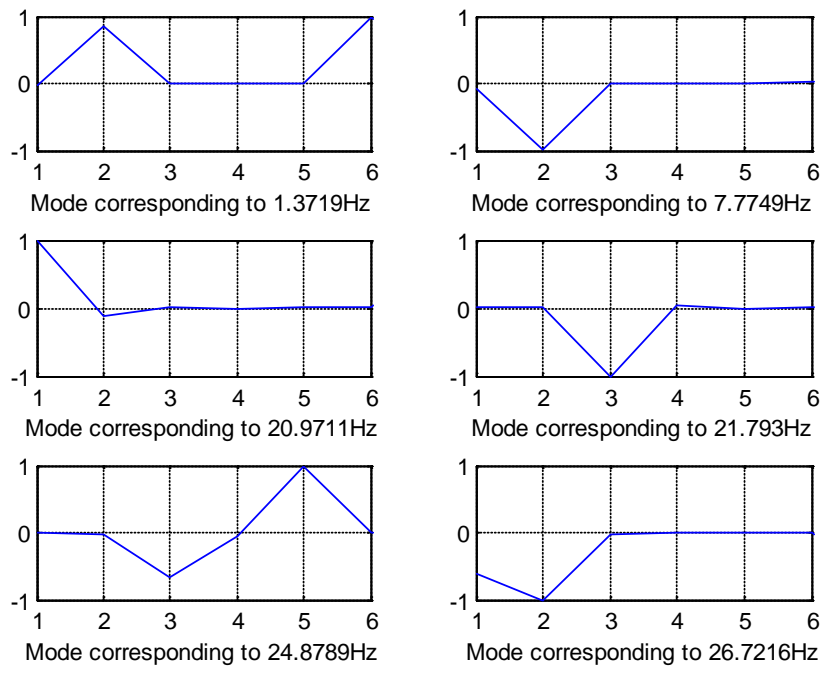


Figure 4.9: Mode Shapes - 1 to 6 (12 DOF Model – Combined Loading)

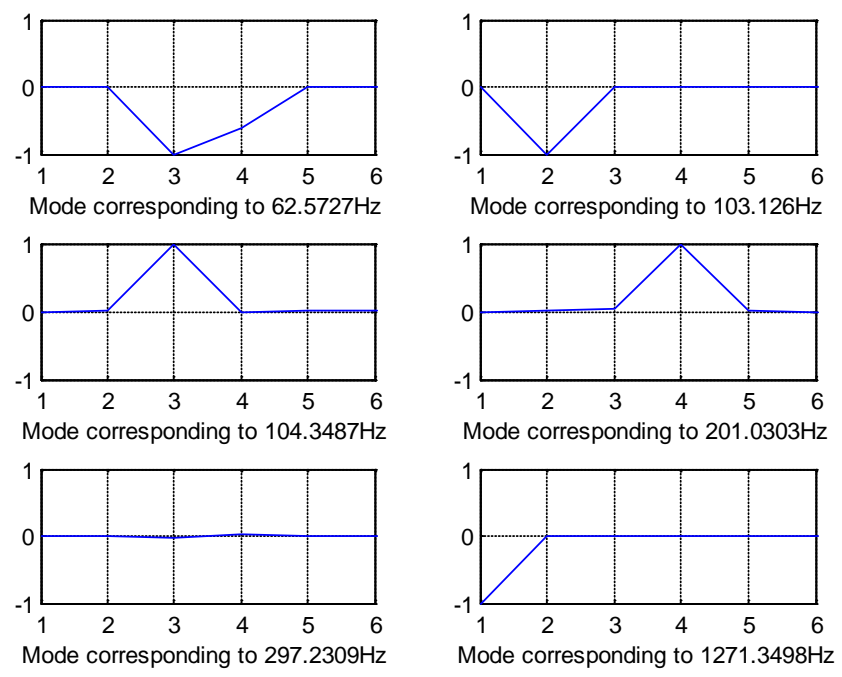


Figure 4.10: Mode Shapes - 7 to 12 (12 DOF Model – Combined Loading)



### 4.2.3.3 Discussion of Results

The results for the two optimization problems presented in sections 4.2.3.1 and 4.2.3.2 are shown in Table 4.6, Table 4.7 and Table 4.8, Table 4.9 respectively. Just like the six DOF model, multiple starting guesses were used due to the nonlinearity of the mount optimization problem. As can be seen from the tables mentioned above, the out-of-plane stiffness values are less sensitive to the transmitted loads. The optimum transmitted load in Tables 4.8 is significantly higher than that shown in Table 4.6. This is due to the use of a combined loading vector. This loading vector contains the shaking load and the road load. The in-plane mount stiffness has increased to satisfy the additional displacement constraint due to the addition of the road load to the input force vector. The location and orientation vectors show a similar trend to the vectors shown in the previous section. The optimized mode shapes that correspond to the results shown in Tables 4.6 and 4.8 are shown in Figs. 4.6, 4.7, 4.9 and 4.10 are normalized. The modes are numbered from 1 to 12 representing the modes that corresponds to the swing-arm assembly (modes from 1 to 6), namely  $(x_{sa}, y_{sa}, z_{sa}, \alpha_{sa}, \beta_{sa}, \gamma_{sa})$ , and the modes that corresponds to the powertrain assembly (modes from 7 to 12), namely  $(x_e, y_e, z_e, \alpha_e, \beta_e, \gamma_e)$ .

The work done thus far characterizes the engine mount by setting up an objective function that minimizes the transmitted loads. In certain application, the goal is to design the mounting system keeping in mind the space limitations where the importance of decoupling the vibration modes becomes very clear. When the vibration modes are decoupled the effect of each mode can be examined independently. Although decoupling vibration modes is not an easy task, a fair bit of work has been done trying to achieve this

goal in the content of vibration isolation. Different approaches have been proposed to come up with clean decoupled modes for a powertrain mounting system. These methods include: inclining the isolators and minimizing the off-diagonal terms of the stiffness matrix.

### 4.3 Isolator Inclining

The natural modes of vibration can be decoupled through a proper orientation of the supporting isolators. By doing so, all the modes will exist independently and vibration of one mode will not excite the other modes. The necessary conditions for decoupling modes can be stated as follows as mentioned in the vibration and shock handbook (Harris, 1961). *“The resultant of the forces applied to mounted body by the isolators when the mounted body is displaced in translation must be a force directed through the center of gravity; or the resultant of the couples applied to the mounted body by the isolators when the mounted body is displaced in rotation must be a couple about an axis through the center of gravity”*.

Decoupling vibration modes can be achieved by placing the isolators in a plane that passes through the center of gravity of the powertrain. If this can't be done, decoupling can be achieved by inclining the isolators as shown in the below.

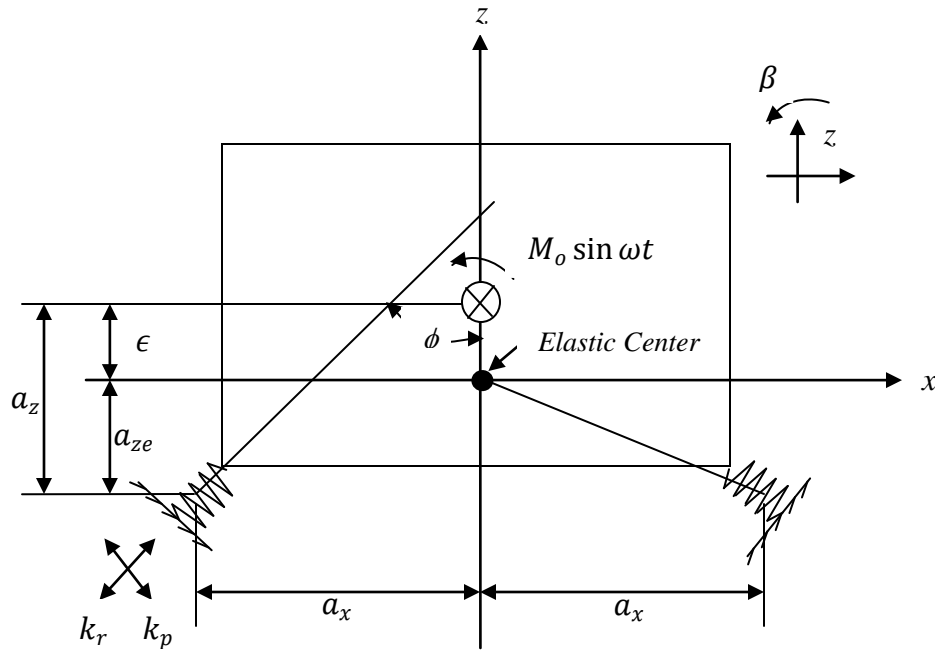


Figure 4.11: Schematic diagram of equipment supported by inclined isolators

If the elastic axis of the mounting system is chosen in a way to pass through the center of gravity of the powertrain, translational and rotational modes will be decoupled. Decoupling occurs because the inertia force is being applied through the center of gravity; as a result the body will not undergo any rotation. To insure complete mode decoupling, the angle in which the isolators must be inclined must satisfy the following relation:

$$\frac{a_z}{a_r} = \frac{\frac{1}{2} \left[ 1 - \left( \frac{k_p}{k_r} \right) \right] \sin 2\phi}{\frac{k_q}{k_r} + \frac{k_p}{k_r} + \left[ 1 - \left( \frac{k_p}{k_r} \right) \right] \sin^2 \phi} \quad (4.40)$$

In Eq. (4.40),  $k_p, k_q, k_r$  are the stiffness values along the principal elastic axes of the isolator and  $\phi$  is the angle between the Z axis and the R axis shown in Fig. 4.11.

### 4.3.1 Numerical Example

Consider the mounts arranged symmetrically as shown in Fig. 4.12. The mounts are arranged symmetrically about the  $z$  axis. They are attached to one end of the cylinder at a distance  $a_r$  from the  $z$  axis and a distance  $a_z$  from the  $x$ - $y$  plane. The mounts are inclined so that their principal axes  $R$  and  $P$  are intersect respectively at two common points on the  $z$  axis. Let the angle between the  $z$  axis and the  $R$  axis for each mount is  $\phi$ . Let the angle between the  $z$  axis and the  $P$  axis be  $90^\circ - \phi$ . The  $Q$  principal elastic axes are tangent to the circle of radius  $a_r$  which bounds the end face of the cylinder. The mass  $m = 200$  kg. The inertia values are  $I_x = I_y = 25 \text{ kg.m}^2$  and  $I_z = 12 \text{ kg.m}^2$ . The inclination angle  $\phi = 30^\circ$ . The stiffness values and the distance are shown in Table 4.10.

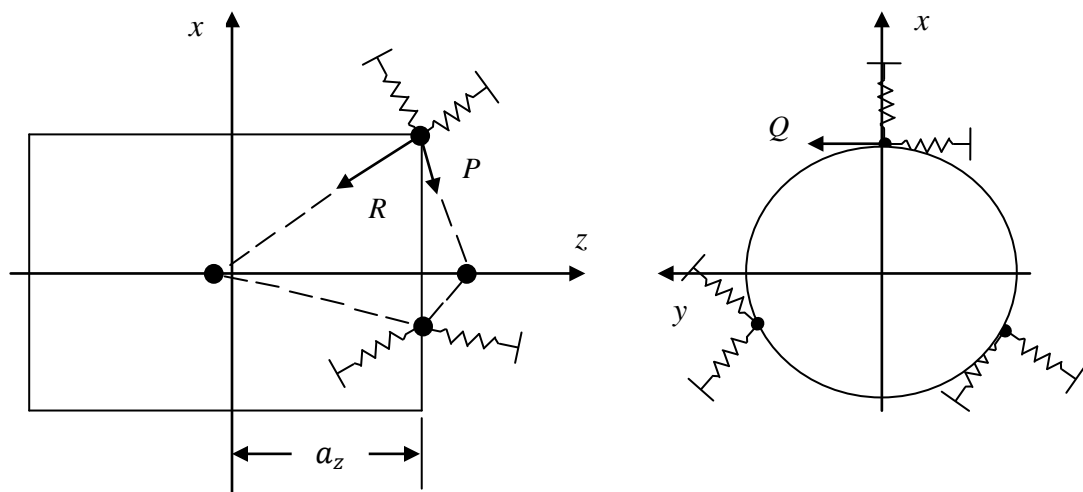


Figure 4.12: Mount Arrangement

Table 4.10: Stiffness Values and the Distance

$k_p$ (N/mm)	$k_q$ (N/mm)	$k_r$ (N/mm)	$a_z$ (mm)
50	100	150	123.72

Results for the example presented in this section are shown in Fig. 4.13. The effect of inclining the mount is clearly seen in Fig. 4:13. This suggests that we need to find the set of angles that will be used to orient the mount about its axis. This will decouple the vibration modes. As it's clearly shown, all of the six modes are completely decoupled. The natural frequencies of each of the modes are also shown in the Fig. 4.13.

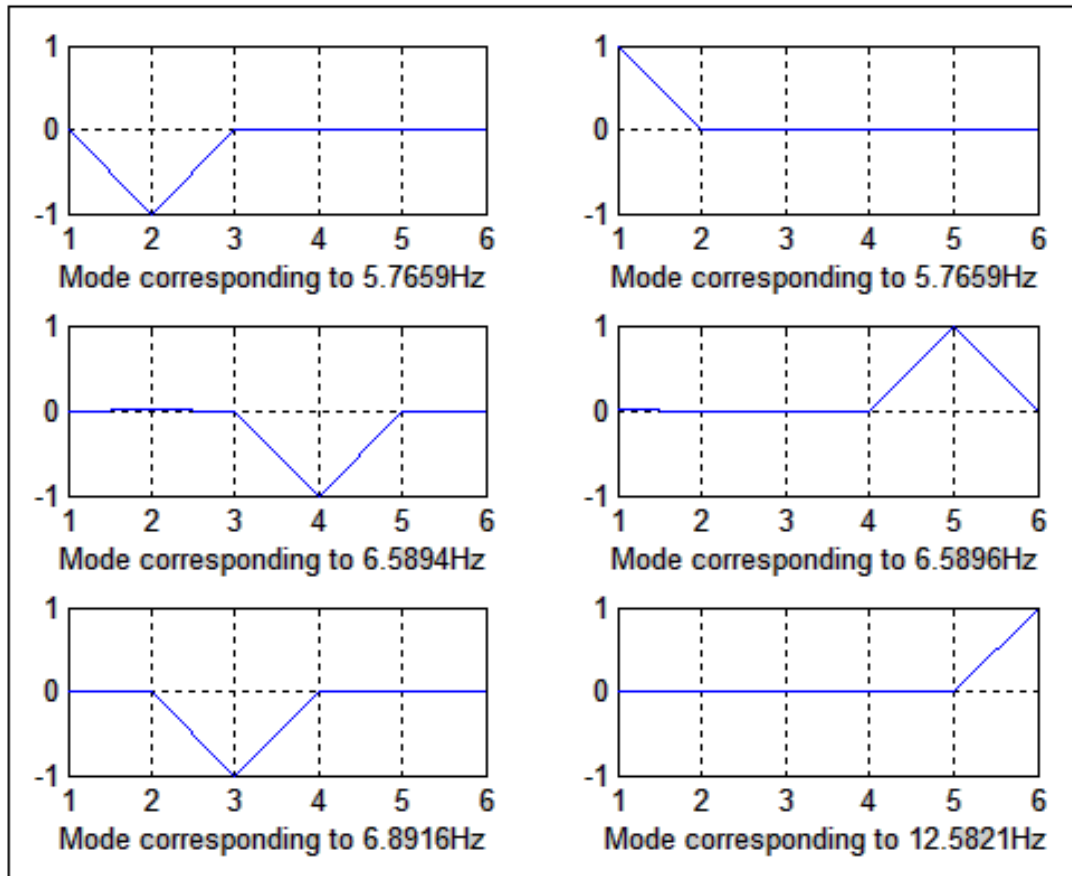


Figure 4.13: Decoupled Modes Along with the Associated Natural Frequency

#### 4.4 Vibration Modes Decoupling

The final approach for mode decoupling considered is formulation of an optimization problem. The objective function that has been used in this section to achieve mode decoupling is to minimize the Frobenius norm of the off-diagonal terms of the overall stiffness matrix. While the value of the objective function is being minimized, the values of the stiffness, orientation and location of the mounts are being estimated the SQP optimization technique. The objective function is given by:

$$F = \left\| \sum_{i=1}^n \sum_{j=1}^n k_{ij} \right\|_{frobenius}, i \neq j \quad (4.41)$$

In Eq. (4.41),  $k_{ij}$  are the terms of the stiffness matrix. The Frobenius norm is defined as follows:

$$Norm_{frobenius} = \sqrt{\sum diag(K_{off\_diag}^T * K_{off\_diag})} \quad (4.42)$$

To illustrate this procedure a numerical example is presented next where three different sets of variables are used to achieve mode decoupling.

##### 4.4.1 Numerical Example

A V-6 engine is supported using four mounts. The mass of the engine is  $m = 276.70 \text{ kg}$ . The inertia tensor for the engine are shown Table 4.11. The mount coordinates were measured from the engine center of gravity to each mount attachment point. The mount's compression, lateral and force/aft axes define the engine's  $x$ ,  $y$  and  $z$  coordinate system. Mount orientation is obtained by rotating about the engine  $x$ -axis, the  $y$ -axis and the  $z$ -axis.

There are three cases through which the approach presented herein is discussed. The first case corresponds to using the mount stiffness values as the only variables in the design vector. The second case is where the mount stiffness and orientation form the design vector. The third and the final case include the mount stiffness values, mount locations and mount orientation combined together in the design vector. The results for the three different cases are shown in the Fig. 4.14 through Fig. 4.16. The initial guess and the final mount parameters along with the matrix showing the minimized off-diagonal terms of the overall stiffness matrix are shown in Table 4.12 through Table 4.20.

Table 4.111: Inertia Tensor for the Engine

	x	y	z
$I_x$	15.8	0	0
$I_y$	0	11.64	0
$I_z$	0	0	15.69

Table 4.12: Initial Guess of the Mount Locations in (m)

Mount	x	y	z
1	-0.2246	-0.3093	-0.1990
2	0.3614	-0.2823	-0.2510
3	-0.1946	0.1407	-0.2290
4	0.2934	0.1667	-0.2450

Table 4.13: Initial Guess of the Mount Orientations (deg.)

Mount	$\theta_x$	$\theta_y$	$\theta_z$
1	0	-45	0
2	0	-39	180
3	0	-75	0
4	0	-45	180

Table 4.14: Initial Guess of the Mount Stiffness (N/m)

Mount	x	y	z
1	223667	44733	44733
2	170167	126050	48619
3	217167	434334	108583
4	232167	464334	116083

Table 4.15: Optimum Mount Stiffness (Case I)

	$k_x$	$k_y$	$k_z$
1	100	100	36437
2	100	100	26427
3	100	100	77636
4	100	100	46833



Table 4.16: Stiffness Matrix Showing Off-Diagonal Terms (Case I)

<b>4.00E+02</b>	0.00E+00	0.00E+00	0.00E+00	-9.24E+01	2.84E+01
0.00E+00	<b>4.00E+02</b>	0.00E+00	9.24E+01	0.00E+00	2.36E+01
0.00E+00	0.00E+00	<b>1.87E+05</b>	2.92E-04	-9.46E-04	0.00E+00
0.00E+00	9.24E+01	2.92E-04	<b>8.45E+03</b>	2.53E-03	7.33E+00
-9.24E+01	0.00E+00	-9.46E-04	2.53E-03	<b>1.23E+04</b>	-5.93E+00
2.84E+01	2.36E+01	0.00E+00	7.33E+00	-5.93E+00	<b>5.28E+01</b>

Table 4.17: Optimum Mount Stiffness (Case II)

	$k_x$	$k_y$	$k_z$	$\theta_1$	$\theta_2$	$\theta_3$
1	253873	36444	10928	-161.81	-57.67	47.57
2	221988	58054	1575	-178.88	55.46	-35.62
3	118594	499001	9737	-106.49	19.36	-78.72
4	135131	410392	12926	108.56	-135.85	169.58

Table 4.18: Stiffness Matrix Showing Off-Diagonal Terms (Case II)

<b>4.73E+05</b>	8.37E-03	-5.32E-03	-1.56E-02	-8.22E-03	2.01E-03
8.37E-03	<b>2.81E+05</b>	1.10E-02	-7.48E-03	5.86E-04	-9.95E-04
-5.32E-03	1.10E-02	<b>1.01E+06</b>	-6.43E-03	1.78E-02	1.50E-02
-1.56E-02	-7.48E-03	-6.43E-03	<b>3.10E+04</b>	2.49E-02	-5.95E-03
-8.22E-03	5.86E-04	1.78E-02	2.49E-02	<b>4.08E+04</b>	3.61E-02
2.01E-03	-9.95E-04	1.50E-02	-5.95E-03	3.61E-02	<b>2.65E+04</b>

Table 4.19: Optimum Mount Stiffness (Case III)

	$k_x$	$k_y$	$k_z$	$\theta_1$	$\theta_2$	$\theta_3$	x	y	z
1	255170	39646	7580	-150.39	47.95	-143.55	-0.32	-0.20	-0.16
2	221410	52800	1005	-173.77	22.53	-43.88	0.46	-0.38	-0.19
3	125570	52542	8132	-153.09	-60.25	-64.77	-0.29	0.24	-0.12
4	133770	408330	12438	104.30	-163.91	173.29	0.19	0.06	-0.24

Table 4.20: Stiffness Matrix Showing Off-Diagonal Terms (Case III)

<b>3.96E+05</b>	-6.74E-02	9.02E-02	1.20E-01	-1.65E-01	-1.09E-01
-6.74E-02	<b>2.78E+05</b>	1.37E-01	1.63E-01	-9.33E-02	-1.22E-01
9.02E-02	1.37E-01	<b>6.45E+05</b>	-8.82E-02	2.16E-02	-2.65E-02
1.20E-01	1.63E-01	-8.82E-02	<b>9.56E+03</b>	-1.40E-01	-4.42E-02
-1.65E-01	-9.33E-02	2.16E-02	-1.40E-01	<b>3.14E+04</b>	9.03E-02
-1.09E-01	-1.22E-01	-2.65E-02	-4.42E-02	9.03E-02	<b>3.28E+04</b>

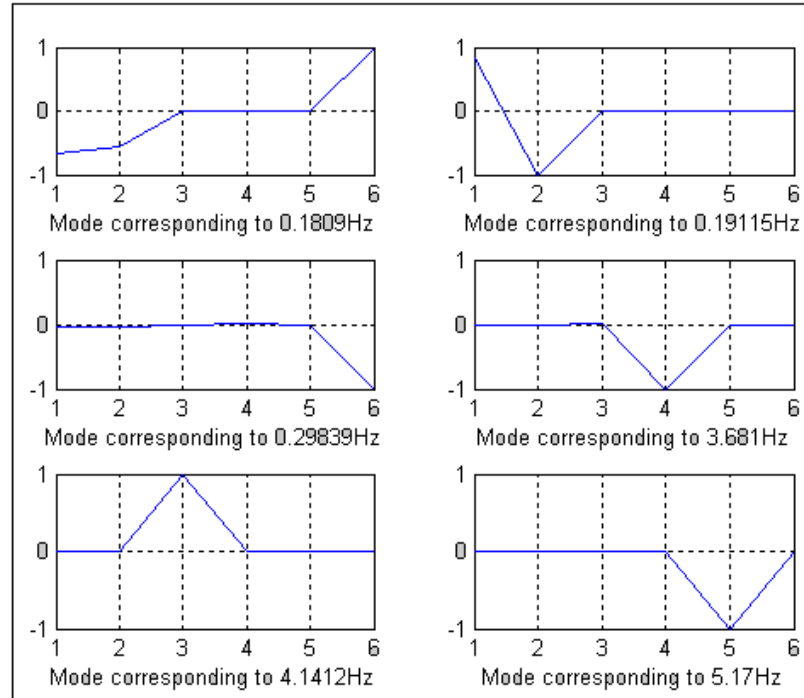


Figure 4.14: Decoupled Modes and the Corresponding Frequencies (Case I)

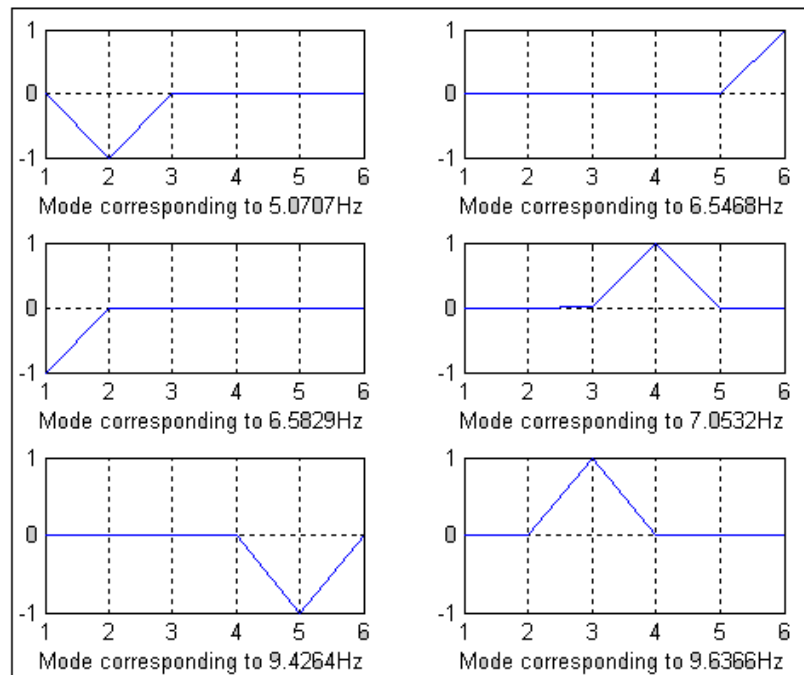


Figure 4.15: Decoupled Modes and the Corresponding Frequencies (Case II)

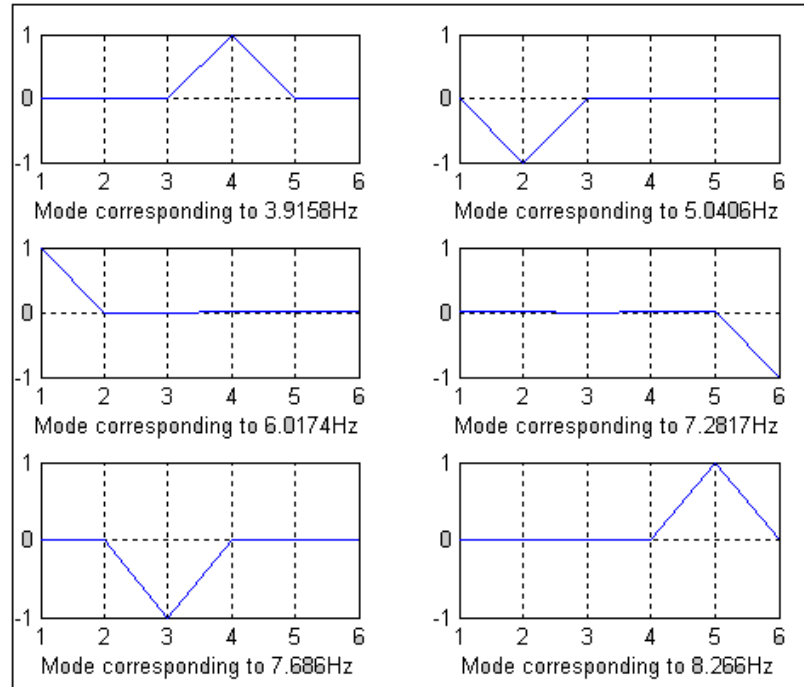


Figure 4.16: Decoupled Modes and the Corresponding Frequencies (Case III)

As can be seen from Fig. 4.14 through Fig. 4.16, the vibration modes are being decoupled. In the first case where the mount stiffness is the only variable, most of the modes were decoupled. In the second and third cases, where on top of mount stiffness, the mount orientations are also considered; all the modes are completely decoupled. This observation is in line with the previous findings that we have found in the earlier sections, which emphasize on the importance of mount orientation in achieving decoupling. These results are seen in Fig. 4.15 and Fig. 4.16 where it can be clearly seen that all the modes are decoupled nicely.

#### 4.5 Summary

This chapter presents different techniques that are used to characterize the engine mounting system. All of the techniques presented use the method of Sequential Quadratic Programming to solve the optimization problem. The SQP method is also introduced in

this chapter as well. The development of two different models of the mounting system is discussed herein. Both models are presented in detail where the equations of motion are described in detail. The first model is a simple six DOF powertrain model that is solved by minimizing the transmitted forces while finding the mount characteristics. The second model is a more comprehensive model that is used to better understand the vibration isolation in the motorcycle. The second model is solved in the same way as the first model. The second model is capable of capturing the effect of the shaking load, the road load or a combination of both loads. Two more techniques were used to characterize the mounting system. These techniques are, isolator inclining and vibration modes decoupling to achieve a complete decoupling of the vibration modes of the system.

## **Chapter 5 – Optimum Design of a Mount System for a V-Twin Engine**

This chapter discusses the V-Twin engine configuration that is commonly used in motorcycle applications. There are two sources of vibration that affect the performance of a motorcycle engine mount system; the first one is due to the shaking forces which are generated due to the engine imbalance in the moving parts inside the engine. This force is transmitted to the frame through the mounting system. The second force is due to the road loads which are caused by the irregularities in the road profile. These forces are transmitted to the frame through the tire patch. The road load could be periodic or non-periodic whereas the shaking load is periodic. Numerical examples are presented for solving the mounting system optimization problem when shaking forces and/or road loads are present.

### *5.1 Shaking Loads*

This chapter focuses on designing the most suitable mounting system that provides isolation against forces transmitted from the powertrain to the frame. It is known that force and motion isolation are the major problems that engineers encounter when designing an engine mount. Motorcycle engines contain reciprocating parts that produce shaking forces due to the movement of various parts of the engine. The main objective herein is to minimize these shaking forces. This objective is achieved by supporting the powertrain by using a resilient support or an isolator. The largest lumped mass that the vehicle carries is the powertrain, which is attached to the frame using rubber mounts. The mounting system that is used in these cases must ensure low vibration transmission from/into the engine. There are a lot of factors to consider when looking at the source of vibration, which could be internal or external or both. In this section, attention will

focused on the internal shaking forces which are created due to the engine imbalance (Paul, 1979). The shaking force is defined as the sum of the inertia and static forces that are transmitted to the frame through the mounting system (Kaul, 2006). Minimizing the transmitted loads from the engine to the frame is discussed as well in the literature (Tao, 2000) and (Snyman, 1995) which is considered in detail in Appendix D.

Before developing the expressions for shaking forces in a V-Twin engine, an analysis will be performed to develop expressions for shaking forces in a single cylinder engine.

### 5.1.1 Transmitted Shaking Loads

Figure 5.1 shows a schematic diagram of a single cylinder slider crank mechanism. The standard slider crank mechanism is the basic building block of virtually all internal combustion engines. Presented next is the position, velocity, acceleration and the forces analysis of the slider-crank mechanism. Let the crank radius be  $r$  and the connecting rod length be  $l$ . The crank angle is  $\theta$  and the angle that the connecting rod makes with the  $x$  axis is  $\phi$ , the crank rotates at a constant speed  $\omega$  then:

$$q = r \sin \theta = l \sin \phi \quad (5.1)$$

$$\theta = \omega t \quad (5.2)$$

$$\sin \phi = \frac{r}{l} \sin \omega t \quad (5.3)$$

$$s = r \cos \omega t \text{ and } u = l \cos \phi \quad (5.4)$$

The distance  $x$  that is measured from the pivot point  $O$  to the slider at point  $B$  is given as follows:

$$x = s + u = r \cos \omega t + l \cos \phi \quad (5.5)$$

$$\cos \phi = \sqrt{1 - \sin^2 \phi} = \sqrt{1 - \left(\frac{r}{l} \sin \omega t\right)^2} \quad (5.6)$$

$$x = r \cos \omega t + l \sqrt{1 - \left(\frac{r}{l} \sin \omega t\right)^2} \quad (5.7)$$

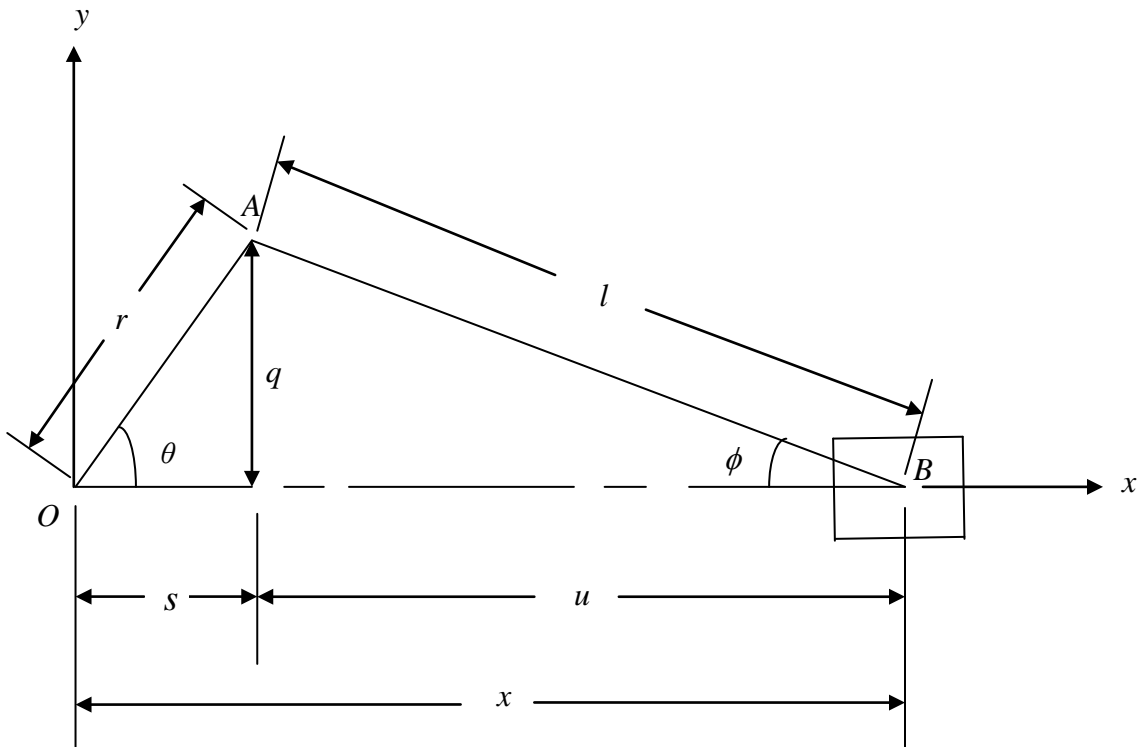


Figure 5.1: Slider Crank Mechanism

The expression given by Eq. (5.7) gives the position of the piston along the x axis as a function of crank angle  $\theta$ . If a derivative of Eq. (5.7) is taken once with respect to time, the velocity of the piston will be determined as shown below:

$$\dot{x} = -r\omega \left[ \sin \omega t + \frac{r}{2l} \frac{\sin 2\omega t}{\sqrt{1 - \left(\frac{r}{l} \sin \omega t\right)^2}} \right] \quad (5.8)$$



If a derivative of the piston velocity is taken once with respect to time, the piston acceleration is obtained as shown below:

$$\ddot{x} = -r\omega^2 \left\{ \cos \omega t - \frac{r[l^2 (1 - 2\cos^2 \omega t) - r^2 \sin^4 \omega t]}{[l^2 - (r \sin \omega t)^2]^{\frac{3}{2}}} \right\} \quad (5.9)$$

In the velocity expression shown in Eq. (5.8) and the acceleration expression shown in Eq. (5.9), a steady state solution is considered where it is assumed that the crank speed  $\omega$  is constant.

Using the binomial theorem, an approximate expression for the position, velocity and acceleration of the piston can be written as follows:

$$\begin{aligned} x &\cong l - \frac{r^2}{4l} + r \left( \cos \omega t + \frac{r}{4l} \cos 2\omega t \right) \\ \dot{x} &\cong -r\omega \left( \sin \omega t + \frac{r}{2l} \sin 2\omega t \right) \\ \ddot{x} &\cong -r\omega^2 \left( \cos \omega t + \frac{r}{l} \cos 2\omega t \right) \end{aligned} \quad (5.10)$$

The inertia force  $F_i$  is the sum of the inertia forces at points  $A$  and  $B$  on the slider crank mechanism.

$$F_i = m_A a_A + m_B a_B \quad (5.11)$$

In Eq. (5.11), the acceleration term  $a_B$  is the acceleration of the piston which is given in Eq. (5.10). The acceleration term  $a_A$  could be found by taking the second derivative of the position vector at point  $A$  with respect to time. The position vector that describes the location of point  $A$  is given as follows:

$$R_A = r \cos \omega t \hat{i} + r \sin \omega t \hat{j} \quad (5.12)$$

Differentiate the position vector given in Eq. (5.12) twice with respect to time and an expression for the acceleration at point  $A$  is achieved as follows:

$$a_A = [-r\alpha \sin \omega t - r\omega^2 \cos \omega t] \hat{i} + [r\alpha \cos \omega t - r\omega^2 \sin \omega t] \hat{j} \quad (5.13)$$

In Eq. (5.12),  $\hat{i}$  and  $\hat{j}$  are unit vectors defined along the  $x$  and  $y$  axis. The inertia force along the  $x$  and  $y$  axis are given as follows:

$$\begin{aligned} F_{ix} &= -(m_A + m_B) r\omega^2 \cos \omega t - m_B \frac{r^2 \omega^2}{l} \cos 2\omega t \\ &\quad - (m_A + m_B) r\alpha \sin \omega t - m_B \frac{r^2 \alpha}{2l} \sin 2\omega t \\ F_{iy} &= m_A r\alpha \cos \omega t - m_A r\omega^2 \sin \omega t \end{aligned} \quad (5.14)$$

In Eq. (5.14),  $m_A$  and  $m_B$  are the equivalent rotating and reciprocating masses respectively. The shaking force is  $F_s = -F_i$ . It is fully described taking into account the equivalent balancing masses as shown below:

$$\begin{aligned} F_{sx} &= (m_A + m_B - m_{cb}) r\omega^2 \cos \omega t + m_B \frac{r^2 \omega^2}{l} \cos 2\omega t \\ &\quad + (m_A + m_B - m_{cb}) r\alpha \sin \omega t + m_B \frac{r^2 \alpha}{2l} \sin 2\omega t \\ F_{sy} &= (m_A - m_{cb}) r\omega^2 \sin \omega t - (m_A - m_{cb}) r\alpha \cos \omega t \end{aligned} \quad (5.15)$$

In Eq. (5.15),  $F_{sx}$  and  $F_{sy}$  denote the net shaking forces in the  $x$  and  $y$  directions respectively and  $m_{cb}$  is the equivalent mass. These shaking forces result from a single cylinder.

Presented next is the development of shaking force expressions for a V-twin engine shown in Fig. 5.2. The shaking force analysis that was done on a single cylinder engine is generalized to accommodate the V-twin engine and the shaking forces will be computed along the global X-Y coordinate system.

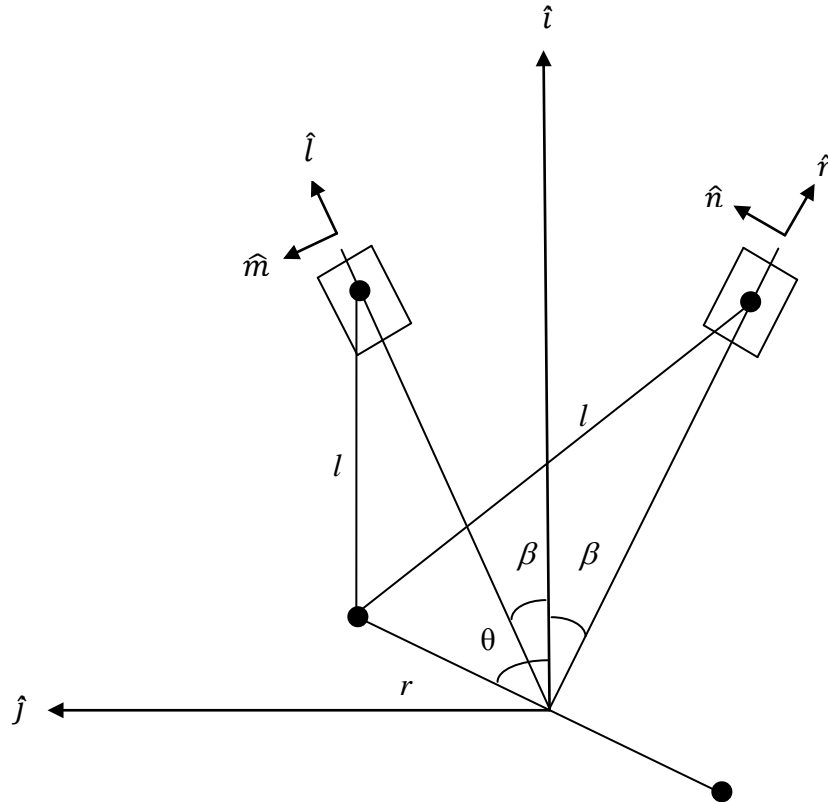


Figure 5.2: V-twin Engine Configuration.

In order to determine the shaking forces for the V-Twin engine, the shaking force expression for single cylinder engine given in Eq. (5.15) are used. The forces in each bank will be computed separately. Then by combining the corresponding terms of the shaking forces in each bank, the total shaking forces and moments can be computed in the global X-Y coordinate system for the V-Twin engine.

The shaking force in the left cylinder (bank)  $(F_s)_{left}$  is given as follows:

$$\begin{aligned}
(F_s)_{left} = & \left\{ (m_A + m_B)r\omega^2 \cos(\theta - \beta) - m_{cb1}r_1\omega^2 \cos(\theta - \beta) \right. \\
& + m_B \frac{r^2\omega^2}{l} \cos 2(\theta - \beta) + (m_A + m_B)r\alpha \sin(\theta - \beta) \\
& \left. - m_{cb1}r_1\alpha \sin(\theta - \beta) + m_B \frac{r^2\alpha}{2l} \sin 2(\theta - \beta) \right\} \hat{l} \\
& + \{ m_A r \omega^2 \sin(\theta - \beta) - m_{cb1} r_1 \omega^2 \sin(\theta - \beta) - m_A r \alpha \cos(\theta - \beta) \\
& + m_{cb1} r_1 \alpha \cos(\theta - \beta) \} \hat{m} \tag{5.16}
\end{aligned}$$

The shaking force in the right cylinder (bank)  $(F_s)_{right}$  is given as follows:

$$\begin{aligned}
(F_s)_{right} = & \left\{ (m_A + m_B)r\omega^2 \cos(\theta + \beta) - m_{cb2}r_2\omega^2 \cos(\theta + \beta) \right. \\
& + m_B \frac{r^2\omega^2}{l} \cos 2(\theta + \beta) + (m_A + m_B)r\alpha \sin(\theta + \beta) \\
& \left. - m_{cb2}r_2\alpha \sin(\theta + \beta) + m_B \frac{r^2\alpha}{2l} \sin 2(\theta + \beta) \right\} \hat{r} \\
& + \{ m_A r \omega^2 \sin(\theta + \beta) - m_{cb2} r_2 \omega^2 \sin(\theta + \beta) - m_A r \alpha \cos(\theta + \beta) \\
& + m_{cb2} r_2 \alpha \cos(\theta + \beta) \} \hat{n} \tag{5.17}
\end{aligned}$$

In Eq. (5.16) and Eq. (5.17),  $\hat{r}$  and  $\hat{n}$  are the unit vectors along the  $x$  and  $y$  axis of the local coordinate system for the right cylinder.  $\hat{l}$  and  $\hat{m}$  are the unit vectors along the  $x$  and  $y$  local coordinate system for the left cylinder.  $m_{cb1}$  and  $m_{cb2}$  are the equivalent masses at distances  $r_1$  and  $r_2$  for the left and right banks respectively. Combining the shaking forces for the right and left cylinders in their corresponding local coordinate system and transferring them into the global coordinate system  $X$ - $Y$  to come up with the overall shaking forces of the V-twin engine yields:

$$\begin{aligned}
F_{sx} = \sin\beta \left\{ 2(m_A + m_B)r\omega^2 \sin\theta\sin\beta - 2(m_A + m_B)r\alpha \cos\theta\sin\beta \right. \\
+ 2m_B \frac{r^2\omega^2}{l} \sin 2\theta\sin 2\beta - m_B \frac{r^2\alpha}{l} \cos 2\theta\sin 2\beta \left. \right\} \\
+ \omega^2 \sin\beta \{ m_{cb2}r_2 \cos(\theta + \beta) - m_{cb1}r_1 \cos(\theta - \beta) \} \\
+ \alpha \sin\beta \{ m_{cb2}r_2 \sin(\theta + \beta) - m_{cb1}r_1 \sin(\theta - \beta) \} \\
+ \cos\beta \{ 2m_A r\omega^2 \sin\theta\cos\beta - 2m_A r\alpha \cos\theta\cos\beta \} \\
+ \alpha \cos\beta \{ m_{cb1}r_1 \cos(\theta - \beta) + m_{cb2}r_2 \cos(\theta + \beta) \} \\
- \omega^2 \cos\beta \{ m_{cb1}r_1 \sin(\theta - \beta) + m_{cb2}r_2 \sin(\theta + \beta) \} \quad (5.18)
\end{aligned}$$

$$\begin{aligned}
F_{sy} = \cos\beta \left\{ 2(m_A + m_B)r\omega^2 \cos\theta\cos\beta + 2(m_A + m_B)r\alpha \sin\theta\cos\beta \right. \\
+ 2m_B \frac{r^2\omega^2}{l} \cos 2\theta\cos 2\beta + m_B \frac{r^2\alpha}{l} \sin 2\theta\cos 2\beta \left. \right\} \\
- \omega^2 \cos\beta \{ m_{cb1}r_1 \cos(\theta - \beta) + m_{cb2}r_2 \cos(\theta + \beta) \} \\
- \alpha \cos\beta \{ m_{cb1}r_1 \sin(\theta - \beta) + m_{cb2}r_2 \sin(\theta + \beta) \} \\
+ \sin\beta \{ 2m_A r\omega^2 \cos\theta\sin\beta + 2m_A r\alpha \sin\theta\sin\beta \} \\
+ \alpha \sin\beta \{ m_{cb2}r_2 \cos(\theta + \beta) - m_{cb1}r_1 \cos(\theta - \beta) \} \\
+ \omega^2 \sin\beta \{ m_{cb1}r_1 \sin(\theta - \beta) - m_{cb2}r_2 \sin(\theta + \beta) \} \quad (5.19)
\end{aligned}$$

The shaking forces shown in Eq. (5.18) and Eq. (5.19) can be employed to find the shaking moments by multiplying each term by the moment arm. The moments exist within each bank and their vectors will be orthogonal to the cylinder planes. For the right bank, a moment unit vector  $\hat{n}$  is defined which is perpendicular to the unit vector  $\hat{r}$ .

Similarly, a moment unit vector  $\hat{m}$  is defined which is perpendicular to the unit vector  $\hat{l}$  for the left bank as shown in Fig. 5.2.

The shaking moment in the left cylinder (bank)  $(M_s)_{left}$  is given as follows:

$$(M_s)_{left} = \left\{ (m_A + m_B)r\omega^2 \cos(\theta - \beta) - m_{cb1}r_1\omega^2 \cos(\theta - \beta) \right. \\ \left. + m_B \frac{r^2\omega^2}{l} \cos 2(\theta - \beta) + (m_A + m_B)r\alpha \sin(\theta - \beta) \right. \\ \left. - m_{cb1}r_1\alpha \sin(\theta - \beta) + m_B \frac{r^2\alpha}{2l} \sin 2(\theta - \beta) \right\} z \hat{m} \quad (5.20)$$

The shaking moment in the right cylinder (bank)  $(M_s)_{right}$  is given as follows:

$$(M_s)_{right} = \left\{ (m_A + m_B)r\omega^2 \cos(\theta + \beta) - m_{cb2}r_2\omega^2 \cos(\theta + \beta) \right. \\ \left. + m_B \frac{r^2\omega^2}{l} \cos 2(\theta + \beta) + (m_A + m_B)r\alpha \sin(\theta + \beta) \right. \\ \left. - m_{cb2}r_2\alpha \sin(\theta + \beta) + m_B \frac{r^2\alpha}{2l} \sin 2(\theta + \beta) \right\} z \hat{n} \quad (5.21)$$

In Eq. (5.20) and Eq. (5.21),  $z$  is the moment arm. Combining the shaking moments for the right and left cylinders that have been shown Eq. (5.20) and Eq. (5.21) in their corresponding local coordinate system and transferring them into the global coordinate system  $X-Y$  to come up with the overall shaking moments for the V-twin engine yields:

$$M_{sx} = \cos\beta \left\{ 2(m_A + m_B)r\omega^2 \cos\theta \cos\beta + 2m_B \frac{r^2\omega^2}{l} \cos 2\theta \cos 2\beta \right. \\ \left. + 2(m_A + m_B)r\alpha \sin\theta \cos\beta + m_B \frac{r^2\alpha}{l} \sin 2\theta \cos 2\beta \right\} . z \\ - \omega^2 \cos\beta \{ m_{cb1}r_1 \cos(\theta - \beta) + m_{cb2}r_2 \cos(\theta + \beta) \} . z \\ - \alpha \cos\beta \{ m_{cb1}r_1 \sin(\theta - \beta) + m_{cb2}r_2 \sin(\theta + \beta) \} . z \quad (5.22)$$

$$\begin{aligned}
M_{sy} = \sin\beta & \left\{ -2(m_A + m_B)r\omega^2 \sin\theta\sin\beta - 2m_B \frac{r^2\omega^2}{l} \sin 2\theta\sin 2\beta \right. \\
& + 2(m_A + m_B)r\alpha \cos\theta\sin\beta + m_B \frac{r^2\alpha}{l} \cos 2\theta\sin 2\beta \left. \right\} .z \\
& + \omega^2 \sin\beta \{ m_{cb1}r_1 \cos(\theta - \beta) - m_{cb2}r_2 \cos(\theta + \beta) \} .z \\
& + \alpha \sin\beta \{ m_{cb1}r_1 \sin(\theta - \beta) - m_{cb2}r_2 \sin(\theta + \beta) \} .z \quad (5.23)
\end{aligned}$$

The shaking torque on one cylinder is calculated using the inertia force acting on the piston  $F_{i14}$  multiplied by the distance  $x$  from the piston at point  $B$  to the origin of the coordinate system at point  $O$  as shown in Fig. 5.1. The free body diagram of the piston showing all the acting forces are shown below in Fig. 5.3.

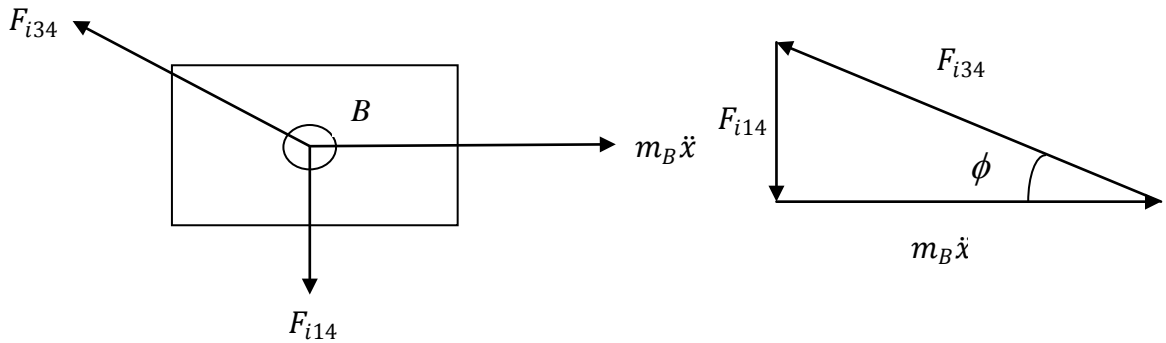


Figure 5.3: Free Body Diagram of the Piston

$$\begin{aligned}
T_s &= (F_{i14} * x)\hat{k} \\
&= m_B \ddot{x} \tan\phi * x \quad (5.24)
\end{aligned}$$

In Eq. (5.24),  $\ddot{x}$  is the piston acceleration represented in Eq. (5.10). Substitute the piston acceleration expressed in Eq. (5.10) into Eq. (5.24), the shaking torque will be expressed as follows:

$$T_s = m_B \left[ -r\omega^2 \left( \cos\omega t + \frac{r}{l} \cos 2\omega t \right) - r\alpha \left( \sin\omega t + \frac{r}{2l} \sin 2\omega t \right) \right] \tan\phi * l$$

$$- \frac{r^2}{4l} + r \left[ \cos\omega t + \frac{r}{4l} \cos 2\omega t \right] \quad (5.25)$$

$$\tan\phi \approx \frac{r}{l} \sin\omega t \left( 1 + \frac{r^2}{2l^2} \sin^2\omega t \right) \quad (5.26)$$

In Eq. (5.25),  $x$  is described in Eq. (5.10) and  $\hat{k}$  is unit vector acting along the  $z$  axis which is perpendicular to the plane of the slider crank mechanism shown in Fig. 5.1. Assume that the angular acceleration  $\alpha$  is zero and approximating  $\tan \phi$  as shown in Eq. (5.26) we get an expression for the shaking torque for both the left and the right banks.

The shaking torque in the left bank  $(T_s)_{left}$  is as follows:

$$(T_s)_{left} = \frac{1}{2} m_B r^2 \omega^2 \left[ \frac{r}{2l} \sin(\theta - \beta) - \sin 2(\theta - \beta) \right. \\ \left. - \frac{3r}{2l} \sin 3(\theta - \beta) \right] \hat{k} \quad (5.27)$$

The shaking torque in the right bank  $(T_s)_{right}$  is as follows:

$$(T_s)_{right} = \frac{1}{2} m_B r^2 \omega^2 \left[ \frac{r}{2l} \sin(\theta + \beta) - \sin 2(\theta + \beta) \right. \\ \left. - \frac{3r}{2l} \sin 3(\theta + \beta) \right] \hat{k} \quad (5.28)$$

The combined shaking torque  $T_s$  due to shaking torque from both left and right banks is the algebraic sum of both  $(T_s)_{left}$  and  $(T_s)_{right}$  shown below:

$$T_s = \frac{1}{2} m_B r^2 \omega^2 \left[ \frac{r}{l} \sin\theta \cos\beta - 2\sin 2\theta \cos 2\beta - \frac{3r}{l} \sin 3\theta \cos 3\beta \right] \hat{k} \quad (5.29)$$

The final shaking force vector is a  $6 \times 1$  vector shown below:



$$F_s = [F_{sx} \ F_{sy} \ F_{sz} \ M_{sx} \ M_{sy} \ T_s]^T \quad (5.30)$$

### 5.1.2 Numerical Example

The example discussed herein is based on the six DOF model presented in section 3.4.1 and the optimization problem of minimizing the transmitted load was formulated in section 4.2. This example is a continuation of the example presented in section 4.2.2.1 where the shaking force is the only input load. The input load is calculated at different steady speeds of 800 rpm, 3000 rpm and 5000 rpm. The powertrain is supported by four identical circular cross section elastomeric mounts. The layout of this system is shown in Fig. 4.4, and the objective function is presented in Eq. (4.38). Mount parameters, which consists of mount stiffness, mount locations and mount orientations are compiled to form the design vector. The powertrain mass and inertia tensor and the lower and upper bounds used for the design variables and the limit that is imposed on the design variables by constraining the deflection of the powertrain are the same as those imposed in the example presented in section 4.2.2.1.

The optimization problem is solved using the SQP technique that employs a function (fmincon) to minimize the value of the objective function. The force vector corresponding to different engine steady speeds is shown in Table 5.1. The design variables resulting from the optimization process are shown in Table 5.2 to Table 5.4. The resulting force plots in the  $x$  and  $y$  directions for different engine speeds are shown in Fig. 5.4 to Fig. 5.6 and the resulting torque plots for different engine speeds are shown in Fig. 5.7 to Fig. 5.9.

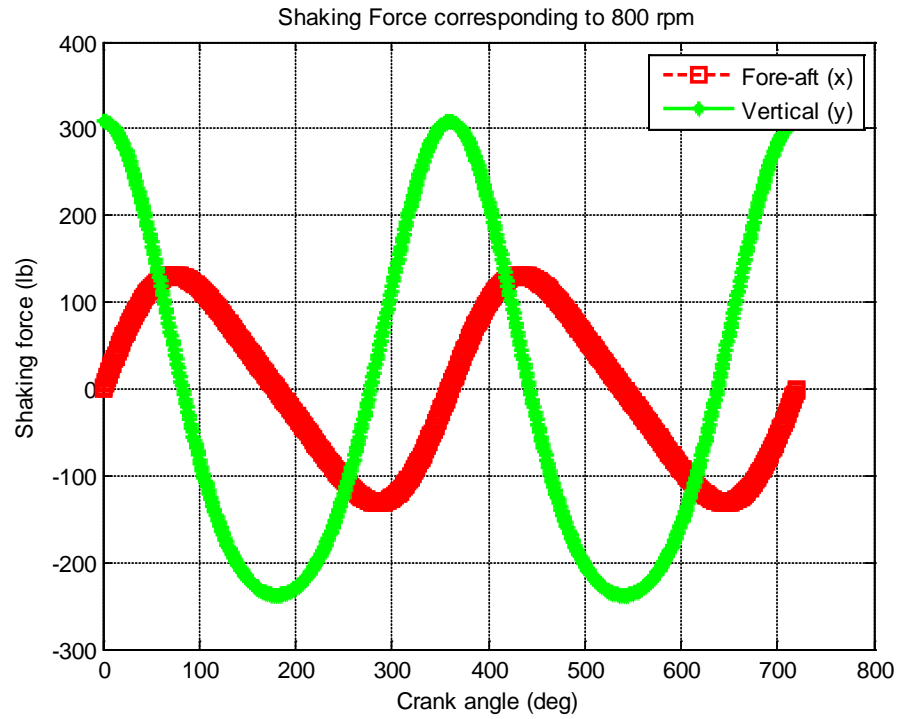


Figure 5.4: Shaking Force in the x and y Directions (800 rpm)

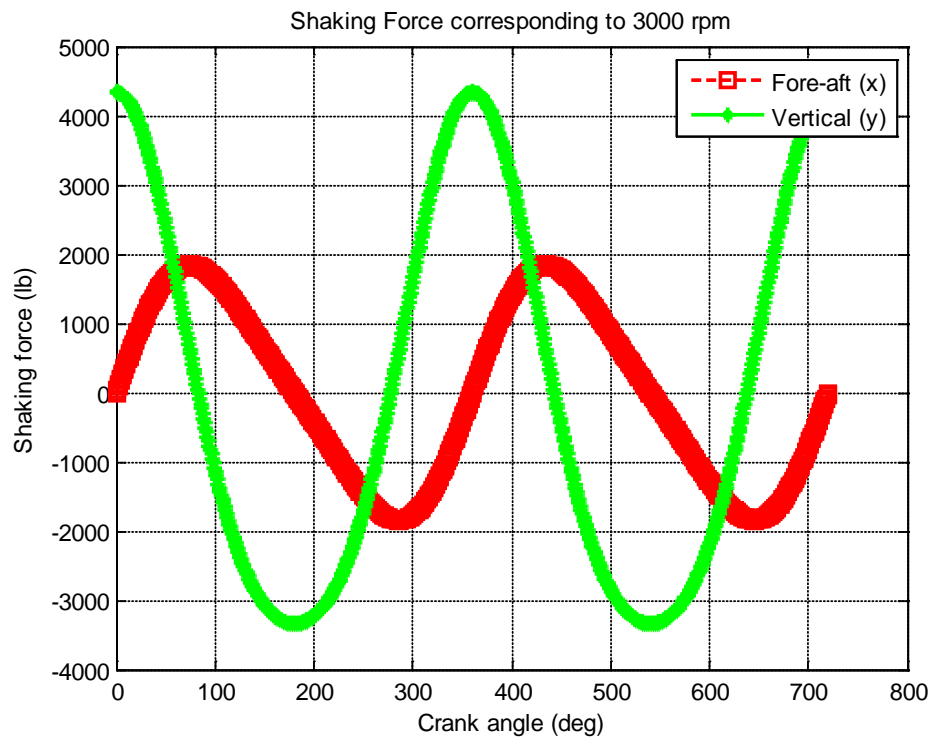


Figure 5.5: Shaking Force in the x and y Directions (3000 rpm)

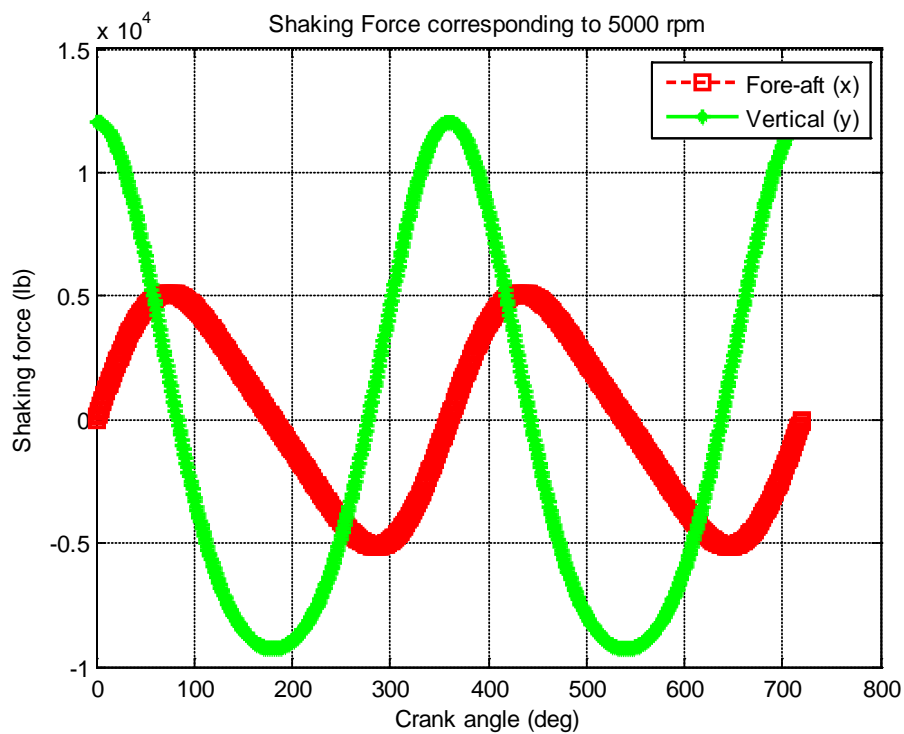


Figure 5.6: Shaking Force in the x and y Directions (5000 rpm)

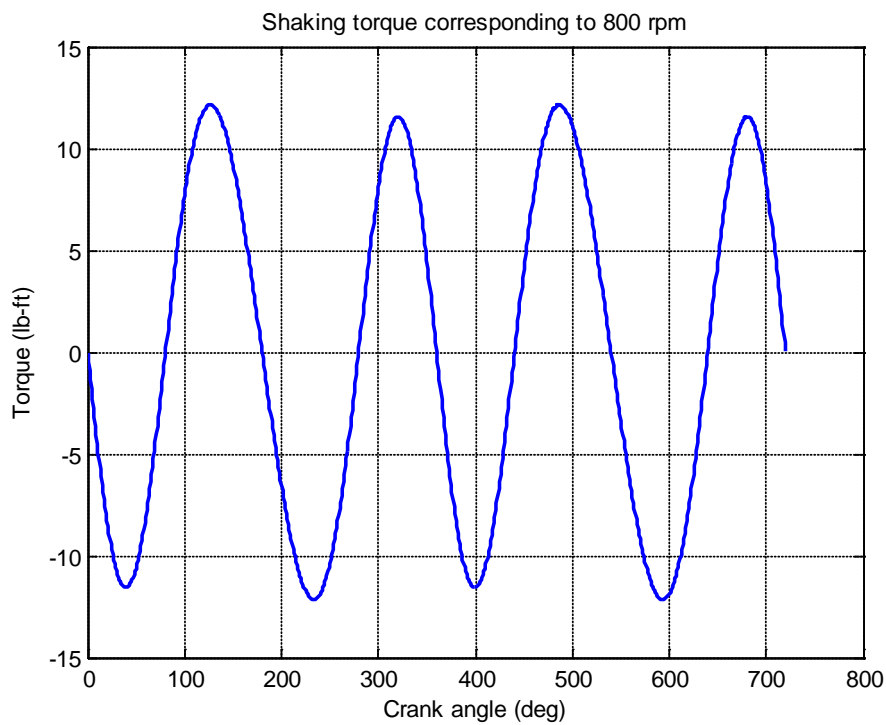


Figure 5.7: Shaking Torque (800 rpm)

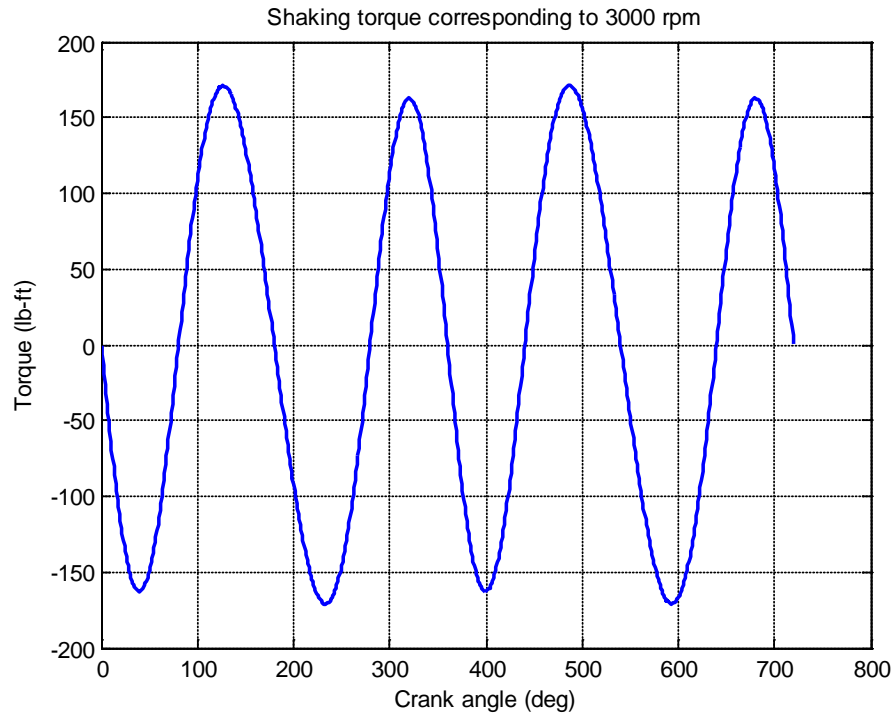


Figure 5.8: Shaking Torque (3000 rpm)

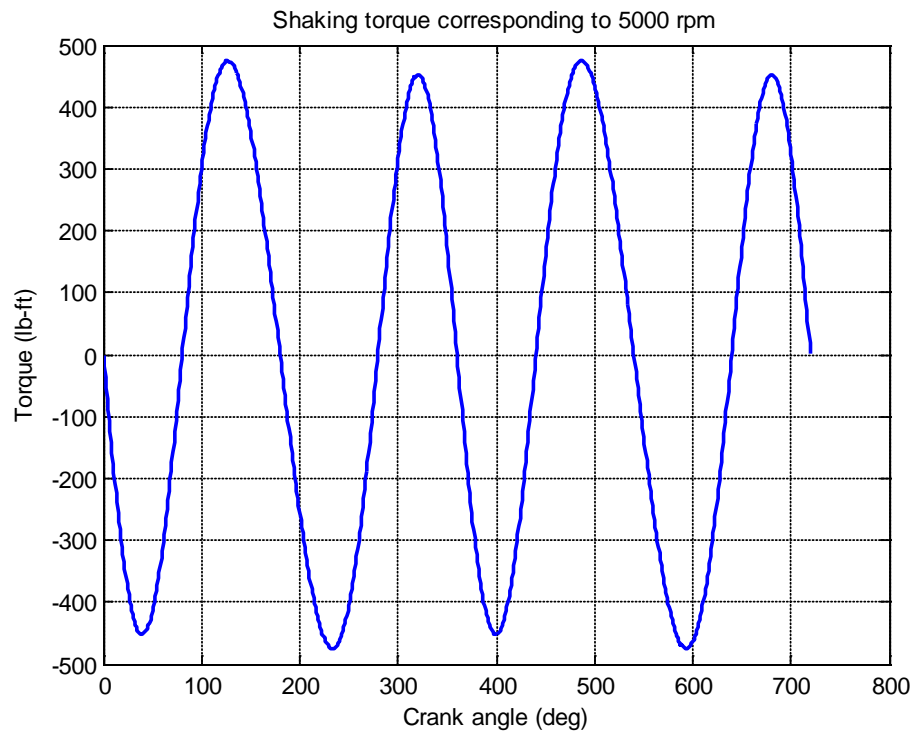


Figure 5.9: Shaking Torque (5000 rpm)

Table 5.1: Shaking Force Vector at Different Speeds

$\omega$ (rpm)	$F_x$	$F_y$	$F_z$	$M_x$	$M_y$	T
	(lb)				(lb.ft)	
800	131.12	308.82	0	0	0	12.15
3000	1843.87	4342.79	0	0	0	170.89
5000	5121.87	12063.3	0	0	0	474.70

Table 5.2: Optimization Results for the Shaking Force Vector Corresponding to 800 rpm

	Load Transmitted	Mount Stiffness (lb/in)		
	(lb)	x	y	z
Initial Guess	412.48	475	475	7500
Optimized Design	188.81	5000	5000	7585.3

Table 5.3: Optimization Results for the Shaking Force Vector Corresponding to 3000 rpm

	Load Transmitted	Mount Stiffness (lb/in)		
	(lb)	x	y	z
Initial Guess	815.49	475	475	7500
Optimized Design	247.18	1728	1728	7993.6

Table 5.4: Optimization Results for the Shaking Force Vector Corresponding to 5000 rpm

	Load Transmitted	Mount Stiffness (lb/in)		
	(lb)	x	y	z
Initial Guess	448.19	475	475	7500
Optimized Design	259.83	1278.2	1278.2	7515.7

As can be seen from the plots shown above, the forces in the  $x$  and  $y$  directions as well as the shaking torque exhibit a periodic behavior. It is clear from Table 5.1 that the value of the forces and moments increase with the increase of the engine operating speed. Table 5.2 through Table 5.4 shows the optimum stiffness values for the mounting system. The results are consistent with the results found in section 4.2.2.1 where the stiffness along the  $z$ -axis was seen to have no influence on the objective function value and thus did not deviate much from the starting guess value whereas the stiffness values in the  $x$  and  $y$  direction do change significantly. This is due to the fact the force transmitted to the frame is less sensitive to the stiffness in the  $z$ -direction.

## 5.2 Road Loads

In this section, the effect of external loads on the mounting system is investigated. One of the main problems that engineers encounter in vibration isolation is the problem of motion isolation. This problem is seen in the case of external loads that are transmitted to the engine. These loads which are due to the irregularities of the road profile are transmitted to the frame through the tire patch. Two different road profiles are investigated in this work with one road profile which is periodic while the other road

profile is non-periodic. The main goal is to come up with an appropriate mounting system that minimizes the transmission of these external loads.

### 5.2.1 Transmitted Road Loads

The road loads are due to irregularities in the road profile which could be periodic or non-periodic. These road profiles are analyzed for a specific displacement functions in which the frequency content is analyzed. For the periodic profiles, the frequency content is obtained by using the Fourier series expansion of the displacement function. For the non-periodic profiles, it's obtained using the Fourier transform. Herein, the Fourier series coefficient and the frequency content are obtained using the Fast Fourier Transforms (FFT) (Chen, 2001). The input force resulting from a certain road profile is determined as follows:

$$F_y = kx + c\dot{x} \quad (5.31)$$

In Eq. (5.31),  $F_y$  is the vertical component of the force that is transmitted through the tire patch due to the displacement  $x$  and the velocity  $\dot{x}$  as a result of the road profile change.  $k$  and  $c$  are the stiffness and damping of the rear wheel in the  $y$ -direction.

The continuous time Fourier series (CTFS) for a periodic road profile is represented as follows:

$$x(t) = \sum_{m=-\infty}^{\infty} c_m e^{jm\omega_o t}; \text{ where } \omega_o = \frac{2\pi}{P} \quad (5.32)$$

In Eq. (5.32),  $c_m$  represents the Fourier series coefficients and are determined as follows:

$$c_m = \frac{1}{P} \int_{-P/2}^{P/2} x(t) e^{-jm\omega_o t} dt \quad (5.33)$$

In Eq. (5.33),  $P$  is the fundamental period of the displacement function  $x(t)$  that corresponds to the fundamental frequency  $\omega_o$ . On the other hand, the discrete time Fourier series (DTFS) is represented for the discrete displacement function as follows:

$$x[n] = x(nT) = \sum_{m=\langle N \rangle} c_{md} e^{jm \omega_o nT} \quad (5.34)$$

where  $\omega_o = 2\pi/NT$  and  $c_{md}$  are the Fourier series coefficients which are determined as follows:

$$c_{md} = \frac{1}{N} \sum_{n=0}^{N-1} x[n] e^{-jm \omega_o nT} \quad (5.35)$$

In Eq. (5.34) and Eq. (5.35),  $\omega_o$  is the fundamental frequency and  $T$  is the sampling period. The DTFS coefficients can be determined using Eq. (5.36), if the band limited displacement function  $x(t)$  and an appropriate sampling period  $T$  is chosen using FFT.

$$c_{md} = \frac{X[m]}{N} \quad (5.36)$$

In Eq. (5.36),  $X[m]$  is the FFT of  $x[n]$  and  $N$  is the number of terms of  $x[n]$  used to compute the FFT.

The continuous time Fourier transform (CTFT) of the displacement function is given in Eq. (5.37) and the Discrete time Fourier transform (DTFT) is given in Eq. (5.38) below.

$$X(\omega) = \int_{-\infty}^{\infty} x(t) e^{-j\omega t} dt \quad (5.37)$$

$$X_d(\omega) = \sum_{n=-\infty}^{\infty} x(nT) e^{-j\omega nT} \quad (5.38)$$



In Eq. (5.37) and Eq. (5.38),  $X(\omega)$  is the spectrum of  $x(t)$  which can be used for periodic and non-periodic displacement functions.

### 5.2.2 Numerical Example

The example presented herein discusses the presence of both the shaking loads and the road loads. The input load vector is a linear combination of the shaking loads and the road loads in which the shaking loads are evaluated at a steady engine speed of 4000 rpm. The example is a continuation for the example presented in section 4.2.3.2. The optimization problem is formulated such that the mount parameters which consist of mount stiffness, location and orientation are compiled to form the vector of design variables. The layout of the problem considered in this example is shown in Fig. 4.4 and all the data are presented in section 4.2.3.2.

The optimization problem is solved using the SQP technique that employs a function (fmincon) to minimize the value of the objective function. Two different road profiles are examined in this example separately in which one is periodic (Profile #1) and the other one is non-periodic (Profile #2). Both of the road profiles along with their displacement functions and their corresponding magnitude spectrum and their reconstructed plots are presented in Fig. 5.10 to Fig. 5.15.

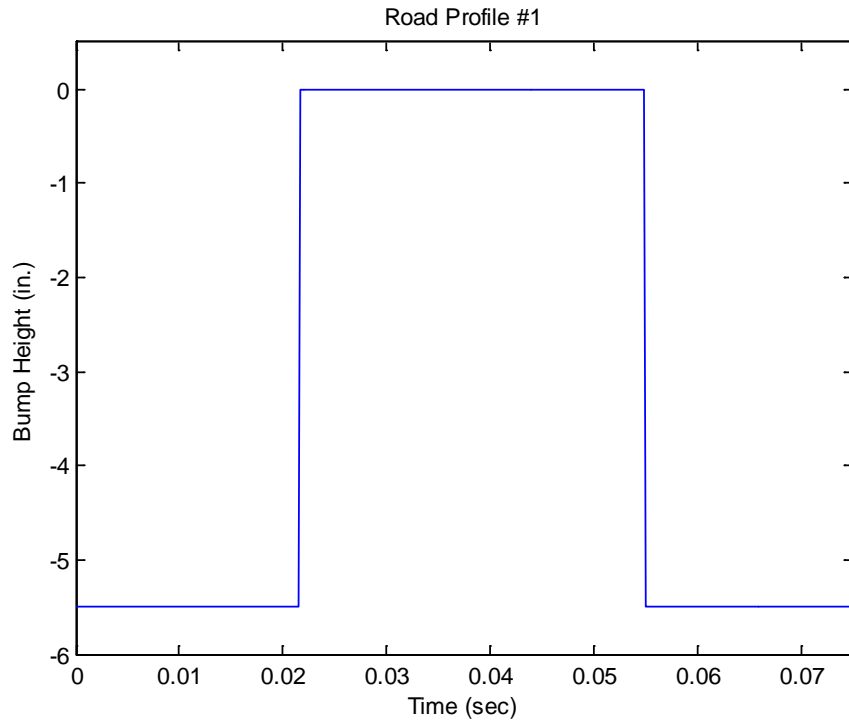


Figure 5.10: Road Profile #1

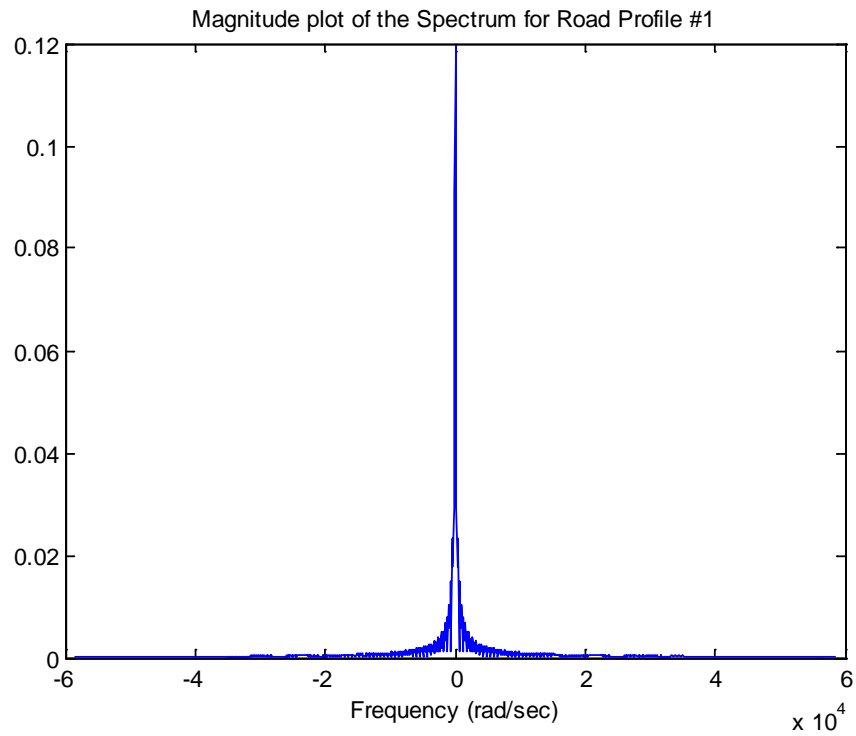


Figure 5.11: Magnitude Plot of the Spectrum for Road Profile #1

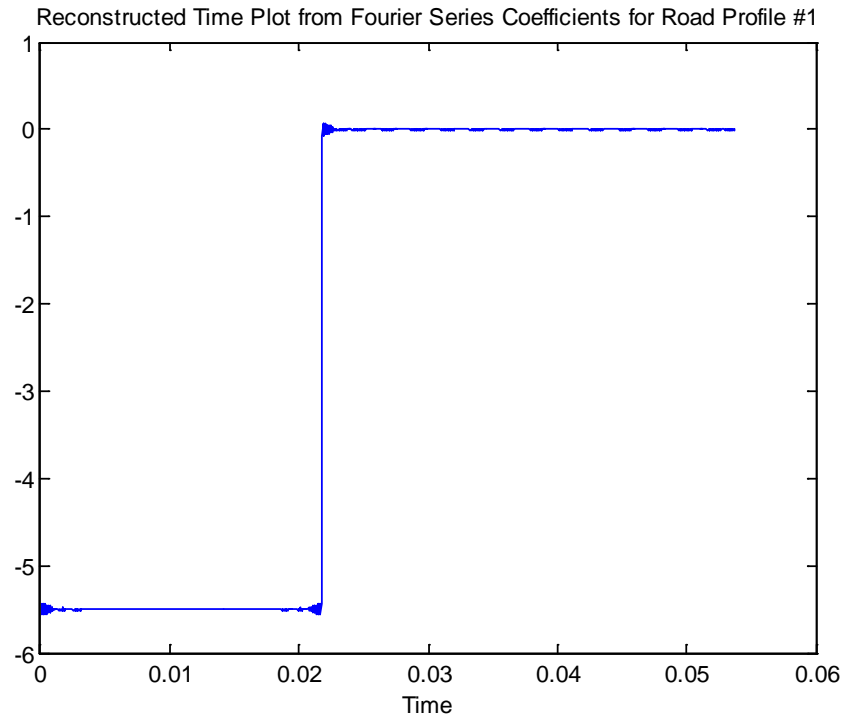


Figure 5.12: Reconstructed Time Plot for Road Profile #1

Figure 5.13 shows road profile #2. This road profile is non-periodic with bump height of 3.5 in. The time displacement plot is shown in Fig. 5.13. The magnitude plot of the spectrum and the reconstructed plot are shown in Fig. 5.14 and Fig. 5.15 respectively.

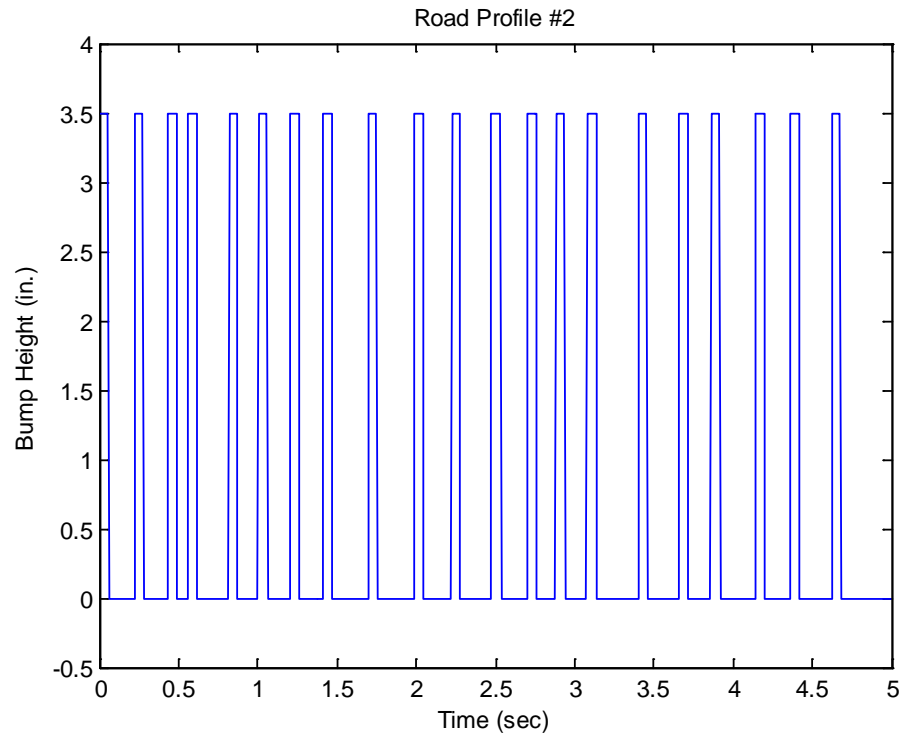


Figure 5.13: Road Profile #2

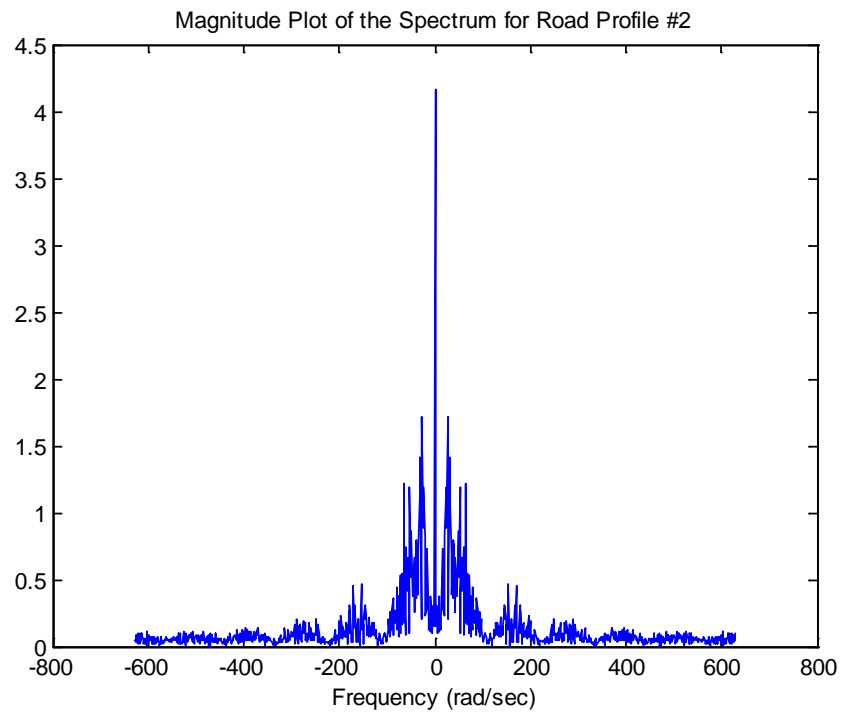


Figure 5.14: Magnitude Plot of the Spectrum of Road Profile #2

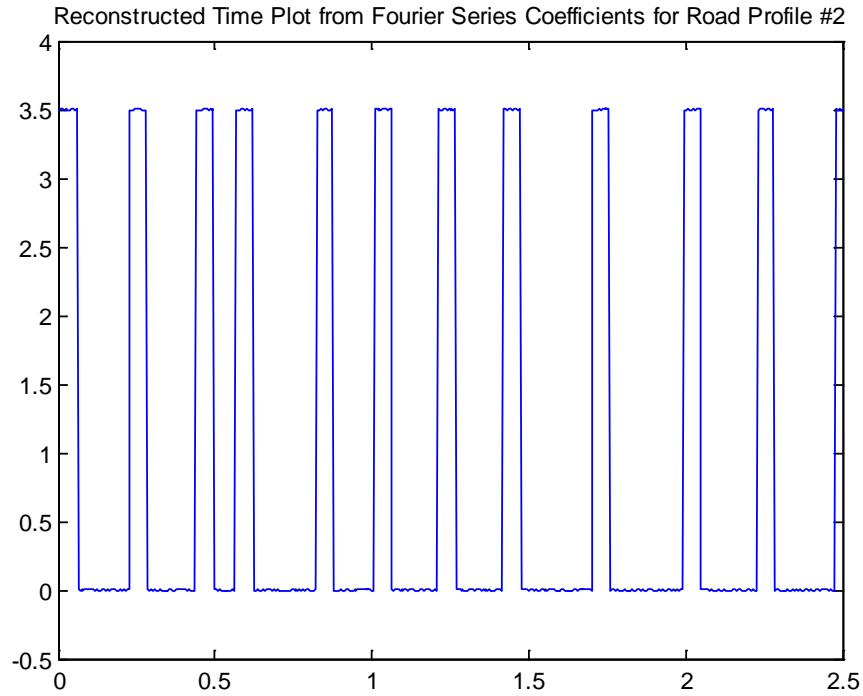


Figure 5.15: Reconstructed Time Plot for Road Profile #2

The design variables resulting from the optimization process are shown in Table 5.5 and Table 5.7, meanwhile the optimum mount location and orientation for both load profiles are shown in Table 5.6 and Table 5.8.

Table 5.5: Optimization Results for Road Profile #1

	Load Transmitted	Mount Stiffness (lb/in)		
	(lb)	x	y	z
Initial Guess	110.40	475	475	2400
Optimized Design	60.01	2336.5	2336.5	2344.8

Table 5.6: Optimization Results for location and Orientation (Profile #1)

	Mount 1	Mount 2	Mount 3	Mount 4
Orientation (deg)				
Starting Guess	(0.1, 50, 0)	(-0.1, -50, 0)	(0.5, 25, 0)	(-0.5, -25, 0)
Results	(0, 50, 0)	(0, -50, 0)	(50,50, 0)	(-50,-50, 0)
Position (in)				
Starting Guess	(12, -9, 0)	(12, -9, 0)	(-19, -5, 0)	(-19, -5, 0)
Results	(12, -8.9, -3)	(12, -8.9, 3)	(-17, -10, -7)	(-17, -10, 7)

Table 5.7: : Optimization Results for Road Profile #2

	Load Transmitted	Mount Stiffness (lb/in)		
	(lb)	x	Y	z
Initial Guess	599.63	475	475	7500
Optimized Design	113.47	2116.2	2116.2	5884.5

Table 5.8: Optimization Results for location and Orientation (Profile #2)

	Mount 1	Mount 2	Mount 3	Mount 4
Orientation (deg)				
Starting Guess	(0.1, 50, 0)	(-0.1, -50, 0)	(0.5, 25, 0)	(-0.5, -25, 0)
Results	(50, 50, 0)	(-50, -50, 0)	(50, 50, 0)	(-50, -50, 0)
Position (in)				
Starting Guess	(12, -9, 0)	(12, -9, 0)	(-19, -5, 0)	(-19, -5, 0)
Results	(12, -5.5,-7)	(12, -5.5,7)	(-11, -10, -3)	(-11, -10, 3)

As can be seen from the tables above, the value of the load transmitted for both cases is larger than the transmitted loads in the corresponding example discussed in section 4.3.2.1 where only the shaking force is considered. This due to the fact that the input force vector contains alongside the shacking load at 4000 rpm the road load due to different road profiles. It is worth mentioning that different starting guess vector is used to insure that the final solution is not at local minima. Again, the influence of mount orientation is seen to be more significant than mount location. The results are consistent with the results found in section 4.2.2.1 where the stiffness along the  $z$  axis does not affect objective function values and therefore does deviate much from the starting guess values whereas the stiffness values in the  $x$  and  $y$  direction do change significantly. An alternate model is used to estimate the forces and moments transmitted through the tire patch using the Pacejka model discussed in Appendix B. This tire model is not used in this dissertation.

### 5.3 *Summary*

In this chapter, the input load vector acting on the mounting system is discussed. The load vector is a linear combination of the shaking force and the road loads. The shaking force vector is developed first for a single cylinder engine and then generalized to accommodate a V-Twin engine configuration. The road loads which are due to irregularities in the road profile are also discussed. Two different road profiles are considered. Road profile #1, which is periodic and road profile #2, which is non-periodic are employed in this work. The frequency content of the road profiles is obtained using the FFT technique. The technique used herein could be used for any other load profile. It is seen that for both examples considered herein significant reduction in the loads transmitted through the mount are obtained by varying the mount stiffness values, location and orientation.



## Chapter 6 – Shape Optimization of Engine Mounts

In this chapter, a parametric approach is presented to determine the optimum geometric shape of an engine mount in order to minimize the vibrations transmitted to and from the engine. The engine mount used in this chapter is an elastomeric mount which is made of rubber. For proper vibration isolation, elastomeric mounts are designed such that they have the necessary stiffness rate in all directions. As shown in chapters 4 and 5, an optimization problem is solved first to determine the optimum values of stiffness, orientation and location of the mount system such that vibrations transmitted are minimized. Besides knowing the mount stiffness values, a determination of the optimum shape of the mount is also vital. This chapter addresses determining the shape of the mount such that it meets the required stiffness of the mounting system obtained from dynamic analysis. A nonlinear finite element analysis is used to determine the final optimum shape corresponding to the desired mount stiffness values.

### 6.1 *Finite Element Modeling*

The general shape of the shear rubber engine mount, also known as bush engine mount, is shown in Fig. 6.1. This type of engine mount is common in motorcycle applications. The finite element model of the mount used herein is created using the finite element software ANSYS<sup>®</sup> and is built to fully describe the geometry of the bush type engine mount. The finite element model is built using solid 186 elements shown in Fig. 6.2. This element is a three dimensional, 20 node structural solid element. The solid element exhibits quadratic displacement behavior. Each node has a 3 DOF, namely translation in the  $x$ ,  $y$  and  $z$  directions. The element supports plasticity, hyperelasticity, stress stiffening and large deformations.

The mount is connected to the frame via metal steel plates on both sides. These plates are bonded to the mount and the connection is at the mount attachment holes. Since the stiffness of the steel plates is higher than the mount stiffness, the constraints are moved from the plate holes directly into the mount surface as shown in Figs. 6.3 and 6.4. The boundary conditions are applied by constraining the displacement of the surface of the mount in all directions. A shaft which is connected to the source of vibration runs through the mount which transmits the loads from the powertrain to the frame. Since load transmitting shaft runs through the center hole of the mount, the loading can be modeled by using rigid bodies that runs from the center node into the inner mount surface or by defining a constraint equation as shown in Figs. 6.5 and 6.6. The input load, which is determined from the dynamic analysis performed in chapters 4 and 5, can be defined by applying a force at the center node in the  $x$ ,  $y$  and  $z$  directions.

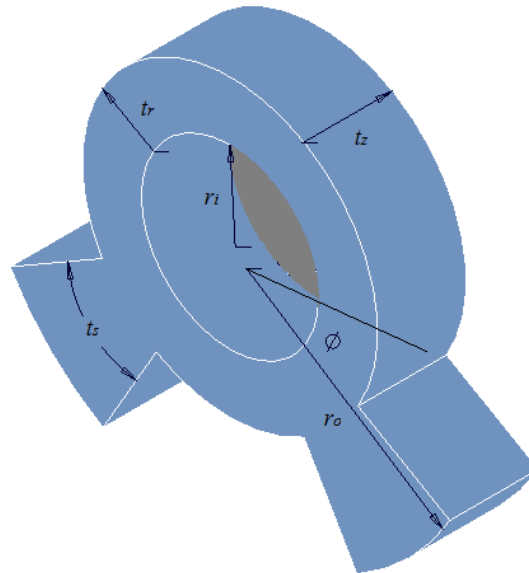


Figure 6.1: Mount Geometry

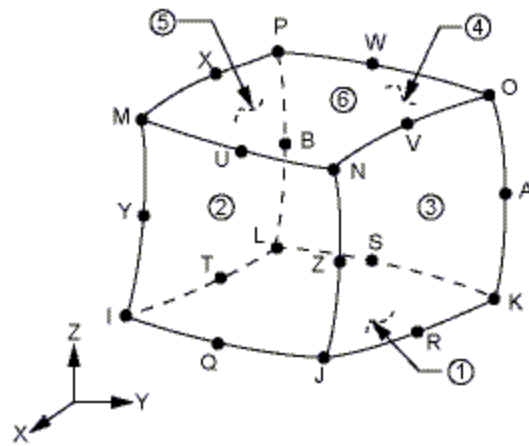


Figure 6.2: Solid 186 Element (ANSYS, 2009)

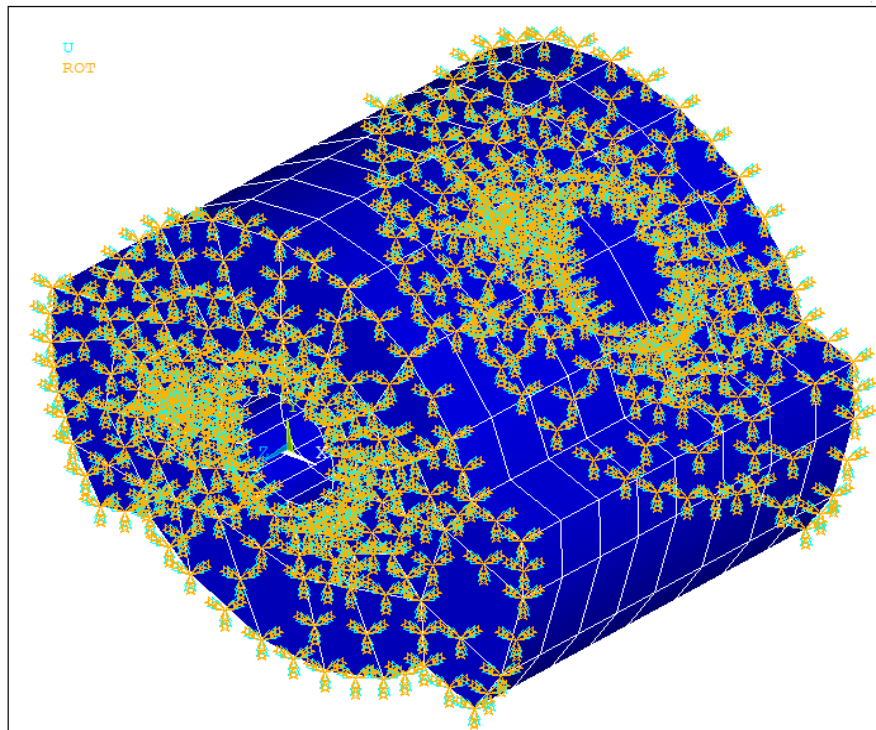


Figure 6.3: Isometric View Showing the Boundary Conditions

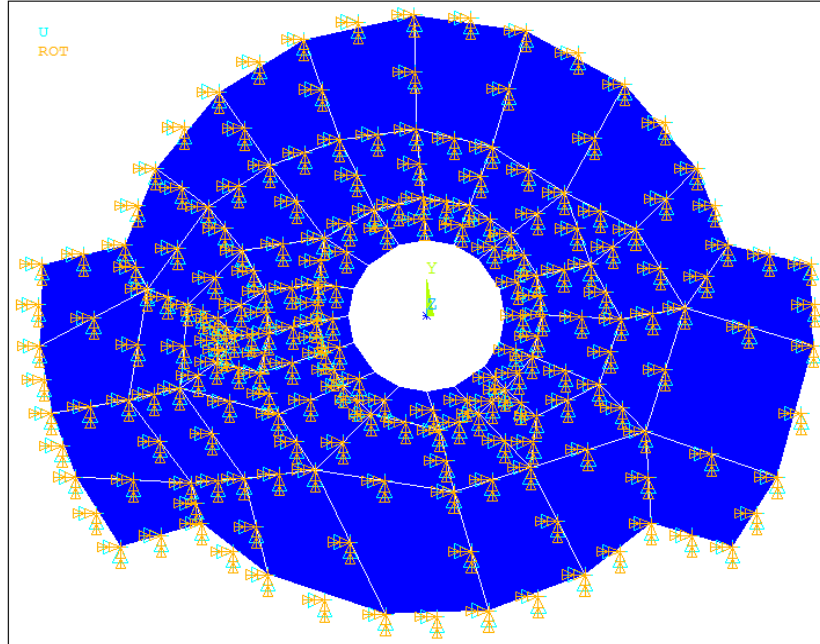


Figure 6.4: Front View Showing the Boundary Conditions

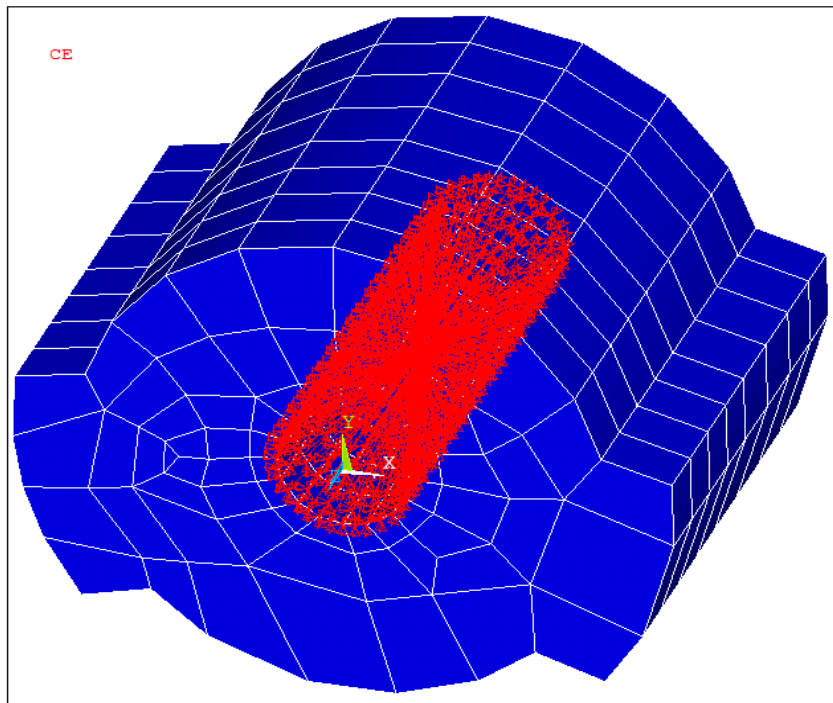


Figure 6.5: Isometric View Showing the Constraint Equation

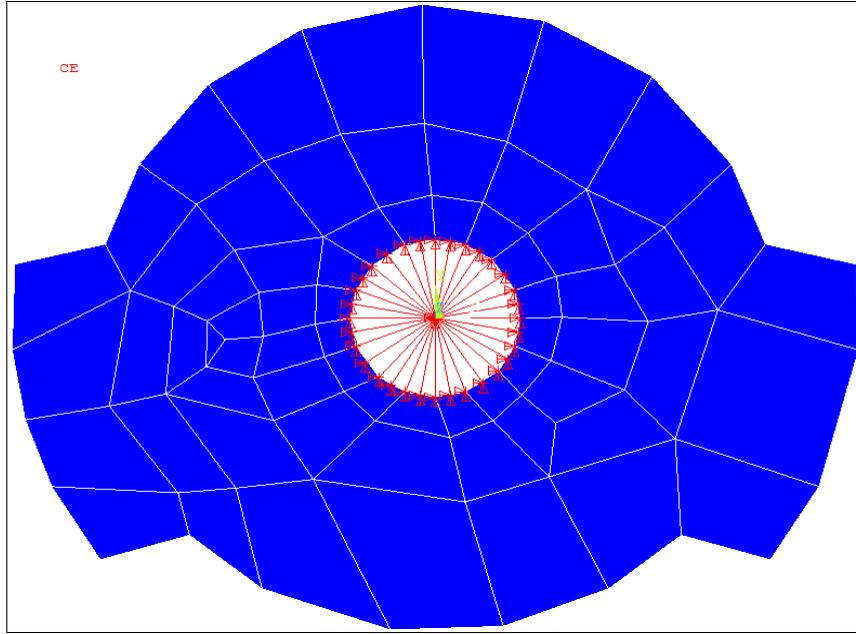


Figure 6.6: Front View Showing the Constraint Equation

## 6.2 Parameter Optimization

A parametric study is employed herein to determine the optimum geometric dimensions of the isomeric mount. These dimensions could be selected to describe the entire mount as shown in Fig. 6.1. The shape of the mount can be determined by matching the stiffness that is determined from the dynamic analysis which is performed in chapter 4 and 5 and the stiffness obtained from the geometry of the mount. Once the design parameters are chosen which are  $t_r$ ,  $t_s$ ,  $t_z$ , and  $\theta$ , the objective function is set up as follows:

$$\psi = wt(1)(k_x - k_x^{des})^2 + wt(2)(k_y - k_y^{des})^2 + wt(3)(k_z - k_z^{des})^2 \quad (6.1)$$

The bounds of the design variables must satisfy the condition described in Eq. (6.2), where  $x_i$  is the  $i^{th}$  design variable and  $n$  is the number of design variables.

$$x_i^{min} \leq x_i \leq x_i^{max} \text{ for } i = 1, \dots, n \quad (6.2)$$

In Eq. (6.1),  $wt(i)$  is the weighting function that corresponds to the stiffness in the  $i^{th}$  direction. The superscript 'des' indicates the desired stiffness that is obtained from the dynamic analysis of the mounting system. Meanwhile the design parameters selected will determine the stiffness values for the geometry that is obtained from the nonlinear finite element analysis. The process of determining the design variables is expensive and time consuming, therefore in order to reduce the number of function evaluations, the least effective stiffness could be dropped from the objective function  $\psi$ .

### 6.3 Design Model and Analysis

The mount that is used herein is a bush type which is typically used in the automotive industry. The actual geometry of such mount is shown in Fig. 6.1 along with the parameters that define its shape. There are a total of six parameters that dictates the shape of the mount of which four are used as the design variables; namely  $t_s, t_z, t_r$  and  $\theta$ . The other two parameters ( $r_i$  and  $r_o$ ) are constants. These design variables affect the mount stiffness directly. The weighting function that is used in the objective function could be used to take into account the importance of the stiffness in a particular direction. The dynamic analysis is done for a motorcycle powertrain in which is supported by four isomeric mounts. The connection between the powertrain and the swing-arm are taken into consideration generating a twelve DOF system (Kaul, 2006). The exciting force will be a mix of the shaking force evaluated at different engine steady state speeds and/or the road loads.

In the work presented in this chapter, the stiffness values corresponding to specific mount geometry are obtained using a nonlinear finite element analysis. The geometry shown in Fig. 6.1 is used to generate a mesh for the analysis. The optimization

is carried out using ANSYS<sup>®</sup>. Solid 186 is the element that has been used for this purpose is shown in Fig. 6.2. Appropriate boundary conditions have been applied to the model as discussed in section 6.2. The boundary conditions along with the constraint equation are shown in Fig. 6.3 to Fig. 6.6. This model is assumed to exhibit small deflections, for this reason the Mooney Rivlin model is sufficient to describe the fully incompressible hyperelastic material behavior of rubber (Kim, 1997), (Rivlin, 1992) and (Ali, 2010). The Mooney Rivlin model of the strain energy is expressed as follows:

$$U = C_{10}(I_1 - 3) + C_{01}(I_2 - 3) \quad (6.3)$$

In Eq. (6.2),  $I_1$  and  $I_2$  are the first and second strain invariants. The coefficients  $C_{10}$  and  $C_{01}$  are determined from the uniaxial tension test. The rubber that is used in this work is carbon black filled natural rubber (Rivlin, 1992). The values of the coefficients are:

$$C_{10} = 0.03622 \text{ and } C_{01} = -0.00335.$$

All the design variables must satisfy the design range which could be considered as inequality constraints that dictates the lower and upper bound of these variables. Each one of these ranges that specify the upper and lower limit of the design variables are considered as inequality constraints and are incorporated in the finite element optimizer. The static deflection that is due to the static weight of the engine is measured along the axis of gravity is given by:

$$\delta = \left| \frac{F_g}{k} \right| \quad (6.4)$$

In Eq. (6.4),  $F_g$  represents the static weight of the engine and  $k$  represents the stiffness in the gravity direction.

The optimization problem described by Eq. (4.8) is solved using the SQP technique that employs a MATLAB built in function (fmincon) to minimize the value of

the objective function formulated in Eq. (4.7). Once the operation is complete, the design vector that corresponds to the optimum value of the objective function is known. The design vector includes the stiffness values of the engine mount. The second part of the problem is initiated by setting the objective function described in Eq. (6.1) to minimize the difference between the desired stiffness values obtained from the first optimization done through the dynamic analysis and the stiffness values obtained from the geometric shape of the mount. As a first step, a static analysis is performed to determine the deflections. The objective function employs the mount geometric data as the design vector. The design vector consists of  $t_s$ ,  $t_z$ ,  $t_r$  and  $\theta$ . The shape optimization takes into account the range of the design variables that acts like lower and upper bounds. These bounds are as shown in Eq. (6.5) below.

$$\begin{aligned}
 0.3 &\leq t_r \leq 0.59 \\
 0.3 &\leq t_s \leq 1.5 \\
 0.5 &\leq t_z \leq 1.77 \\
 -\pi/18 &\leq \theta \leq -\pi/6
 \end{aligned} \tag{6.5}$$

#### 6.4 Examples

In this section two examples dealing with shape optimization of mounts are presented. The first example is based upon the six DOF model formulated in section 4.1.1. The second example will be based upon the twelve DOF model formulated in section 4.1.2. For both of these examples, the final geometrical shape of the mount will be determined. The systems in both of the examples are subjected to different types of loading conditions.



### 6.4.1 Example I

The example presented herein is a continuation of the example presented in section 4.2.2.1. This example is based on the six DOF model presented in section 4.1.1. The input load vector corresponds to the engine shaking load at the steady engine speed of 4000 rpm. The design variables resulting from the optimization process are shown in Table 4.3. The data given in Table 4.3 which represent the stiffness values of the mounts are used to set up the objective function presents in Eq. (6.1). The optimization problem is formulated and solved using the finite element software ANSYS<sup>®</sup>. The design vector consists of the four parameters that fully describe the geometry of the mount  $t_s, t_z, t_r$  and  $\theta$  as shown in Fig. 6.1. The optimized design variables must satisfy the lower and upper bounds set in Eq. (6.5). The final values of the design vector are shown in Table 6.1 along with the minimum value of the objective function. The initial shape of the mount is shown in Figs. 6.7 and 6.8 and the final optimized shape of the mount is shown in Figs. 6.9 and 6.10. An analysis was also performed for three different engine speeds corresponding to idling (800 rpm), steady state cruising (3000 rpm) and over revving situation (5000 rpm). The results for the shaking force vectors calculated at 800 rpm, 3000 rpm and 5000 rpm are shown in Table 5.1. The corresponding design variable vector  $t_s, t_z, t_r$  and  $\theta$  that corresponds to these different shaking force vectors are shown in Table 6.2 and Fig. 6.11.

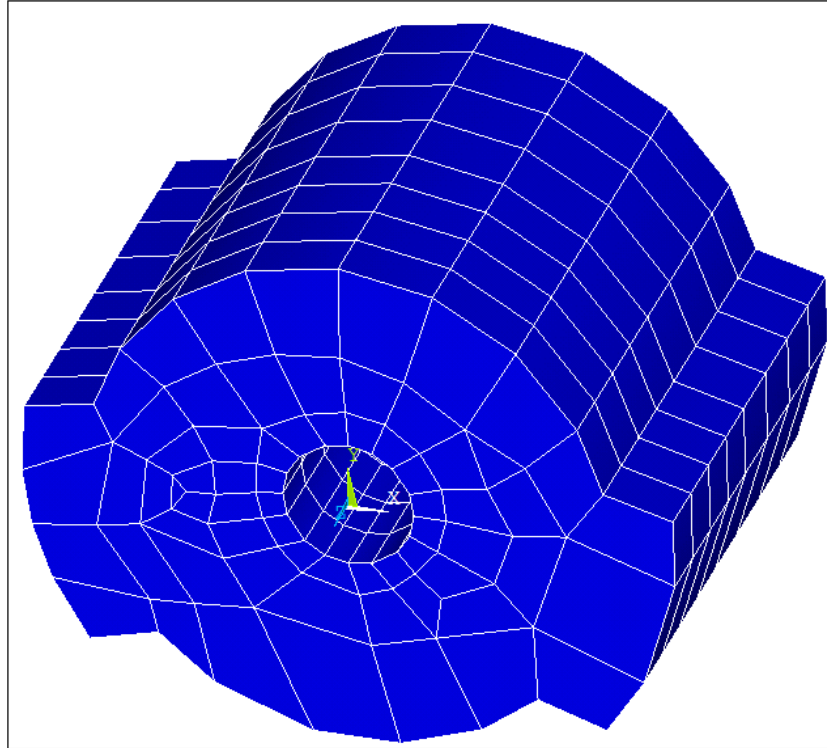


Figure 6.7: Isometric View of the Initial Geometry

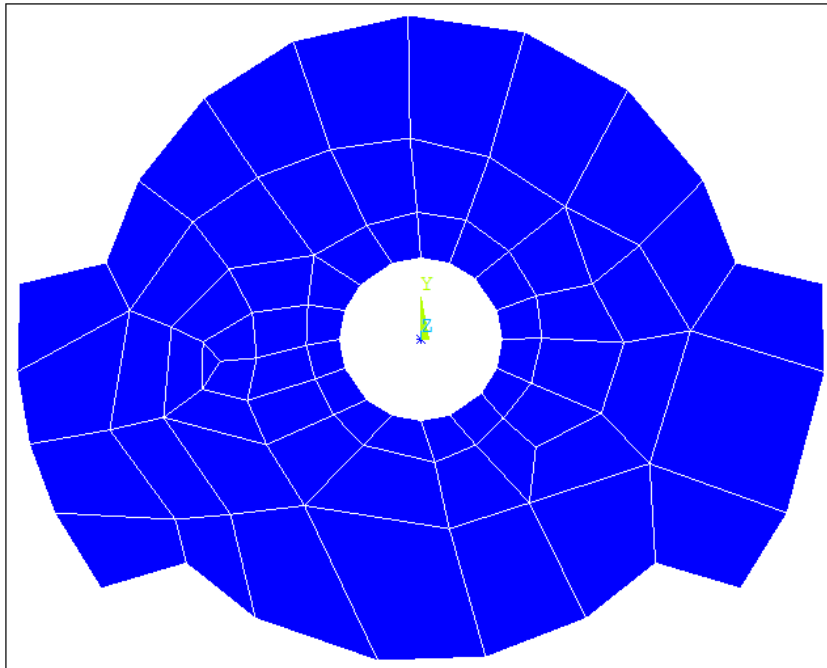


Figure 6.8: Front View of the Initial Geometry

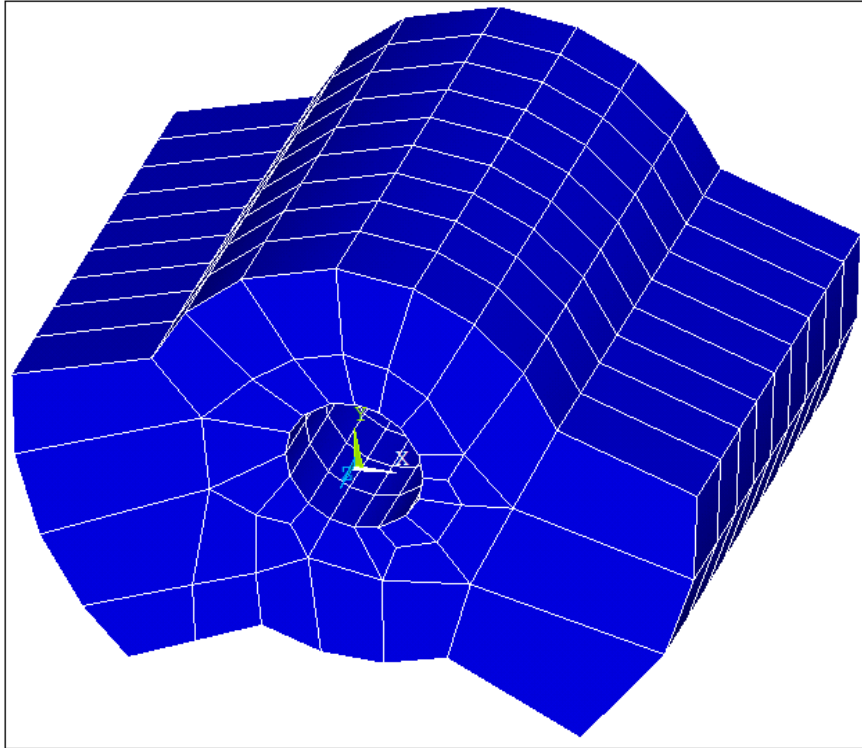


Figure 6.9: Isometric View of the Optimized Geometry (Example I)

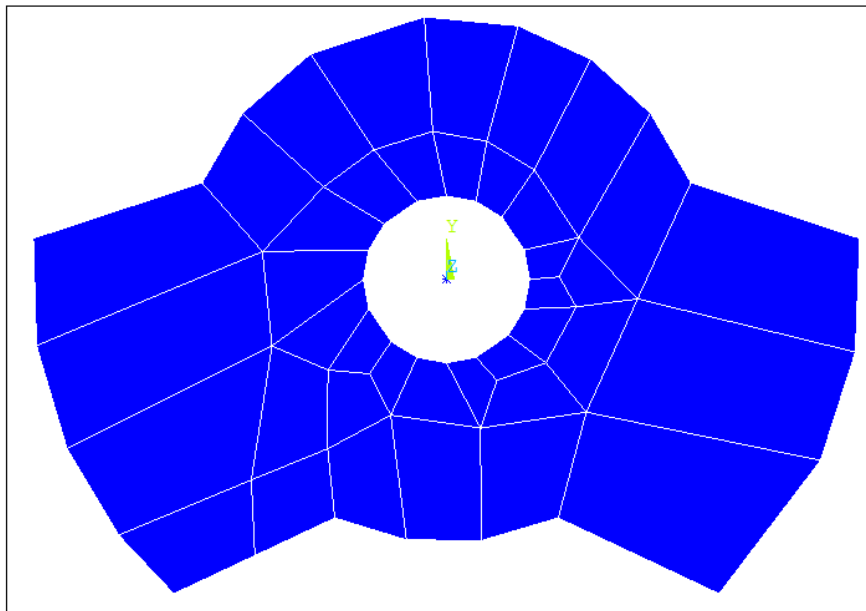


Figure 6.10: Front View of the Optimized Geometry (Example I)

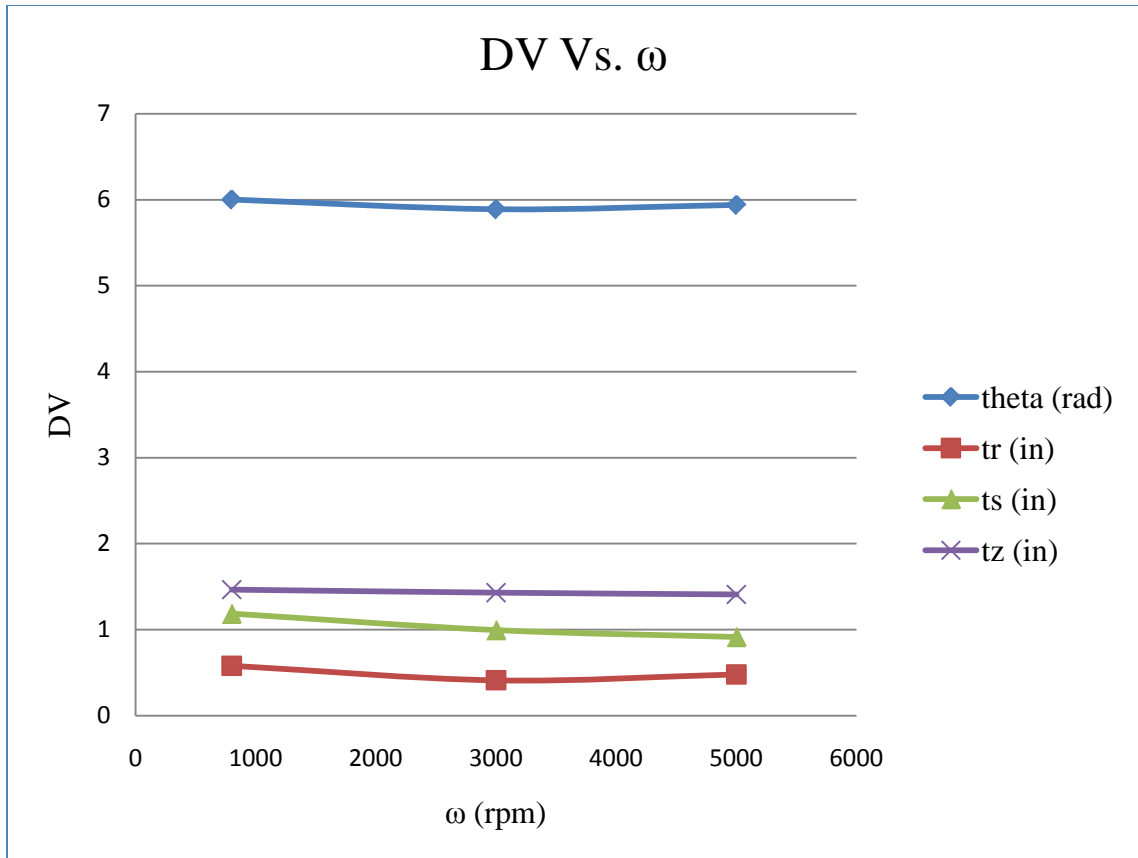


Figure 6.11: Design Variables Vector Vs. Steady State Speed

Table 6.1: Parameter Optimization Results

		Initial	Optimized	Target Stiffness
Design Variables	$\theta$ (rad)	6.021	5.9052	
	$t_r$ (in)	0.591	0.4259	
	$t_s$ (in)	0.787	0.9387	
	$t_z$ (in)	1.378	1.4016	
Stiffness (lb/in)	kx	3411.3	1065.5	1016.6
	ky	9183.8	1042.7	1016.6
	kz	1852.5	7520.6	7503.5
Obj. Function	$\psi$	104371544.93	3364.83	

Table 6.2: Design Variables Vector Corresponding to different Steady State Speeds

	$\omega$ (rpm)		
	800	3000	5000
$\theta$ (rad)	6.00189	5.8888	5.9394
$t_r$ (in)	0.57968	0.4110	0.4795
$t_s$ (in)	1.18617	0.9951	0.9154
$t_z$ (in)	1.46379	1.4299	1.4100

Table 6.3: Transmitted Loads at Different Operating Speeds

	$\omega$ (rpm)		
	800	3000	5000
Transmitted Load	188.807	266.812	258.616
Transmitted Load for Optimum values at 3000 rpm	189.727	266.812	259.62

Figure 6.11 shows the variation in the optimized mount geometry parameters  $t_s, t_z, t_r$  and  $\theta$  as a function of the engine speed. Table 6.3 shows the optimum transmitted force at different engine speeds as a result of having the optimum stiffness values at 3000 rpm which are obtained from the geometrical optimization. As can be clearly seen from Table 6.3, that there is minimal change to the transmitted loads at 800 rpm and 5000 rpm when selecting an optimum geometry corresponding to 3000 rpm

#### 6.4.2 Example II

The example presented herein is a continuation of the example presented in section 4.2.3.1. This example is based on the twelve DOF powertrain-swing-arm model

presented in section 4.1.2. The input load vector in this example is a linear combination of the engine shaking load at the steady speed of 4000 rpm and road loads due to road load profile #1 shown in Fig. 5.10. The design variables resulting from the optimization process are shown in Table 4.8. The data given in Table 4.8, which represent the stiffness values of the mounts are used to set up the objective function presents in Eq. (6.1). The optimization problem is formulated and solved using the finite element software ANSYS<sup>®</sup>. The design vector consists of the four parameters that fully describe the geometry of the mount  $t_s, t_z, t_r$  and  $\theta$  as shown in Fig. 6.1. The optimized design variables must satisfy the lower and upper bounds set in Eq. (6.5). The final values of the design vector are shown in Table 6.4 along with the minimum objective function value. The initial shape of the mount is shown in Figs. 6.7 and 6.8 and the final optimized shape of the mount is shown in Figs. 6.12 and 6.13.

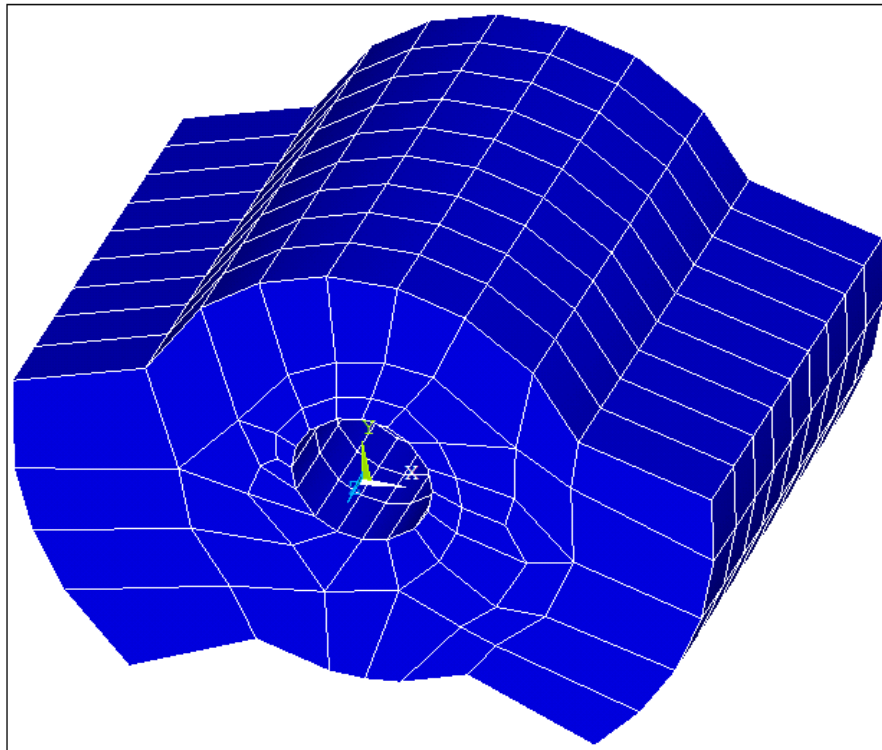


Figure 6.12: Isometric View of the Optimized Geometry (Example II)

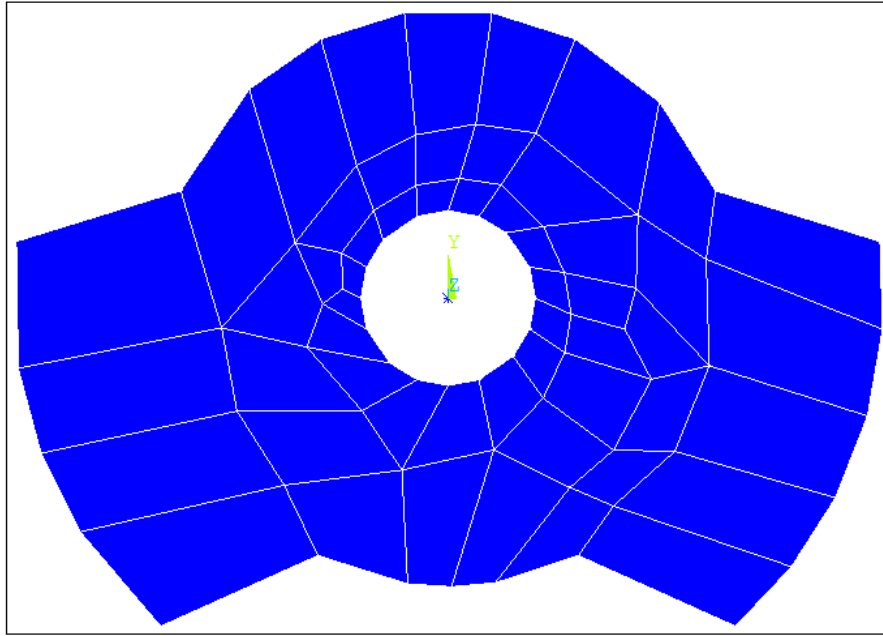


Figure 6.13: Front View of the Optimized Geometry (Example II)

Table 6.4: Parameter Optimization Results

		Initial	Optimized	Target Stiffness
Design Variables	$\theta$ (rad)	6.021	5.923	
	$t_r$ (in)	0.591	0.454	
	$t_s$ (in)	0.787	0.965	
	$t_z$ (in)	1.378	1.430	
Stiffness (lb/in)	$k_x$	3411.3	2410.40	2405
	$k_y$	9183.8	2400.10	2405
	$k_z$	1852.5	1572.80	1564.5
Obj. Function	$\psi$	47047713.13	122.06	

The design of a shear (bush) type mount has been obtained using the geometrical shape optimization using the parameterization technique. The method was done through utilizing a nonlinear finite element analysis. Part of the design was done using SQP

method in MATLAB<sup>®</sup> in order to find the target stiffness values. More details regarding these results are available in sections 4.2.2.1 and 4.2.3.2. As can be noticed from the results above, the optimum shape of the mount is acceptable and can be used as the final shape. It is worth mentioning that this approach is applicable for any type of engine mounts. The stiffness values that are obtained from the shape optimization are slightly different than those values obtained from the dynamic analysis; however, the shape obtained from the parametric optimization is acceptable and can be used in real design situations.

## 6.5 *Summary*

In this chapter, a determination of the geometrical shape of the engine mount is discussed. The shape optimization is performed using ANSYS<sup>®</sup>. The process begins by performing dynamic analysis which is represented in chapter 4 and then the shape optimization is performed. Two different examples are considered in this chapter. The first example is based on the six DOF model in which the objective function is formulated using the shaking force vector as the only input load. The second example is based on the twelve DOF model in which the objective function is formulated using a combination of the force vector consisting of both the shaking force and forces transmitted through the tire patch.



## Chapter 7 - Conclusion

The mount system modeling work presented in this dissertation can be generally divided into three main areas. The first area deals with development of mathematical models of the mount and the mounting system that varies in complexity, in order to examine their vibration isolation quality. The second area makes use of the developed theoretical models in order to come up with the design of an optimum passive engine mounting system such that the forces transmitted to the frame to the system are minimized. The third area explores finding the optimum engine mount geometrical shape with desired stiffness and damping characteristics.

This chapter summarizes the work that has been done in this dissertation and provides an outline for possible future work on this topic.

### *7.1 Theoretical Modeling*

Several engine mounting system were discussed in chapter 3 which the model complexity varied from a simple Voigt model to more complex Voigt model with Bouc-Wen element and nonlinear stiffness. In all of the models that have been discussed, the major concern was to eventually enhance the vibration isolation quality. A close attention was paid to the problem of mechanical snubbing when the isolated mass undergoes large displacements.

All the models proposed in this work are generic and are applicable to a wide range of motorcycle layouts. All the models account for motorcycle systems that exhibit very rigid frames. The overall motorcycle stiffness is affected by the structural compliance of some components such as the frame, the swing-arm, the powertrain and

the connecting elements between these components. All of these components are discussed in detail in this dissertation.

Unlike the automobile vibration isolation problem, the motorcycle vibration isolation depends heavily on the loading conditions where the engine excitation force is not the only source of vibration; the motorcycle is affected by the engine excitation force and the road loads as well. In addition, the overall motorcycle stiffness and the ride quality is strongly affected by the isolation system. The work presented in this dissertation discusses both loading conditions in order to come up with the optimum mounting system configuration. The road loads are calculated using the vertical stiffness and damping characteristics of the tire patch and the displacement profile of the road surface. The engine excitation loads are computed from the shaking forces present in a V-Twin engine.

Two major mounting system models were used in this dissertation. The first model is formulated by considering the mounting system to be a six degree of freedom system and the second model is formulated by considering the mounting system to be a twelve degree of freedom model. In both models, the frame is assumed to infinitely rigid. In the second model, the powertrain assembly and the swing-arm assembly are connected via a coupler shaft at a pivot point. The second model allows for the road loads to be in the problem solution.

## *7.2 Mounting system optimization*

The major role of the mounting system in addition to physically mount the powertrain to the vehicle frame is to provide vibration isolation. It is important to insure sufficient clearance between the powertrain and the surrounding components. This is

achieved by imposing the appropriate boundaries when designing the mounting system. The mounting system should be able to isolate the frame under steady state loading conditions at the same time limiting the maximum excursion of the powertrain under transient loading conditions.

In chapter 4, the mount models were developed to determine the optimum mounting system characteristics by minimizing the load transmitted from the engine to the frame through the mounting system under multiple loading conditions. This objective was achieved while satisfying the displacement constraints to limit the maximum excursion at specific locations on the powertrain. In the design process, the mount location, orientation and stiffness parameters were used as the design vector. It was found that the mount orientation is significant and very important in achieving enhanced vibration isolation. The optimization problem was solved using MATLAB<sup>®</sup>.

### *7.3 Shape Optimization*

Finding the mounting system characteristics, which was done in chapters 4 and 5 has proven to be very important when it comes to vibration isolation. Finding the optimum geometrical mount shape has proven to be vital also. The shape optimization of the engine mount is done with the help of a finite element model that employs a nonlinear analysis technique. This work is done using ANSYS<sup>®</sup>. The mount geometry is built in ANSYS<sup>®</sup> using the major dimensions that will fully describe the geometry. The finite element model is generated using a suitable element to accommodate the nonlinear properties of rubber from which the mount is made off. A Mooney Rivlin rubber model is used to describe the fully incompressible hyperelastic material behavior of rubber.

The geometrical parameters of the mount such as the mount diameter, rubber thickness, etc. are used as the design vector. All the assumptions that are necessary to find the best loading conditions as well as boundary conditions are discussed in chapter 6. The loading and boundary conditions are important when it comes to considering different sources of vibration and physically mounting the powertrain on the frame.

#### *7.4 Future Work*

There are some issues that have surfaced in the work discussed in this dissertation which are related to this work. These issues have not been addressed in this work, but could be investigated in the future research.

All the models that have been discussed in this work were used to optimize the engine mount which is a passive mount. Future models could be modified such that engine mounting system consists of active mounts in addition to or in line of passive mounts. The mounting system could include a variable stiffness and damping properties that are under a control law based on accelerations at certain points on the frame.

The focus of this work was on the in-plane stiffness properties. The out-of plane stiffness properties could be considered by considering an enhanced representation of the front and rear end of the motorcycle.

All the models presented in chapters 4 and 5 of this dissertation are based on simple Voigt model that employs simple linear spring stiffness. Future work could consider more complex model that used a nonlinear stiffness. Mechanical snubbing will be better represented using such models which in turn will enhance the understanding of the mounting system vibration isolation.

External loads are transmitted through the tire patch to the engine through the mounting system. The load calculation is based on the vertical stiffness and damping of the tire which is affected by the displacement profile of the road. An alternative technique for load estimation that could be used in the future research is treating the structure as a load transducer. In this technique, strains are measured by placing strain gauges at some specific locations on the frame which can be used to provide a history of the loads acting on it. A finite element analysis can be used to find the appropriate locations and orientations of the strain gauges to be mounted on the frame.

## References

1. Akanda, A. and Adulla, C., 2005, "Engine Mount Tuning for Optimal Idle and Road Shake Response of Rear-Wheel-Drive Vehicles," *Society of Automotive Engineers*, technical paper series 01-2528.
2. Akanda, A. and Adulla, C., 2006, "Application of Evolutionary Commutation in Automotive Powertrain Mount Tuning," *Shock and Vibration*, Vol. 13, pp. 85-102.
3. Ali, A., Hosseini, M and Sahari, B. B., 2010, "A Review of Constitutive Models for Rubber Like Materials," *American Journal of Engineering and Applied Science*, Vol. 3, pp. 232-239.
4. ANSYS 12.0, Help Documentation, 2009, ANSYS Inc.
5. Atkinson, A. C. and Donev, A. N., 1992, *Optimum Experimental Design*, Oxford Science Publications.
6. Bretl, J., 1993, "Optimization of Engine Mounting Systems to Minimize Vehicle Vibration," *SAE*, paper no. 931322, pp. 475-482.
7. Carfagni, M., Lenzi, E. and Pierini, M., 1998, "The Loss Factor as a Measure of Mechanical Damping," *Proceedings of the 16<sup>th</sup> International Modal Analysis Conference*, pp. 580-584.
8. Chen, C. T., 2001, *Digital Design Processing – Spectral Computation and Filter Design*, Oxford University Press, Chapters 2, 3 and 4.
9. Cocco, G., 2001, *Motorcycle Design and Technology*, Giorgia Nada.
10. Courteille, E. and Mortier, F., 2005, "Multi-Objective Robust Design Optimization of an Engine Mounting System," *SAE*, paper no. 01-2412.
11. Crede, C. E., 1965, *Shock and Vibration Concepts in Engineering Design*, Prentice Hall Inc Englewood Cliffs, N.J.
12. Crede, C. E., 1951, *Vibration and Shock Isolation*, John Wiley and Sons Inc, New York, 1951.
13. Derby, F. T., 1973, "Decoupling the Three Translational Modes from the Three Rotational Modes of a Rigid Body Supported by Four Corner-Located Isolators," *Shock and Vibration Bulletin*, Part 4, Vol. 43, pp. 91-108.
14. Dhingra, A. K. and Hunter, T. G., 2003, "Optimum Experimental Design of A General Purpose Load Transducer," *NAFEMS World Congress*, Orlando, FL.

15. Ford, M. D., 1985, "An Analysis and Application of a Decoupled Engine Mount System for Idle Isolation", *SAE*, paper no. 850976, pp. 133-142.
16. Garmaroudi, M. A. and Mosayebi, J., 2008, "Design and Optimization of Engine Mount," *International Review of Mechanical Engineering*, Vol. 2, No. 5, pp. 682-692.
17. Geck, P. E. and Patton, R. D., 1984, "Front Wheel Drive Engine Mount Optimization," *Society of Automotive Engineering*, No. 840736, pp. 123-134.
18. Harris, C. M. and Crede, C. E., 1961, *Shock and Vibration Handbook*, McGraw-Hill New York, Chapter 30, pp. 18-38.
19. Ikhouane, F., Manosa, V. and Rodellar J., 2006, "Dynamic Properties of the Hysteretic Bouc-Wen Model," *Systems and Control Letters*. Vol. 56, pp. 197-205.
20. Iwahara, M., 1999, "The Optimum Layout of Engine Mounting by Dynamic Analysis," *SAE*, paper no. 01-3717.
21. Jeong, T. and Singh, R., 2000, "Analytical Methods of Decoupling the Automotive Engine Torque Roll Axis," *Journal of Sound and Vibration*, Vol. 234, pp. 85-114.
22. Jianqiao, Y. and Williams, F. W., 1997, "Quadratic Representation of Nonlinear Dynamic Stiffness Matrix and Related Eigenvalue Problems," *Computer Methods in Applied Mechanics and Engineering*, Vol. 146. pp. 313-323.
23. Kaul, S., 2006, *Modeling Techniques for Vibration Isolation in Motorcycles*, PhD Thesis, University of Wisconsin, Milwaukee.
24. Kaul, S., Dhingra, A. K., and Hunter, T. G., 2005, "Two Approaches for Optimum Design of Motorcycle Engine Mount Systems," *Engineering Optimization*, Vol. 37, No. 3, pp. 307-324.
25. Kaul, S., Dhingra, A. K., and Hunter, T. G., 2007, "Frame Flexibility Effects on Engine Mount Optimization for Vibration Isolation in Motorcycles," *Journal of Vibration and Acoustics*, Vol. 129, pp. 590-600.
26. Kim, J. J. and Kim, H. Y., 1997, "Shape Design of an Engine Mount by a Method of Parameter Optimization," *Computers and Structures*, Vol. 65, No.5, pp. 725-731.
27. Lee, D. H., Hwang, W. S. and Kim, C. M., 2002, "Design Sensitivity Analysis and Optimization of an Engine Mount System Using an FRF Based Substructuring Method," *Journal of Sound and Vibration*, Vol. 255, pp. 383-397.

28. Liu, C. Q., 2003, "A Computerized Optimization Method of Engine Mounting System," *SAE*, paper no. 01-1461.
29. Masroor, S. A. and Zahary, L. W., 1990, "Design an All-Purpose Force Transducer," *Experimental Mechanics*, Vol. 31, No.1, pp. 33-35.
30. MATLAB User Guide, Version 7.0, Release 14, Math Works.
31. Norton, R. L., 2004, *Design of Machinery: An Introduction to the Synthesis and Analysis of Mechanisms and Machines*, 3<sup>rd</sup> edition, McGraw Hill.
32. Pacejka, H. B., and Bakker, E., 1993, "The Magic Formula Tyre Model," *Vehicle System Dynamics*, Vol. 21, pp. 1-18.
33. Pacejka, H. B., and Besselink, I. J. M., 1997, "Magic Formula Tyre Model with Transient Properties," *Vehicle System Dynamics*, Vol. 27, pp. 234-249.
34. Pacejka, H. B., 1995, "The Role of Tyre Dynamic Properties," *Smart Vehicle*, pp. 55-68.
35. Pacejka, H. B., 2002, *Tyre and Vehicle Dynamics*, Butterworth-Heineman.
36. Paul, B., 1979, *Kinematics and Dynamics of Planner Machinery*, Prentice Hall INC, New Jersey.
37. Rao, S. S., 2000, *Engineering Optimization Theory and Practice*, 3<sup>rd</sup> edition, John Wiley & Sons, Chapter 7.
38. Rao, S. S., 1990, *Mechanical Vibrations*, Addison Wesley, Reading, MA.
39. Rivlin, R. S., 1992, "The Elasticity of Rubber," *Rubber Chem. Technol.* 65, G51-G66.
40. Scharnhorst, T. and Pain, T. H., 1978, "Finite Element Analysis of Rubber-Like Materials by Mixed Model," *International Journal for Numerical Methods in Engineering*, Vol. 12, pp. 665-676.
41. Singh, R., 2000, "Dynamic Design of Automotive Systems: Engine Mounts and Structural Joints," *Sadhana*, Vol. 25, Part 3, pp. 319-330.
42. Singh, R. and Royston, T. J., 1996, "Optimization of Passive and Active Non-linear Vibration Mounting Systems Based on Vibration Power Transmission," *Journal of Sound and Vibration*, Vol. 194, pp. 295-316.



43. Singh, R. and Park, J. Y., 2007, "Effect of Engine Mount Damping on the Torque Roll Axis Decoupling," *SAE International*, No. 01-2418, pp. 1-9.
44. Snyman, J. A. and Heyns, P.S. and Vermeulen, P. J., 1995, "Vibration Isolation of a Mounted Engine Through Optimization," *Mechanical and Machine Theory*, Vol. 30, No.1, pp. 109-118.
45. Soroka, W. W., 1965, "Hysteretically Damped Vibration Absorber and an Equivalent Electrical Circuit," *Experimental Mechanics*, Vol. 5, pp. 53-58.
46. Spiekermann, C. E., Radcliff, C. J. and Goodman, E. D., 1985, "Optimal Design and Simulation of Vibrational Isolation Systems," *Journal of Mechanisms, Transmission and Automation in Design*, Vol. 107, pp. 271-276.
47. Suh, M. W., Shim, M. B., Kim, M. S. and Hong, S. K., 2003, "Multidisciplinary Design of Engine Mounts with Consideration of the Driveline", *Automobile Engineering*, Vol. 217, pp. 107-114.
48. Sui, S. J., 2003, "Powertrain Mounting design Principles to Achieve Optimum Vibration isolation with dimension Tools," *Society of Automotive Engineers*, paper no. 01-1476.
49. Swanson, S. R., 1985, "Large Deformation Finite Element Calculations for Slightly Compressible Hyperelastic Materials," *Computers and Structures*, Vol. 21, pp. 81-88.
50. Tao, J. S. and Liu, G. R. and Lam, K. Y., 2000, "Design Optimization of Marine Engine-Mount System," *Journal of Sound and Vibration*, Vol. 253, No.3, pp. 477-494.
51. Timpner, F. F., 1965, "Design Consideration in Engine Mounting," *SAE*, paper no. 650093 (966B).
52. Wen-ku, S., Jiang-hua, F., Hao, Y. and Teng, T., 2009, "Multi Objective Optimization of Powertrain Mounting Based on MATLAB," *Second Asia-Pacific Conference on Computational Intelligence and Industrial Application*, No. 978-4244-4607, pp. 484-487.
53. Wickham, M. J., Riley, D. R. and Nachtsheim, C. J., 1995, "Integrating Optimal Experimental Design of a Multi Axis Load Transducer," *Journal of Engineering for Industry*, Vol. 117, pp. 400-405.
54. Ye, M., Wang, X., 2007, "Parameter Identification of the Bouc-Wen Hysteresis Model Using Particle Swarm Optimization," *Smart Materials and Structures*, Vol. 16, pp. 2341-2349.

55. Yunhe, Y., Naganathan, G. N. and Dukkipati V. R., 2001, "A Literature Review of Automotive Vehicle Engine Mounting System," *Mechanism and Machine Theory*, Vol. 36, pp. 123-142.
56. Zhang J., Richards, M. C., 2006, "Dynamic Analysis and Parameter Identification of a Single Mass Elastomeric Isolation System Using a Maxwell-Voigt Model," *Journal of Vibration and Acoustics*, Vol. 128, pp. 713-721.

## APPENDIX A

The transformation matrix ( $A$ ) is used extensively throughout this dissertation to transform the stiffness matrix values from one coordinate to another. This transformation matrix is a composition of three successive rotations through angles  $\theta_1$ ,  $\theta_2$ , and  $\theta_3$  about the  $x$ ,  $y$  and  $z$  axes respectively of a global coordinate system (Crede, 1965). The transformation matrix is defined as follows:

$$A = R_z(\theta_3) R_y(\theta_2) R_x(\theta_1) \quad (A.1)$$

Substituting all the rotation matrices represented in Eq. (A.1) yields the following:

$$A = \begin{bmatrix} C\theta_3 & -S\theta_3 & 0 \\ S\theta_3 & C\theta_3 & 0 \\ 0 & 0 & 1 \end{bmatrix} \begin{bmatrix} C\theta_2 & 0 & S\theta_2 \\ 0 & 1 & 0 \\ -S\theta_2 & 0 & C\theta_2 \end{bmatrix} \begin{bmatrix} 1 & 0 & 0 \\ 0 & C\theta_1 & -S\theta_1 \\ 0 & S\theta_1 & C\theta_1 \end{bmatrix} \quad (A.2)$$

In Eq. (A.2),  $C\theta_i = \cos\theta_i$  and  $S\theta_i = \sin\theta_i$ . The expression represented in Eq. (A.2) can be rewritten in the following form:

$$A = \begin{bmatrix} C\theta_2 C\theta_3 & -C\theta_1 S\theta_3 + S\theta_1 S\theta_2 C\theta_3 & S\theta_1 S\theta_3 + C\theta_1 S\theta_2 C\theta_3 \\ C\theta_2 S\theta_3 & C\theta_1 C\theta_3 + S\theta_1 S\theta_2 S\theta_3 & -S\theta_1 C\theta_3 + C\theta_1 S\theta_2 S\theta_3 \\ -S\theta_2 & S\theta_1 C\theta_2 & C\theta_1 C\theta_2 \end{bmatrix} \quad (A.3)$$

The expression given in Eq. (A.3) is the same expression for the transformation matrix that has been used throughout this dissertation.

Beside the rotation matrix expressed in Eq. (A.3), Euler angles could be used as an alternative way of computing the rotation matrix ( $A$ ). Euler angle transformation matrix is composed by using a rotation through angle  $\phi$  about the  $z$  axis followed by a rotation through angle  $\theta$  about the  $y$  axis followed by a rotation through angle of  $\psi$  about the  $x$  axis. All of the above rotations are performed about the latest frame or the current frame. The composition is expressed as follows:

$$A = R_z(\phi) R_y(\theta) R_z(\psi) \quad (A.4)$$

Eq. (A.4) can be rewritten as follows:

$$A = \begin{bmatrix} C\phi & -S\phi & 0 \\ S\phi & C\phi & 0 \\ 0 & 0 & 1 \end{bmatrix} \begin{bmatrix} C\theta & 0 & S\theta \\ 0 & 1 & 1 \\ -S\theta & 0 & C\theta \end{bmatrix} \begin{bmatrix} C\psi & -S\psi & 0 \\ S\psi & C\psi & 0 \\ 0 & 0 & 1 \end{bmatrix} \quad (A.5)$$

After computing the rotation matrices represented in Eq. (A.5), the following transformation matrix results:

$$A = \begin{bmatrix} C\phi C\theta C\psi - S\phi S\psi & -C\phi C\theta S\psi - S\phi C\psi & C\phi S\theta \\ S\phi C\theta C\psi + C\phi S\psi & -S\phi C\theta S\psi + C\phi C\psi & S\phi S\theta \\ -S\theta C\psi & S\theta S\psi & C\theta \end{bmatrix} \quad (A.6)$$

Other representations such as the Bryant angles or roll-pitch-yaw angles can also be used in order to construct the transformation matrix.

## APPENDIX B

A comprehensive tire model has been developed by Pacejka to represent the tire dynamics. This model which is referred to as the magic formula has been used extensively in the motorcycle industry. This model generates a set of equations for the forces and moments as a result of the interaction of the tire with road surface which is calculated at different slip conditions. These slip conditions contains a pure longitudinal slip, pure lateral slip or a combination of the mentioned slip conditions.

The governing equation of the Pacejka tire model for a specific vertical load and a camber angle is as follows:

$$y(x) = D \sin\{C \tan^{-1} [B x - E(B x - \tan^{-1} (B x))]\} \quad (B.1)$$

In Eq. (B.1),  $y$  is the output variable which could be either the longitudinal force or the lateral force or the aligning torque and  $x$  is the input variable which could be the slip ratio or the slip angle. Eq. (B.1) generates a curve that passes through the origin. In order for this curve to offset with respect to the origin, a shift coordinate system is introduced as follows:

$$\begin{aligned} Y(X) &= y(x) + S_v \\ x &= X + S_h \end{aligned} \quad (B.2)$$

In Eq. (B.2),  $S_v$  and  $S_h$  are the two shift parameters along the  $x$  and  $y$  axes respectively,  $Y$  represents the output variable which could be the longitudinal force  $F_x$ , or the lateral force  $F_z$  or the aligning torque  $M_y$ .  $X$  represents the input variables which could as a result of the lateral or longitudinal slip. Fig. B.1 shows the Pacejka curve with the terms listed above.  $B$ ,  $C$ ,  $D$  and  $E$  are semi-empirical constants with physical meaning associated to each constant. For example  $B$ ,  $C$  and  $D$  represent the cornering stiffness of the tire. These

constants are function of the wheel load, slip, slip angle and slip ratio. The computation of these constants is based on the experimental results multiple wheel loads, slip angles, slip ratios and chamber angles.

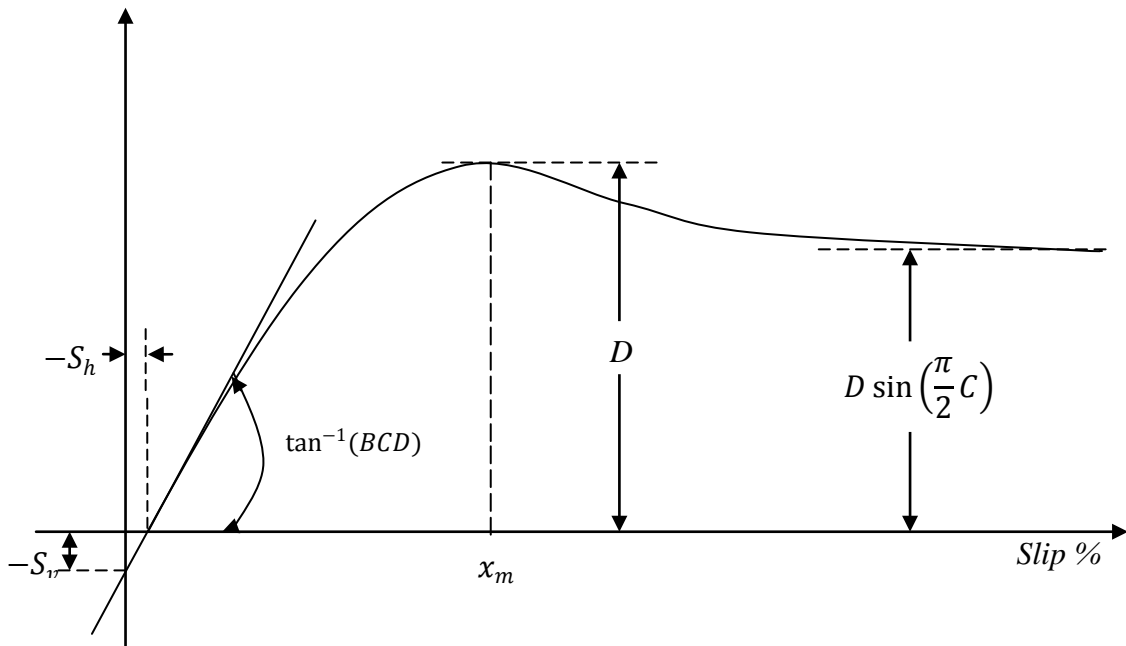


Figure B.1: Pacejka Tire Model Plot [35]

## APPENDIX C

Some models discussed in this dissertation are developed by assuming that the powertrain is connected to the swing-arm via a coupler. This model is presented in section 3.4.2. The coupler shaft is modeled as a simply supported beam with bearing supports at both ends of the beam.

The stiffness matrix of the coupler shaft  $K_c$ , is developed by using a two-element finite element model. Each node is assigned six degrees of freedom. The complete stiffness matrix is  $18 \times 18$ . By imposing the boundary conditions which consists of translational and rotational displacements, the stiffness matrix is reduced to a diagonal matrix. All the translational degrees of freedom of the end points are restrained for the coupler shaft. Zero moment inputs are used at the end nodes to reduce the overall stiffness matrix to six degrees of freedom at the center node in which assigned at the midpoint of the shaft.

$K_c$

$$= \begin{bmatrix} \frac{24 E_1 I_{y1}}{L_1^3 (4 + \phi_{z1})} & 0 & 0 & 0 & 0 & 0 \\ 0 & \frac{24 E_1 I_{z1}}{L_1^3 (4 + \phi_{y1})} & 0 & 0 & 0 & 0 \\ 0 & 0 & \frac{2A_1 E_1}{L_1} & 0 & 0 & 0 \\ 0 & 0 & 0 & \frac{\begin{bmatrix} (4 + \phi_{y1})^2 \\ -(2 - \phi_{y1})^2 \end{bmatrix} 2E_1 I_{z1}}{L_1 (1 + \phi_{y1}) + (4 + \phi_{y1})} & 0 & 0 \\ 0 & 0 & 0 & 0 & \frac{\begin{bmatrix} (4 + \phi_{z1})^2 \\ -(2 - \phi_{z1})^2 \end{bmatrix} 2E_1 I_{y1}}{L_1 (1 + \phi_{z1}) + (4 + \phi_{z1})} & 0 \\ 0 & 0 & 0 & 0 & 0 & 0 \end{bmatrix} \quad (C.1)$$

In Eq. (C.1), the diagonal terms of  $K_c$  are referred to as  $k_{cx}$ ,  $k_{cy}$ ,  $k_{cz}$ ,  $k_{crx}$ ,  $k_{cry}$  and  $k_{crz}$  respectively in the section 4.2.3.1.  $\phi_{y1}$  and  $\phi_{z1}$  are defined as follows:

$$\phi_{y1} = \frac{12 E_1 I_{z1}}{G_2 A_{sy1} L_1^2} = 24(1 + \nu_1) \frac{A_1}{A_{sy1}} \left( \frac{r_{z1}}{L_1} \right)^2 \quad (C.2)$$

$$\phi_{z1} = \frac{12 E_1 I_{y1}}{G_2 A_{sz1} L_1^2} = 24(1 + \nu_1) \frac{A_1}{A_{sz1}} \left( \frac{r_{y1}}{L_1} \right)^2 \quad (C.3)$$

In Eq. (C.2) and Eq. (C.3),  $r_{z1}$  and  $r_{y1}$  are the radii of gyration,  $\nu_1$  is the poisson ratio and  $A_{sy1}$  and  $A_{sz1}$  are the effective cross sectional areas in shear. In the above equations,  $E_1$  is the modulus of elasticity,  $A_1$  is the cross sectional area,  $G_1$  is the shear modulus of the shaft,  $I_{y1}$  and  $I_{z1}$  are the area moments of inertia in which they are equal since the shaft cross sectional area is circular and  $L_1$  is the half the length of the shaft.



## APPENDIX D

The engine is modeled as a rigid body of mass  $M$  which is attached to the frame by means of the mounting system as shown in Fig. D.1. The origin of the global coordinate system  $G$  is located at the center of mass of the engine  $C$ . However, this not necessarily true when the engine is idling. The  $Z$ -axis of the global coordinate system is parallel to the crankshaft and the  $X$  axis is in the vertical direction.

The general translational EOM of the engine is given by:

$$M \ddot{r} = f \quad (D.1)$$

In Eq. (D.1),  $M$  is the mass of the engine and  $f = [f_x, f_y, f_z]^T$  is the sum of all forces acting on the engine block.  $r = [x, y, z]^T$  is the position of the center of mass  $C$ .

The general rotation EOM is given by:

$$I \dot{\omega} + \omega \times I \omega = \eta \quad (D.2)$$

In Eq. (D.2),  $\eta = [\eta_x, \eta_y, \eta_z]^T$ , is the sum of the moments of the individual forces about  $C$ ,  $\omega = [\dot{\theta}_x, \dot{\theta}_y, \dot{\theta}_z]^T$  is the angular velocity with  $\theta_x, \theta_y$ , and  $\theta_z$  are the rotational angles about the  $x, y$  and  $z$  axis respectively.  $I$  is the inertia tensor which is given by Eq. (D.3).

$$I = \begin{bmatrix} I_{xx} & -I_{xy} & -I_{xz} \\ -I_{yx} & I_{yy} & -I_{yz} \\ -I_{zx} & -I_{zy} & I_{zz} \end{bmatrix} \quad (D.3)$$

There are two types of forces acting on the engine body that one needs to be aware of. The first one is the shaking force and moments that are generated as a result of the movement of the internal components in the cylinder. The second one is the reaction force that is applied to the engine at each supporting mount.

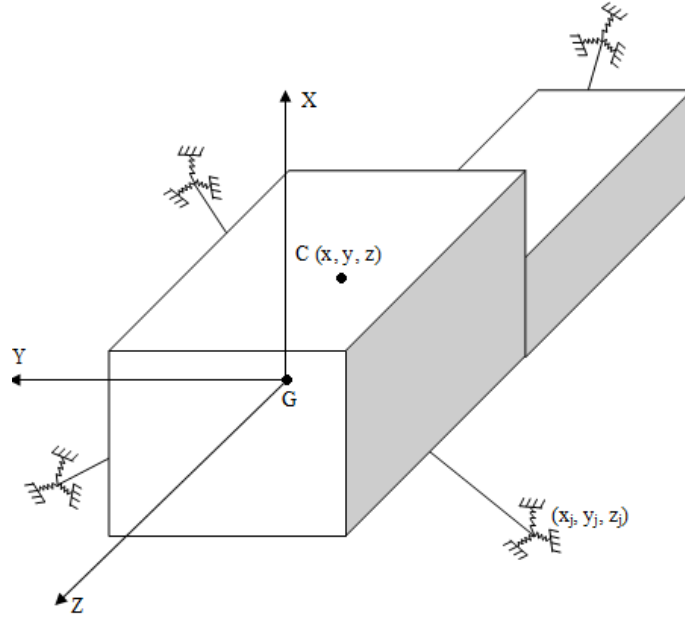


Figure D.1: Rigid body engine model

Consider an engine that is supported by  $N_m$  mounts located at  $(x_{mi}, y_{mi}, z_{mi})$ , where  $i = 1, 2, \dots, N_m$ . It is assumed the three principal stiffness  $(k_{xi}, k_{yi}, k_{zi})$  of each mount are independent of each other. The force moments that are exerted by the elastic mounts on the engine is given by Eq. (D.4). and Eq. (D.5). It is assumed that the displacements at the supports are small compared to their distance from the center of gravity C.

$$\begin{aligned}
 f_{xmi} &= -k_{xi}(x + z_{mi}\theta_y - y_{mi}\theta_z) \\
 f_{ymi} &= -k_{yi}(y + x_{mi}\theta_z - z_{mi}\theta_x) \\
 f_{zmi} &= -k_{zi}(z + y_{mi}\theta_x - x_{mi}\theta_y), \text{ for } i = 1, 2, \dots, N_m
 \end{aligned} \tag{D.4}$$

$$\begin{aligned}
 \eta_{xmi} &= f_{zmi}y_{mi} - f_{ymi}z_{mi} \\
 \eta_{ymi} &= f_{xmi}z_{mi} - f_{zmi}x_{mi} \\
 \eta_{zmi} &= f_{ymi}x_{mi} - f_{xmi}y_{mi}, \text{ for } i = 1, 2, \dots, N_m
 \end{aligned} \tag{D.5}$$

A set of differential equations shown in Eq. (D.6) and Eq. (D.7) may be solved numerically over a period of time  $[0, T]$ .

$$\begin{aligned} M\ddot{x} &= f_{xm} + f_{xc} + f_{xb} \\ M\ddot{y} &= f_{ym} + f_{yc} + f_{yb} \\ M\ddot{z} &= f_{zm} + f_{zc} + f_{zb} \end{aligned} \quad (D.6)$$

$$\begin{aligned} I_{xx}\ddot{\theta}_x &= (I_{yy} - I_{zz})\dot{\theta}_y\dot{\theta}_z + \mu_{xm} + \mu_{xc} + \mu_{xb} \\ I_{yy}\ddot{\theta}_y &= (I_{zz} - I_{xx})\dot{\theta}_z\dot{\theta}_x + \mu_{ym} + \mu_{yc} + \mu_{yb} \\ I_{zz}\ddot{\theta}_z &= (I_{xx} - I_{yy})\dot{\theta}_x\dot{\theta}_y + \mu_{zm} + \mu_{zc} + \mu_{zb} \end{aligned} \quad (D.7)$$

In Eq. (D.6) and Eq. (D.7),  $f_{xm}$ ,  $f_{ym}$ ,  $f_{zm}$ ,  $\mu_{xm}$ ,  $\mu_{ym}$  and  $\mu_{zm}$  are the forces and moments exerted by the mount on the engine. The terms  $f_{xc}$ ,  $f_{yc}$ ,  $f_{zc}$ ,  $\mu_{xc}$ ,  $\mu_{yc}$  and  $\mu_{zc}$  are the inertial forces and moments exerted by the engine. The terms  $f_{xb}$ ,  $f_{yb}$ ,  $f_{zb}$ ,  $\mu_{xb}$ ,  $\mu_{yb}$  and  $\mu_{zb}$  are the forces and moments associated by the balancing masses.

The solution yields dynamic forces represented in Eq. (D.4) and moments represented in Eq. (D.5) exerted by the mounts on the supporting structure due to the displacement of the engine supports. A suggested objective function is compiled as the sum of the squares of the forces over the interval  $[0, 0.4 \text{ sec}]$  as follows:

$$F = \frac{1}{T} \int_0^T \left[ \sum_{i=1}^{N_m} (|f_{xmi}|^2 + |f_{ymi}|^2 + |f_{zmi}|^2) \right] dt \quad (D.8)$$

The proposed objective function may be used as an alternate function to find the minimum transmitted internal loads from the engine to the frame in order to achieve the desired vibration isolation. The transmitted force may be minimized with respect to any set system parameters such as balancing masses and the associated phase angles.

## VITA

Fadi Alkhatib

Place of Birth: Ramallah, Palestine

Education:

Ph.D., University of Wisconsin-Milwaukee, December 2013  
Major: Mechanical Engineering  
Minor: Engineering Mechanics

M.S., University of Wisconsin-Milwaukee, Dec 2003  
Major: Engineering Mechanics

B.S., BirZeit University, Palestine, June 2000  
Major: Mechanical Engineering

Publications:

Alkhatib, F., Dhingra, A. K., "Shape Optimization of Engine Mounts for Enhanced Vibration Isolation," # IMECE2013-64476, *ASME 2013 International Mechanical Engineering Congress & Exposition*.

Alkhatib, F., Dhingra A. K., "Road Loads and Their Effect on the Mount Characteristics," Submitted to *Journal of Vibration and Control*, 2013.

Alkhatib, F., Dhingra A. K., "The Effect of Shaking Forces on the Mount Shape and Design," Submitted to *International Journal of Advanced Manufacturing and Technology*, 2013.